MODULATION AND CODING STUDY OF DATA TRANSMISSION FROM THE GATEWAY STATION TO THE MOBILE AND VICE VERSA

FINAL REPORT

MILLER COMMUNICATIONS SYSTEMS LTD.

MODULATION AND CODING STUDY OF DATA TRANSMISSION FROM THE GATEWAY STATION TO THE MOBILE AND VICE VERSA

FINAL REPORT

MCS File No: 8530
DSS Contract No: OST84-00490
DSS File No: 21ST.36001-4-2612
Date: August 23, 1985

Prepared by: SWC for Stewart Crozier
M. Moher, S. Crozier

Approved by: Stewart Crozier
S. Crozier

SUBMITTED BY:
MCS MILLER COMMUNICATIONS SYSTEMS LTD.
300 Legget Drive,
Kanata, Ontario,
Canada K2K 1Y5

Delivered-To: carole.laplante@crc.ca
X-Sender: jlodge@pop.crc.ca
X-Mailer: QUALCOMM Windows Eudora Version 4.3.2
Date: Wed, 28 Jun 2000 13:00:06 -0400
To: Carole Laplante <carole.laplante@crc.ca>
From: John Lodge <john.lodge@crc.ca>
Subject: Re: Old contractor report - still classified?

Hi Carole:

You can make the document available.

John

At 11:16 AM 6/28/00 -0400, you wrote:

Hello John!

We have a report in the vault made by Miller Communications Systems in 1985. The title is: Modulation and Coding Study of Data Transmission from the Gateway Station to the Mobile and Vice Versa (Final Report and Executive Summary). This report was classified because it may contain information of commercial value. Is it still the case? Is it not covered by a patent now?

Please let me know if I can make the document available or if it should remain in the vault.

Thank you.

Carole Laplante
998-2705

TABLE OF CONTENTS

1.0 INTRODUCTION

The purpose of this study was to evaluate several different modulation strategies which have been proposed for mobile satellite communications.

One of the most difficult technical problems to overcome in mobile satellite communications is the multipath fading nature of the propagation channel. The fading process is due in general to attenuation (or blockage) of the direct path, plus the interference caused by a multitude of reflections from the earth's surface. The aeronautical, maritime, and land mobile channels are progressively more difficult to handle (in some respects), since:

(i) in the aeronautical channel, the fading is due entirely to multipath reflections from the earth's surface (neglecting effects of the aircraft skin, ionosphere, troposphere etc.),

(ii) in the maritime channel, the antenna is closer to the earth's surface (resulting in stronger individual reflections), and some direct path blockage will usually result from large waves and elements of the ship's superstructure, and

(iii) in the land mobile channel, the antenna is even closer to the earth (resulting in strong individual reflections), and there will frequently be severe blockage (or shadowing) of the direct path due to tall buildings, forests, etc.

A particular model of the mobile satellite communications channel is shown in Figure 1.1 [8, 14], which has been shown to be valid for the land mobile case under certain

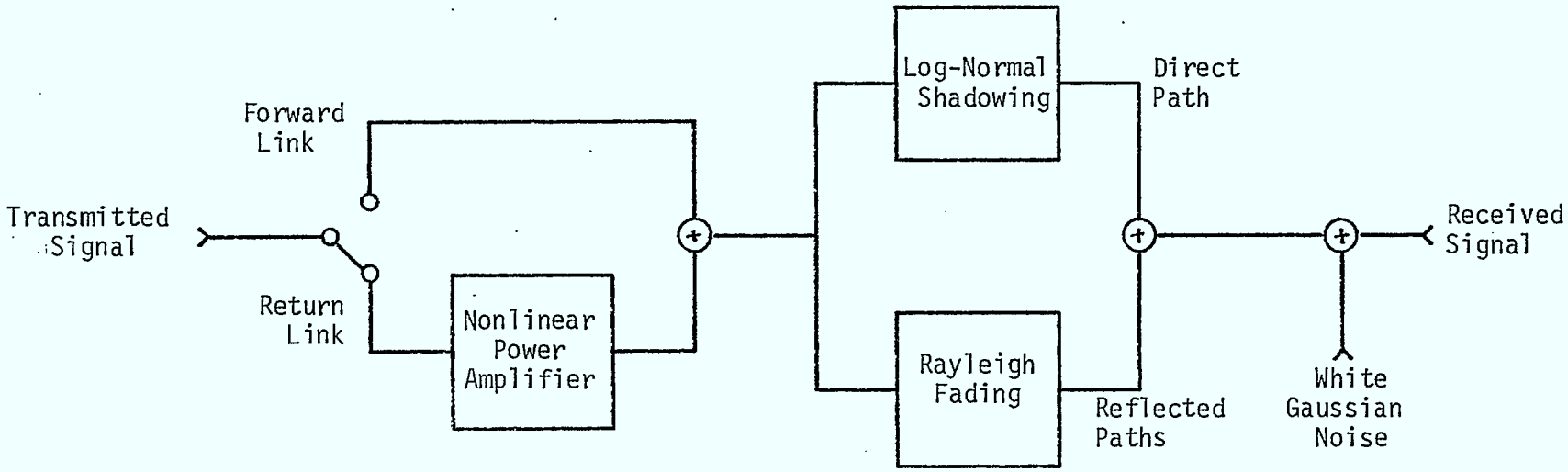

Figure 1.1 : A Model of the Satellite-Mobile Channel

circumstances [15]. The log-normal shadowing of the direct path is typical of forested terrain. Note that in the aeronautical case, the shadowing would not be present, and in the maritime case, it would not be log-normal.

In Figure 1.1, the fading rates of the Rayleigh and log-normal processes differ typically by at least an order of magnitude, with the former rate being typically 100 Hz, and the latter being perhaps a few Hz. (Both rates are proportional to the radial velocity of the vehicle.) Hence, during a few fade cycles of the Rayleigh process, the log-normal process is essentially constant, so that the short-term fading statistics will be seen as Rician, with a K-factor* determined by the direct path attenuation and the multipath power. Over a longer term, the overall process can be viewed as a Rician process with a varying K-factor.

Although strictly speaking, the individual reflections comprising the Rayleigh process will have different propagation delays, it is easy to show that this delay spread is negligible for the geometries and data rates of interest here.

The remainder of the channel is self-evident. There may (will) be a non-linear power amplifier in the (mobile) transmitter, and there will certainly be additive white Gaussian noise in the receiver.

The communications problem thus posed is to design a system that can provide reliable and satisfactory communications over the fading channel described above and specifically modelled in Figure 1.1.

*The K-factor is defined as 10 log (multipath power/direct power).

1.1 System Trade-Offs and Objectives

The degrees of freedom available to the systems designer, as reflected in the model of Figure 1.1, through which to realize a satisfactory system are:

(i) provide sufficient link margins to overcome the direct path shadowing,

(ii) minimize the multipath power through careful antenna design etc, and

(iii) adopt a modulation and coding strategy which is best suited to communicating over the resulting fading channel.

The subject study deals specifically with only the last of these, since effects of the first two will simply show up through choice of parameters in the channel model of Figure 1.1. In particular the specific objectives of the study were to evaluate, through computer simulation, and compare the performance of several candidate modulation strategies, with the channel modelled in Figure 1.1.

To be specific, the three modulation strategies evaluated were:

(i) Differential Minimum Shift Keying (DMSK)

(ii) Differential Offset Four Phase PSK (DOQPSK)

(iii) Coherent Binary Phase Shift Keying (BPSK) in conjunction with an Amplitude Companding Single Sideband modem (ACSSB)

All three strategies were tested at a data rate of 2.4 kbps and were restricted to a 5 kHz channel bandwidth.

1.2 Computer Simulation

The main focus of the evaluation of the three proposed modulation strategies was their computer simulation. MCS has previously developed and delivered a fading channel communications simulation under an MSAT Data Services contract. The main disadvantage of this existing simulation structure is that the instantaneous probability of error is computed for each bit from the (noise-free) demodulator output and the known (or assumed) noise distribution at that point in the system. Although efficient, this approach is rather restrictive in that exact and tractable expressions for detector noise statistics (first and second order) become unmanageable for all but relatively simple demodulators (e.g. CPSK and DPSK with no noise correlation from bit to bit). In addition, if the simulation is to be used to test coding strategies, actual (hard and soft) data sequences (rather than error probability sequences) are required for codec evaluation. In fact, for soft decision decoding, "signal" sequences are required. For these reasons, it was necessary to revert to a direct simulation approach, whereby AWGN is added at the receiver, and bit errors are counted. This of course implies large amounts of processing time to run the long sequences necessary in obtaining reasonably accurate performance estimates.

The channel simulation was developed in Fortran-77 under a VAX/VMS operating environment. In addition to the completely VAX compatible version, some time-consuming routines were also coded to make use of MCS's FPS-5100 Array Processor for evaluating performance at lower bit error rates.

In some cases the array processor provided a speed improvement of up to a factor of seventy-five over the VAX only version. This not only allowed evaluating the proposed modulation strategies at lower bit error rates but allowed faster debugging and testing of more scenarios than originally envisioned.

1.3 The Modulation Strategies

1.3.1 DMSK

Minimum Shift Keying (MSK), which is also known as Fast Frequency Shift Keying (FFSK), is a phase coherent binary FSK modulation with modulation index h = 0.5 [4-6, 16-22]. It has the following significant properties:

(a) 99.5% of the signal energy is contained within an IF bandwidth of 1.5 x (data rate),

(b) the signal envelope is constant and therefore MSK is suitable for use in nonlinear channels,

(c) the ideal error rate (coherent detection) is the same as that of 2- and 4-phase PSK.

As a result of these properties, MSK has received widespread interest [4, 18, 22] because of its potential in band-limited and power-limited systems.

For coherent detection in bursty signal environments such as TDMA, DAMA signalling, and voice activated SCPC, the

demodulator must re-acquire at the beginning of each burst (assuming that there is no phase coherence from burst to burst). PSK demodulators have been developed that can acquire the signal within 30 symbols. The design of carrier recovery loops for these modems is non-trivial [23]. Furthermore, these designs are usually restricted to applications where the available E_b/N_o is relatively large (>8 dB).

Differential detection can be used in PSK systems to avoid the carrier recovery problem. A differential PSK demodulator (DPSK) compares the phase of adjacent symbol intervals by using a 1 symbol delayed version of the received signal as the local reference signal. The need for a coherent recovery circuit is thereby removed.

It has been shown in [6] that MSK signals can also be demodulated by differential detection. While there may be implementation similarities between DMSK and DPSK, DMSK exhibits bandwidth and potentially power efficiency advantages over DPSK that make it a more attractive technique for development. A DMSK modem can use the usual FFSK/MSK modulator but recovers data by differential detection. Signal acquisition times for DMSK are primarily based upon clock recovery while joint carrier and clock recovery determine acquisition times for MSK. This is of prime concern for DAMA signalling for the MSAT mobile radio service.

The major disadvantage of differential detection is a theoretical E_b/N_o penalty arising from the use of an essentially noisier reference signal and ISI imposed by the

receive filter. Filtering, as it relates ultimately to bit error rate performance, is a major concern. This penalty can be reduced, however, by observing [6, 11] that phase comparison of alternate symbol intervals provides a parity check for successive symbols. Single errors can be corrected by a simple circuit without the need for the transmission of redundant bits. Such circuitry has been shown to be particularly useful for the correction of errors due to intersymbol interference. For example, in [6], for BT = 0.6, a 2.5 dB improvement was measured.

1.3.2 Differentially Detected OQPSK

The main problem with the DMSK signal format is that filters with BT products on the order of 1.0 cause quite severe ISI which results in degraded performance. Thus for the most part, optimizing the performance of the DMSK detector corresponds to trading off noise bandwidth against ISI.

This loss is often justified for DMSK because it is a modulation scheme with a constant envelope signal, and is relatively insensitive to frequency offsets. This constant envelope property is very desirable when the power amplifier is driven into saturation. The power amplifier used for ACSSB radios will not be driven into saturation, however, but must be somewhat more linear. For this reason, it may be advantageous to allow some envelope variation in exchange for tighter filtering (or even matched filtering) without the introduction of severe ISI. This more general approach can be viewed as differentially detected OQPSK. The modulator and demodulator for differential OQPSK is essentially the same as that for DMSK; the major difference is in the pulse shaping and/or transmit filtering and receive filtering.

To overcome the ISI problem of DMSK, a Nyquist pulse shape can be used in the DOQPSK format and then matched filtered at the receiver. Theoretically, this format should suffer from no ISI, but because of the envelope variations of the transmitted signal, it is expected to suffer some degradation due to a nonlinearity.

1.3.3 BPSK with TTIB ACSSB

As outlined in [8], it may be advantageous to place the data modem in series with the ACSSB modem, thereby taking advantage of the ACSSB processing. Transparent tone-in-band (TTIB) ACSSB is the approach under consideration. Since an ACSSB modem with TTIB can be used to perform unambiguous carrier recovery [9], coherent modulation strategies are thought to be most appropriate.

2.0 SYSTEM DESCRIPTION

The MSAT land mobile communications system has for the purposes of analysis and simulation been modelled as shown in Figure 2.1. This report describes the performance of this system for three different modulation techniques, DMSK, DOQPSK, and BPSK in conjunction with an ACSSB modem. The remaining portion of the system is held relatively constant throughout these tests. It should be noted that some of the components shown in Figure 2.1, e.g. transmit filtering, non-linearity and error correction, may or may not be present, depending upon the desired system configuration.

The following sections give a high level description of the components of the block diagram of Figure 2.1.

2.1 Data Generation

It is assumed throughout, that the data source is white, that is, the data bits are independent and uncorrelated. The data rate depends upon the modulation scheme chosen, but in all cases studied, the baud rate was a multiple of 1200 symbols per second. In the simulation independent and uncorrelated data bits were generated using the Fortran random number generator.

2.2 Modulation

This was the variable portion of the study, with the three modulation techniques mentioned above being implemented. As well, two additional modulation techniques using coherent detection, MSK and OQPSK, were also included in the simulation for benchmarking purposes. The underlying strategy of all the modulation techniques was to convert the data bits, $\{a_i\}$, $i=1,\ldots,N$, to an impulse train described by

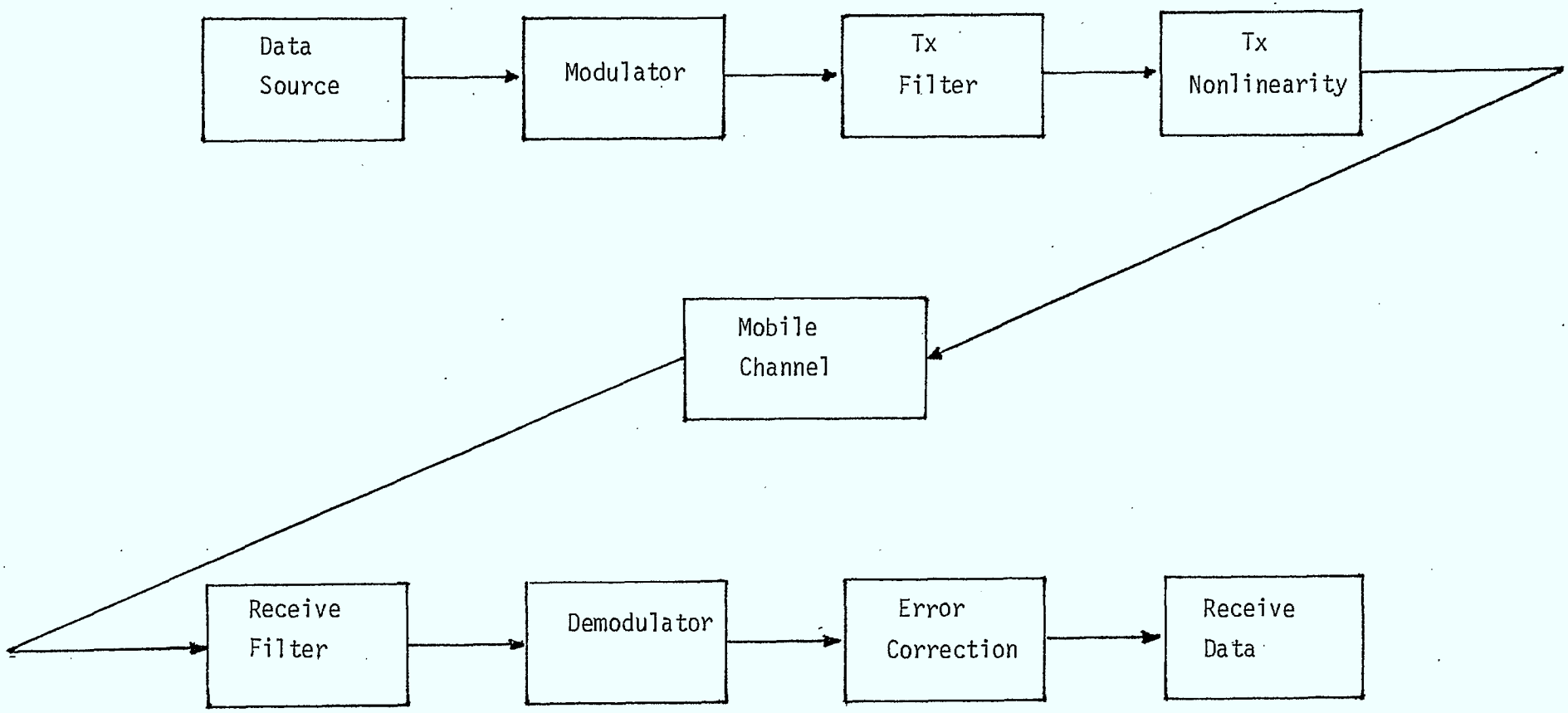

Figure 2.1 Simplified Model of Mobile Satellite Communications Channel

$$m(t) = \sum_{i=1}^{N} b_i \delta(t-T)$$

where T is the bit period, and $\{b_i\}$ is an encoded form of the data $\{a_i\}$. In the case of differential detection then $\{b_i\}$ must be a differentially encoded version of $\{a_i\}$, that is,

$$b_i = -a_i \, b_{i-1}$$

If in addition, we are using a signalling scheme which has two orthogonal channels (e.g. MSK and OQPSK), then every second b_i must be rotated in the complex domain to become purely imaginary. This is accomplished by rotating each successive b_i by 90°, that is,

$$b_i \leftarrow b_i \, e^{j\frac{i\pi}{2}} \qquad i = 1,\ldots,N$$

Note that this type of continuous rotation is required for a differential detection scheme using two orthogonal channels.

All modulation strategies studied for signalling over two orthogonal channels, only included the case when the bits are offset in the two channels. Strategies such as QPSK, where the bits are not offset, were not considered.

Once the impulse train, m(t), is generated the desired pulse shape can be obtained by passing it through a filter with the appropriate impulse response.

Note that one part of the study included an ACSSB modem. This additional form of modulation is described in Section 5.

2.3 Transmit Filtering

Transmit filtering is performed to reduce the sidelobes of the signal, and thus possible adjacent channel interference. It can optionally be performed as part of the pulse shaping but it has been separated in this system description because of the somewhat different purpose.

2.4 Nonlinearity

The communications link from the mobile user to the gateway station will include a transmit power amplifier which will be operating near its saturation point. This is expected to cause some distortion of the signal and for this reason has been included as part of the model.

It is assumed that a general AM-AM and AM-PM type nonlinearity is a sufficiently accurate model of the power amplifier and this has been included as part of the simulation.

The nominal transmit nonlinearity as specified by the Scientific Authority is a memoryless nonlinearity with AM-AM distortion and is described by the equation

$$s_o(t) = \frac{s_i(t)}{1+(\sqrt{2}-1)\left|s_i(t)\right|} .$$

where $s_i(t)$ is the input signal and $s_o(t)$ is the output signal. The input-output amplitude characteristic of this device is shown in Figure 2.2. The nominal operating point of the nonlinearity was at an input amplitude of 1.0.

With MSK modulation and no transmit filtering the input to the nonlinearity should be of constant amplitude, and thus

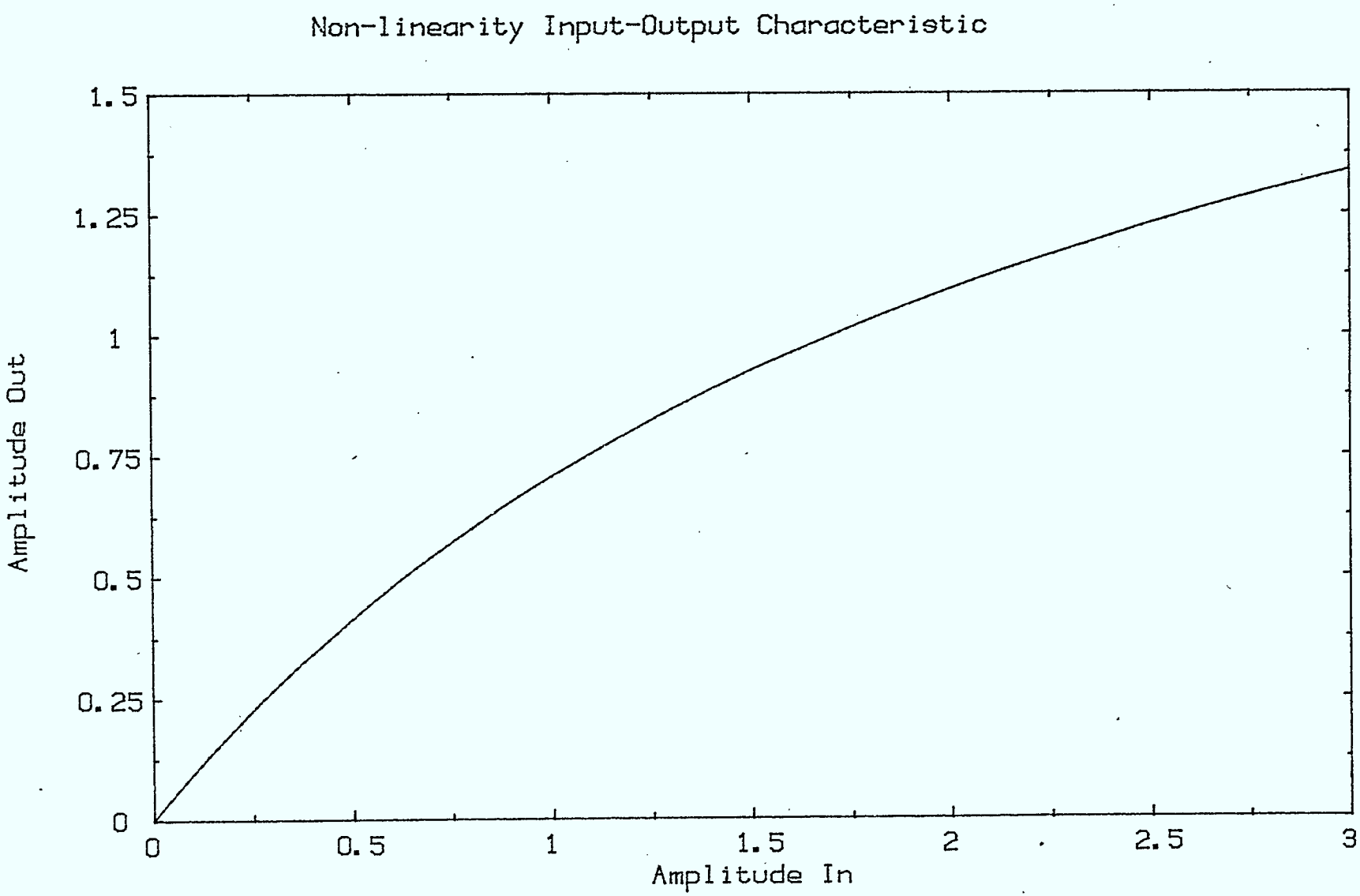
Non-linearity Input-Output Characteristic
Amplitude Out
1.5
1.25
1
0.75
0.5
0.25
0
0
0.5
1
1.5
2
2.5
3
Amplitude In

Figure 2.2

the nonlinearity should cause no distortion. For other modulation types, with fluctuating amplitudes, some distortion is expected.

2.5 The Mobile Channel

The MSAT mobile communications channel was modelled as a Rician fading channel [7] as shown in Figure 2.3. It includes a direct path and a Rayleigh fading path and it assumes that for the bit rates under consideration (1.2 to 2.4 kbps), the delay of the fading path is negligible relative to the bit period. The bandwidth of the Rayleigh fading process is assumed to be approximately 100 Hz.

The nominal spectral shaping filter for the Rayleigh process is that which is described in [1] and was used in [3]. In the analog domain this filter is described by the equation

$$H_m(s) = \frac{1}{(.897s^2+0.31s+1)(1.543s^2+0.841s+1)(1.944s+1)}$$

where the frequency has been scaled to give a bandwidth of 1 radian/second. At present, an FIR approximation to this filter is used (a large number of coefficients is required) and the filter coefficients are scaled to provide a one-sided bandwidth equal to the Doppler frequency of 100 Hz.

Figure 2.4 shows both the analog spectral shape for the Rayleigh fading process and the FIR approximation.

In addition to the multipath channel characteristic, it is also assumed that there will be additive white Gaussian noise at the receiver.

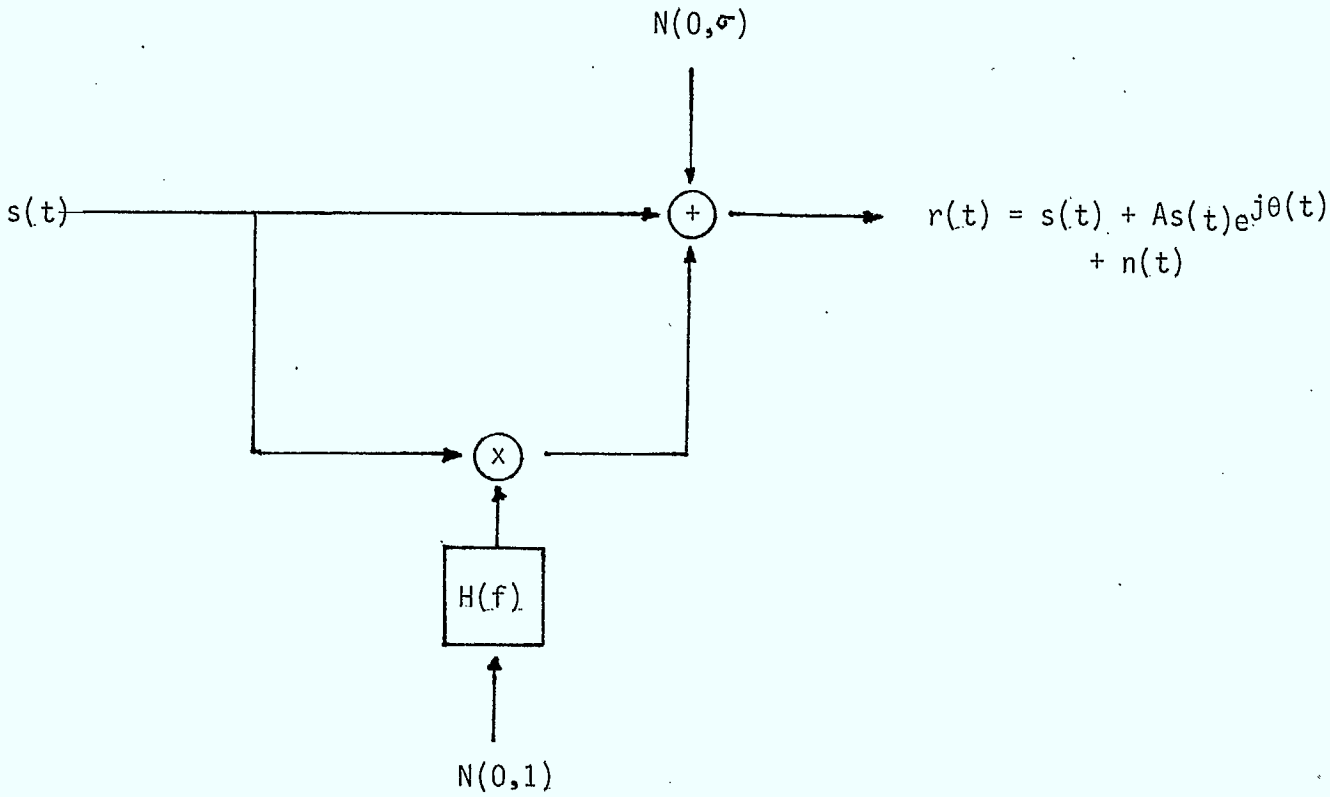

Figure 2.3 Rician Fading Channel

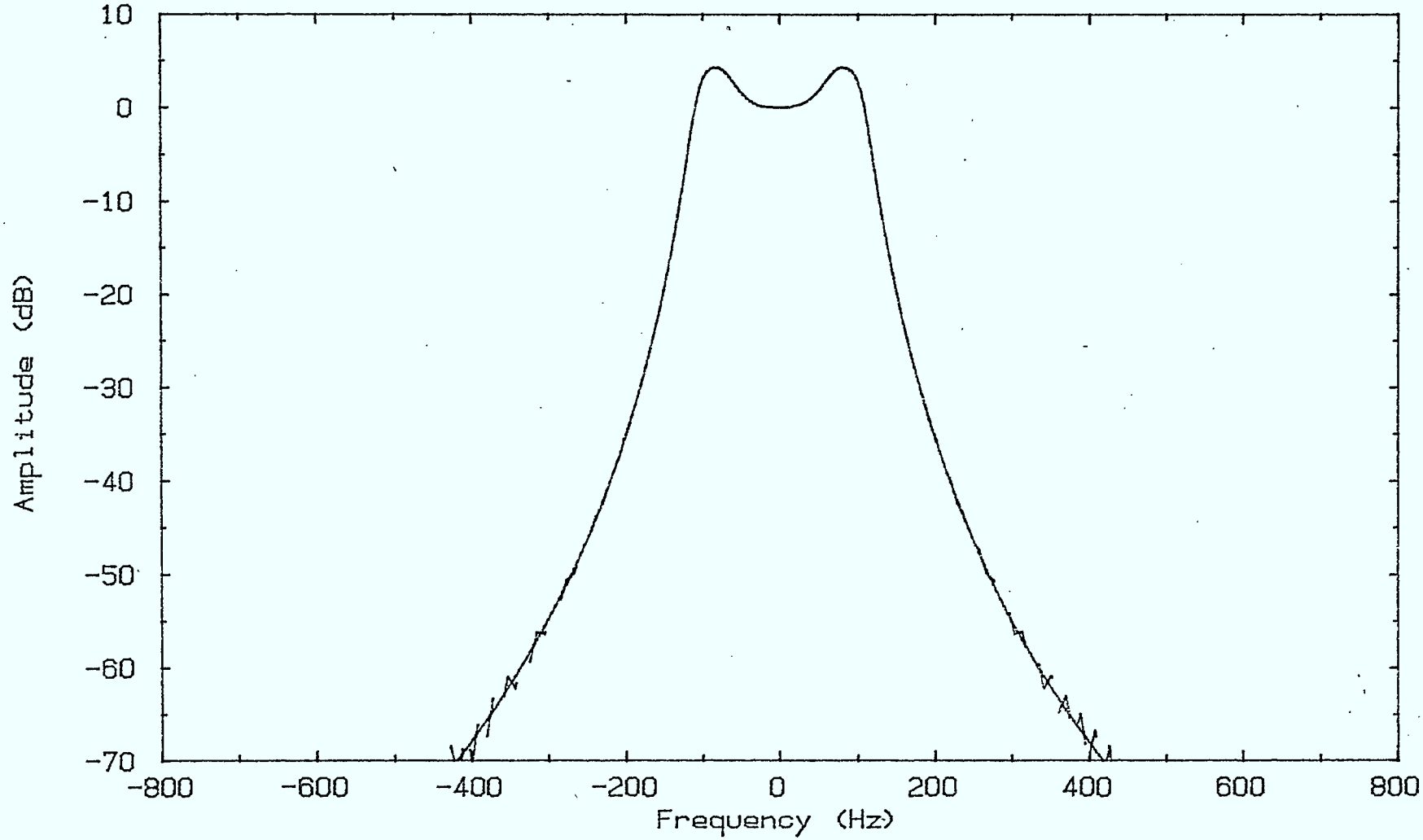

Multipath Spectral Shaping Filter

---------- analog approximation

--- --- --- digital approximation

Figure 2.4

The Rician channel is characterized by its K factor. Let the received signal be described by

$$r(t) = s(t) + A(t)\ e^{j\theta(t)}s(t) + n(t)$$

where s(t) is the transmitted signal, $A(t)e^{j\theta(t)}$ is the complex gain associated with the Rayleigh fading path and n(t) represents the additive white Gaussian noise. Then assuming the fading process is independent of the signal, the ratio of the fading path to direct path power is given by

$$k = \frac{E[\,|A(t)e^{j\theta(t)}s(t)|^2]}{E[\,|s(t)|^2]}$$

$$= E[A^2(t)]$$

where $E[\cdot]$ denotes the expected value, and the channel K factor (dB) is given by $K = 10 \log k$. Note that when there is no fading ($A(t)=0$), K is defined to be $-\infty$ dB.

The performance of the various modulation schemes is usually gauged by their bit error rate (BER) versus E_b/N_o performance curves. The received energy per bit, E_b, was calculated to include both the contribution from the direct path and that from the fading path. If the direct path E_b is denoted by E_b^o, then the total received energy per bit can be determined from the channel K factor by the relationship

$$E_b = (1 + k)\ E_b^o$$

where k is as defined above.

In the case of the ACSSB modem, the power of the pilot and subpilot are also included as part of the direct path energy per bit. For example, if E_b^d is the pure data energy per bit (excluding pilots), and the power in the pilots is a fraction α of the power in the data then

$$E_b^o = (1 + \alpha)E_b^d.$$

2.6 Receive Filter

The receive filter is dependent on the modulation type and where appropriate it is usually matched to the pulse shaping filter to provide an overall Nyquist pulse shape with no intersymbol interference.

2.7 Demodulation

The demodulator obviously must be matched to the modulation, and the basic strategies can be broken down to differential or coherent detection, with one or two channel signalling.

2.7.1 Differential Detection

A circuit incorporating the differential detector with a single-error correction circuit is shown in Figure 2.5. The upper circuit comprising the T second delay line, 90° phase shifter and phase comparator represents the differential detector, while the circuit consisting of the 2T delay line and phase comparator is the parity generator. The balance of the circuit consists of the syndrome generator and error correction elements.

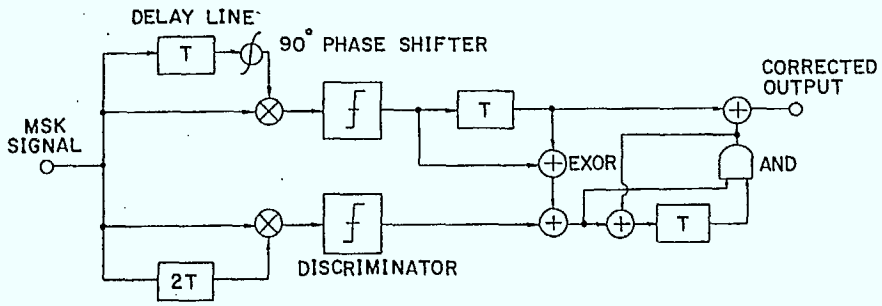

Figure 2.5 Differential Detector and Error Correction Circuit (6).

The received complex baseband DMSK signal with noise is given by r(t), and the reference signal is given by $r(t-T)e^{j\frac{\pi}{2}}$. The demodulated signal is then

$$y(t) = \mathrm{Re}\left[r(t)\ r^*(t-T)e^{-j\frac{\pi}{2}}\right]$$

The single error correction circuit requires an additional demodulated waveform, y'(t), similar to that of y(t), and is defined by

$$y'(t) = \mathrm{Re}\left[r(t)\cdot r^*(t-2T)\right]$$

A complex baseband equivalent DMSK demodulator, with the parity branch, can thus be implemented using the above two expressions. Note that the complex baseband equivalent modulator and demodulator are the same as those for DOQPSK except for the pulse shaping filter.

2.7.2 Coherent Detection

In the case of coherent detection, the received signal is sampled at the appropriate time. Ideal bit synchronization was assumed and no attempt was made to study the effects of non-ideal carrier recovery.

2.8 Error Correction

With the differential demodulation schemes, there is the possibility of performing non-redundant single error correction using a parity check which is inherent in the differential encoding of the data.

The single error correcting mechanism is based on the following [6,11]. Let $\dot{D}_i$, $\dot{D}_{i-1}$ represent the error free data bits in the i-th and (i-1)-th data intervals. Let

$$\dot{P}_i = \dot{D}_i + \dot{D}_{i-1} \tag{2.1}$$

where + is the XOR function.

If e_{D_i} and e_{P_i} represent channel errors in D_i and P_i respectively, then at the receiver

$$D_i = \dot{D}_i + e_{D_i} \tag{2.2}$$

$$P_i = \dot{P}_i + e_{P_i} \tag{2.3}$$

The syndrome (error detection variable) is given by

$$S_i = D_i + D_{i-1} + P_i \tag{2.4}$$

and is 0 when no errors occur and equal to 1 when a single error occurs in one of D_i, D_{i-1}, or P_i. S_i can be expanded using (2.2) and (2.3) as follows:

$$\begin{aligned} S_i &= D_i + D_{i-1} + P_i \\ &= \dot{D}_i + e_{D_i} + \dot{D}_{i-1} + e_{D_{i-1}} + \dot{D}_i + \dot{D}_{i-1} + e_{P_i} \qquad (2.5) \\ &= e_{D_i} + e_{D_{i-1}} + e_{P_i} \end{aligned}$$

Assuming that the effect of $e_{D_{i-2}}$ has been eliminated in the previous decoding interval, the syndrome of the previous interval is given by

$$S_{i-1} = e_{D_{i-1}} + e_{P_{i-1}} \tag{2.6}$$

The error bit can be determined by

$$S_i \cdot S_{i-1} = (e_{D_i} + e_{D_{i-1}} + e_{P_i}) \cdot (e_{D_{i-1}} + e_{P_{i-1}}) \tag{2.7}$$

If only one of $(e_{D_i}, e_{D_{i-1}}, e_{P_i}, e_{P_{i-1}})$ is in error then $S_i \cdot S_{i-1}$ is always 0 except for

$$S_i \cdot S_{i-1} = e_{D_{i-1}} \tag{2.8}$$

In other words the syndrome circuitry can detect an error in D_{i-1}. Adding $e_{D_{i-1}}$ to the T-delayed data will correct the error. The assumption made in stating (2.6) above is justified by feeding $e_{D_{i-1}}$ back into the circuit to eliminate its effect on the next decoding interval.

2.8.1 Performance

Assuming uncorrelated noise samples and no ISI the probability of bit error at the output of the error correction circuit is shown [6] to be given by

$$\begin{aligned} P_o &= 0.89\ P_i^{1.06} \\ &= 0.43\ e^{-1.06\ \mathrm{SNR}} \end{aligned} \tag{2.9}$$

where P_i is the bit error rate (BER) probability at the circuit input.

For an error rate of 10^{-4}, the advantage of this circuit relative to differential detection alone is given by

$$SNR_i - SNR_o = 9.30 - 8.99$$

$$= 0.31 \text{ dB} \tag{2.10}$$

For DMSK the above result only holds for very large bandwidths. When trying to optimize performance in terms of E_b/N_o, both ISI and noise correlation are introduced. As shown in [6] the improvement with SEC increases dramatically when BT products on the order of 1.0 are used.

The performance gains which could be obtained with this single error correction technique were also studied through simulation.

3.0 DMSK STUDY

This task was concerned with the simulation of a DMSK data modulation scheme in the context of the system description given in Section 2.0. DMSK is attractive as a modulation scheme because of its constant envelope property and thus should suffer no degradation when passed through most of the nonlinearities found in practice. Also DMSK has the property that most of its power is concentrated in the main lobe and has significantly less power in the sidelobes when compared to other forms of modulation [4]. This implies that DMSK will cause less adjacent channel interference. The major disadvantage of DMSK is that it can't be match filtered without intersymbol interference. Intersymbol interference can cause up to 3 dB and more degradation in performance depending upon the filtering approach. Fortunately some of this degradation can be recovered using single error correction. It is the purpose of this task to study all of these aspects in the context of a Rician fading channel.

3.1 Pulse Shape

When MSK is considered as a two-channel orthogonal signalling scheme, with the data bits in one channel offset from those in the other [4] then the MSK pulse shape is that of the half cosine pulse shown in Figure 3.1 and described by

$$p(t) = \begin{cases} \sin\left(\frac{\pi t}{2T}\right) & 0 \leq t \leq 2T \\ 0 & \text{otherwise} \end{cases}$$

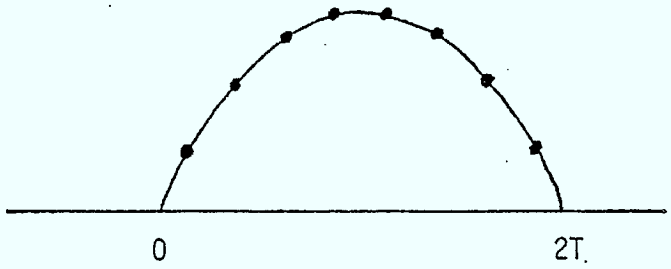

Figure 3.1 MSK Pulse Shape (showing typical sample points).

where T is the bit period. This pulse shape is implemented as an FIR filter with coefficients given by evenly spaced and symmetric samples of p(t) as shown in Figure 3.1. Typically, the pulse shape is sampled at four times the bit rate, and the resulting pulse shape spectrum is shown in Figure 3.2. As this figure shows the MSK spectrum falls off quite rapidly, the first null occurring at ±.75 of the bit rate, and thus the effects of aliasing at this sampling rate should be negligible.

Note also that if this technique is implemented digitally, then the sampling technique shown in Figure 3.1 of sampling the pulse shape symmetrically about the peak but not at the peak (using an even number of samples) forces the spectrum to be zero at the Nyquist frequency. This technique is explained further in Appendix B but from a practical viewpoint its main advantage is that for a channel spacing of approximately twice the bit rate it significantly reduces the interference into the centre of an adjacent channel.

3.2 Transmit Filter

The nominal transmit filter is a 13-tap FIR filter which was specified by the Scientific Authority. Assuming a sampling rate at four times the bit rate, the spectral response of this filter is shown in Figure 3.3.

The result of the combination of the MSK pulse shaping filter and the transmit filter is shown in Figure 3.4. As this figure indicates the transmit filter significantly reduces the level of the sidelobes, reducing the possibility of causing interference into the adjacent channel. This is accomplished with minimal distortion of the main lobe of the MSK spectrum.

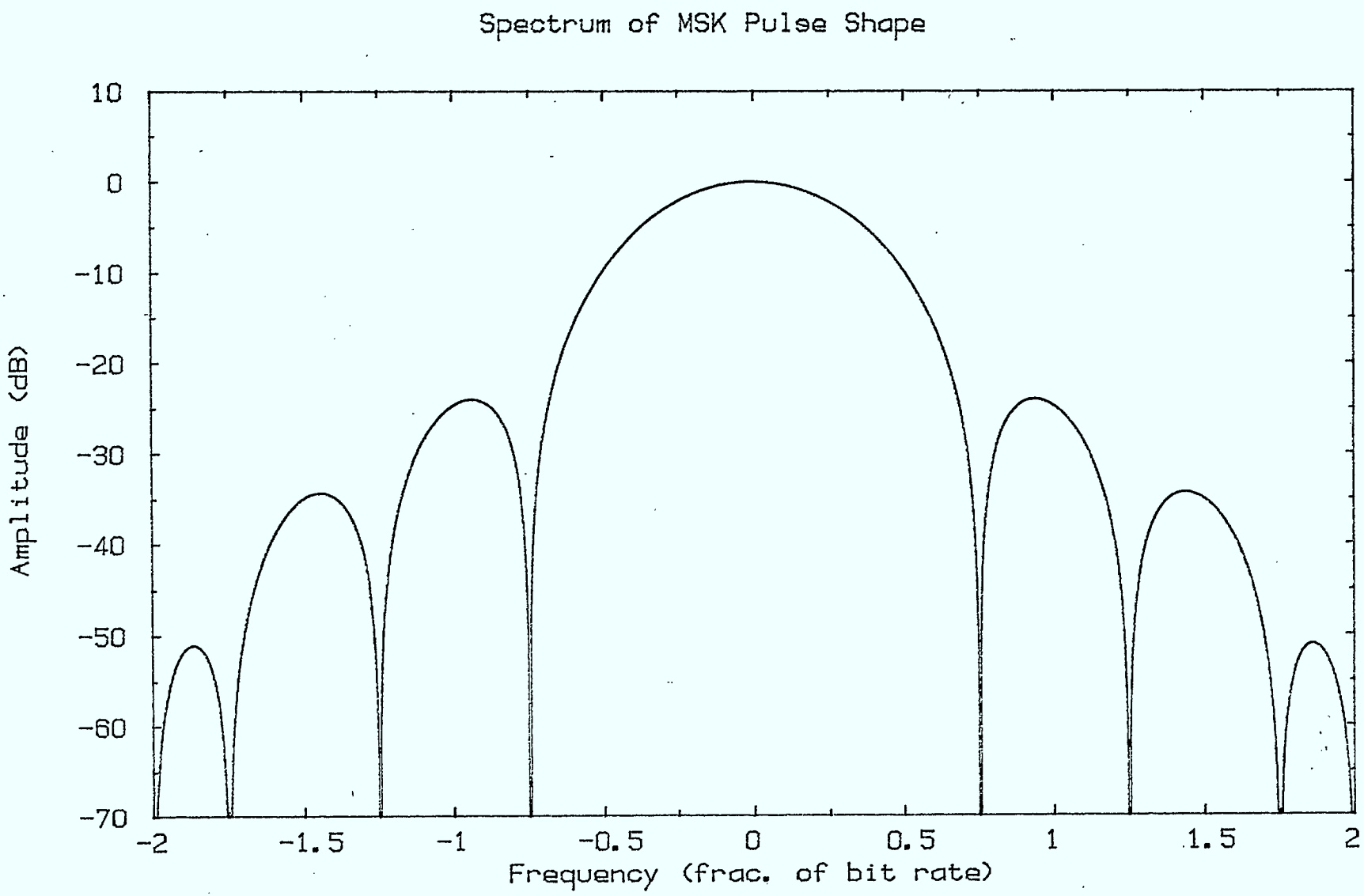
Spectrum of MSK Pulse Shape
Amplitude (dB)
10
0
-10
-20
-30
-40
-50
-60
-70
-2
-1.5
-1
-0.5
0
0.5
1
1.5
2
Frequency (frac. of bit rate)

Figure 3.2

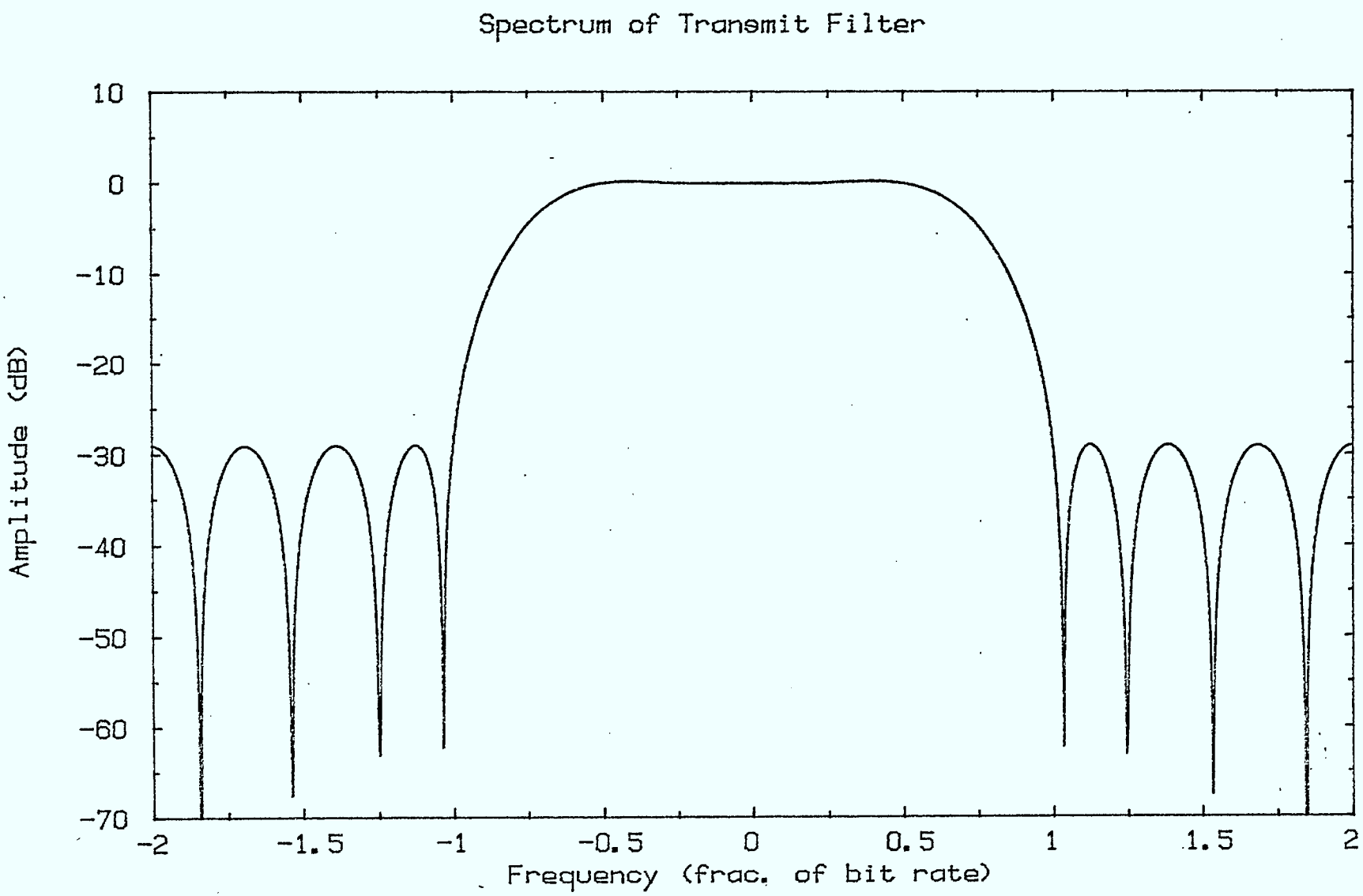
Spectrum of Transmit Filter
Amplitude (dB)
10
0
-10
-20
-30
-40
-50
-60
-70
-2
-1.5
-1
-0.5
0
0.5
1
1.5
2
Frequency (frac. of bit rate)

Figure 3.3

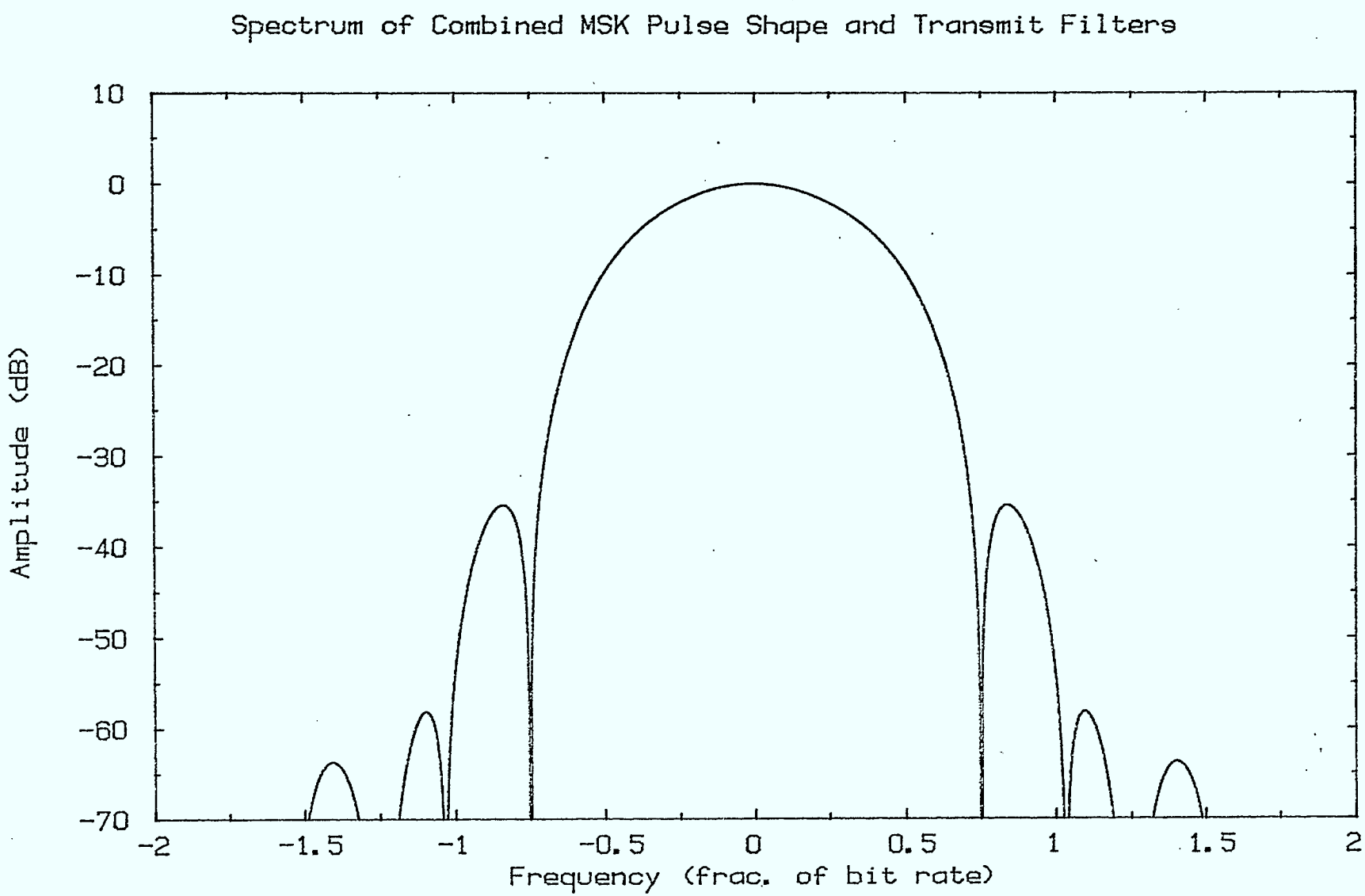
Spectrum of Combined MSK Pulse Shape and Transmit Filters
Amplitude (dB)
10
0
-10
-20
-30
-40
-50
-60
-70
-2
-1.5
-1
-0.5
0
0.5
1
1.5
2
Frequency (frac. of bit rate)

Figure 3.4

3.3 Receive Filter

The nominal receive filter chosen for the following simulation tests was a fourth-order phase-equalized Butterworth filter (i.e. linear phase), with a BT product of 1.1. From a study done in [2], this filter provided the least degradation of conventional DMSK from ideal CMSK of those filters tested (approximately 2.9 dB at a bit error rate of 5×10^{-4}).

This filter was implemented as a 31-tap FIR filter, using a windowed version of the impulse response to define the filter coefficients. Figure 3.5 shows the amplitude response of a 4th order Butterworth and the amplitude response of the FIR approximation. The only difference that can be noticed is a very small ripple in the stopband of the FIR approximation.

The performance of the DMSK system with this receive filter (with various BT products), no transmit filter and an ideal Gaussian channel was compared to that obtained in [2]. The results were in fairly close agreement over the range tested. There was no attempt made to optimize the BT product of the receive filter with the nominal transmit filter present.

3.4 Analytical Results

3.4.1 Ideal Coherent MSK (CMSK)

MSK modulation can be viewed as antipodal signalling on two orthogonal channels [4] and thus the probability of error in a white Gaussian noise channel under ideal conditions is given by

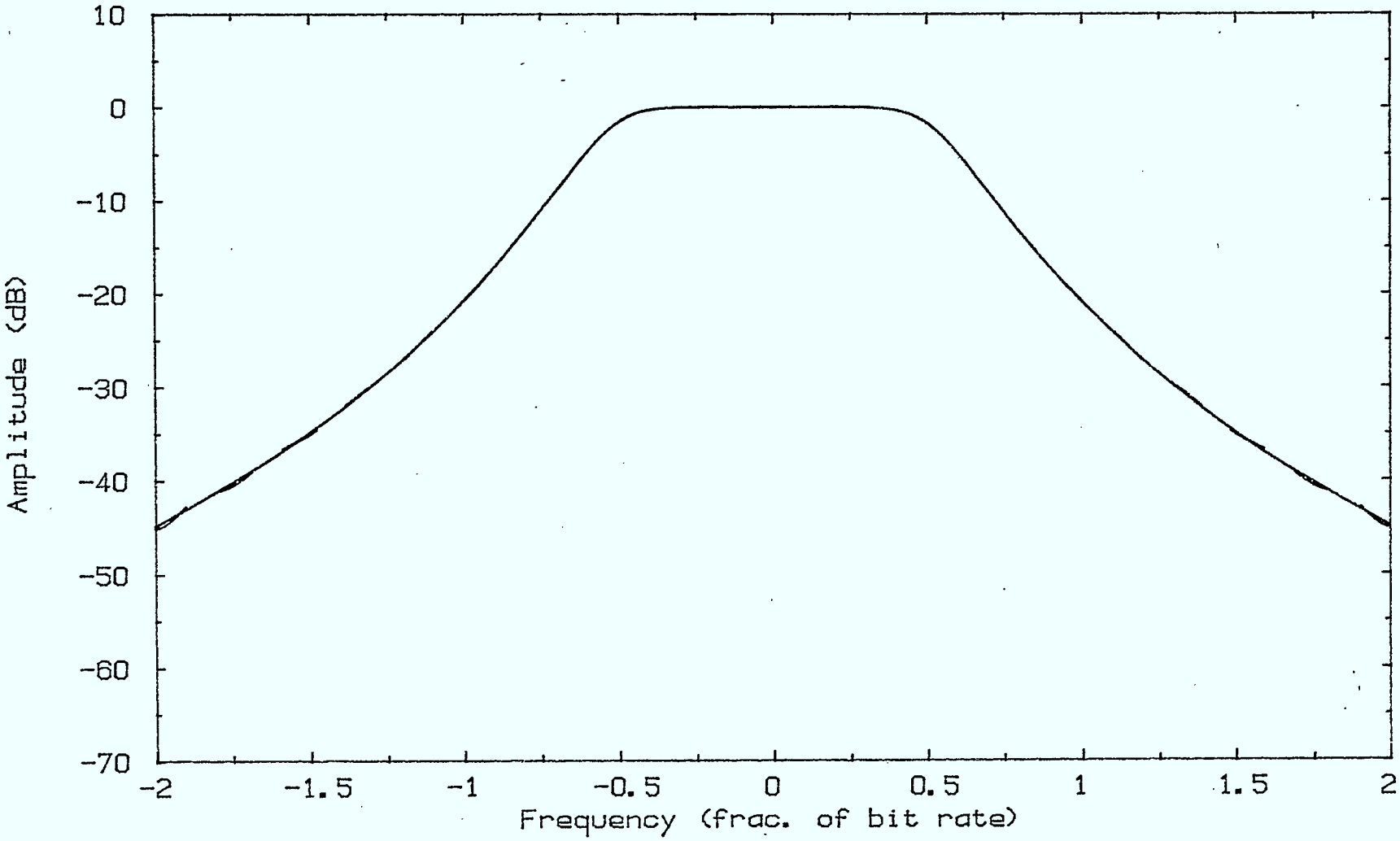

Spectrum of 4th Order Butterworth Receive Filter

---------- analytic spectrum

--- --- --- FIR approximation

Figure 3.5

$$P_e = Q(\sqrt{2E_b/N_o}) \tag{3.1}$$

$$= \int_{\lambda}^{\infty} \frac{1}{\sqrt{2\pi}} e^{\frac{-y^2}{2}} dy.$$

where $\lambda = \sqrt{2\ E_b/N_o}$.

To benchmark the simulation, an ideal white Gaussian channel configuration was used with MSK matched filtering and coherent detection.

The simulation sampling rate was set at four samples per bit and the number of bits simulated depended upon the bit error rate being characterized. A comparison of the simulation results and theory is made in Figure 3.6. The error bars on each sample point indicated the estimate of one standard deviation obtained from a number of simulation runs. As seen in Figure 3.6, there is very good agreement between simulation and theory. Note that the same set of random number seeds were used to generate each point on the curve and this explains any consistent bias observed.

3.4.2 Differential MSK (DMSK)

3.4.2.1 Ideal Differential Detection

Assuming no-ISI, the probability of bit error for the differential or comparison detection of binary FM (including DMSK) is given by [5]

$$P_e = \frac{1}{2} \exp(-SNR) \tag{3.2}$$

where the signal-to-noise power ratio (SNR) is given by

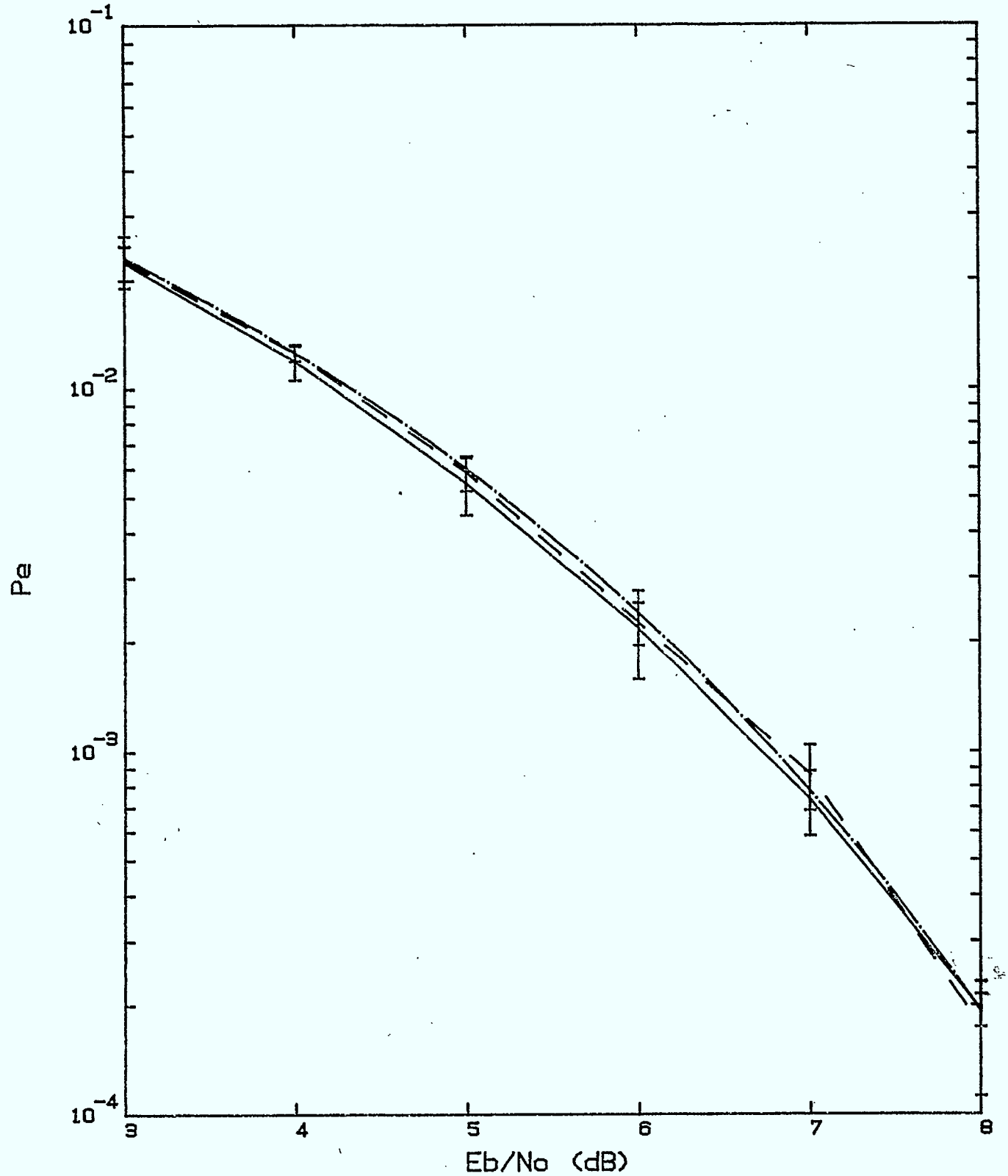

Comparison of AP and VAX Results (Ideal Coherent Case)

——————— AP results

— — — — VAX results

—·—·—·— Ideal Coherent Performance

Figure 3.6

$$SNR = \frac{P_s}{P_n} . \tag{3.3}$$

The noise power P_n is given by

$$P_n = N_o B \tag{3.4}$$

where N_o is the single-sided power spectral density of the additive white Gaussian noise and B is the IF noise bandwidth of the receive (Rx) filter. The validity of (3.2) also depends on the assumption that the autocorrelation function of the noise, $R_n(\tau)$, is zero at $\tau = T$, where T is the bit period.

The differential detector performs optimally only when the transmitted signal is Nyquist, i.e. when the signal format is such that matched filtering may be used at the receiver and the resultant signal is free of ISI. For this case the instantaneous SNR at the desired comparison points is given by SNR = E_b/N_o. Thus the corresponding probability of bit error is given by

$$P_e = \frac{1}{2} \exp(-E_b/N_o) \tag{3.5}$$

This represents a degradation relative to CMSK of about 1 dB at a BER of 10^{-4}. The DMSK signal format does not possess the above desired property and thus exhibits inferior performance to that of (3.5).

The main problem with the DMSK signal format is that filters with BT products on the order of 1.0 cause quite severe ISI which results in degraded performance. Thus for

the most part, optimizing the performance of the differential detector corresponds to trading off noise bandwidth against ISI.

3.4.2.2 No-ISI Degradation Lower Bound

As already stated, equation (3.2) only holds true for an Rx bandwidth approaching infinity (assuming no attempt is made to equalize for ISI), i.e. any bandwidth constraint causes undesirable ISI. For the most part, the problem of finding the best Rx filter reduces to the problem of trading off noise bandwidth B against imposed intersymbol interference. When comparing detection schemes, an appropriate reference is the ratio of energy per bit to noise power spectral density, E_b/N_o, which is required to give the same bit error rate (BER) performance. In terms of E_b/N_o the signal-to-noise ratio is given by

$$SNR = \frac{E_b}{N_o} \cdot \frac{1}{BT} \tag{3.6}$$

To determine the no ISI degradation of DMSK with respect to CMSK, equation (3.6) is substituted in (3.2) and compared to (3.1) for a given probability of error, P_e, and BT product.

As an example, for $P_e = 5x10^{-4}$ and BT = 1.1 we obtain a fundamental no-ISI degradation of 2.0 dB for conventional DMSK over CMSK. Thus the actual degradation with ISI must be greater than 2.0 dB under these conditions.

This example corresponds to the receive filter used in this portion of the simulation. A fourth order phase-equalized Butterworth filter with a BT product of 1.1, as described in Section 3.3.

Note that some of the degradation due to ISI can be recovered through the use of a single error correction technique as discussed in Section 2.8.

3.5 DMSK Simulation Results

3.5.1 Conventional DMSK

Conventional DMSK refers to differentially detected MSK with no attempt at error correction. For this series of tests, the transmit and receive filters were as described in Sections 3.2 and 3.3. The same series of tests were performed both with and without the nonlinearity; the non-linearity followed the transmit filter. The tests were performed with varying amounts of multipath corresponding to K factors of $-\infty$, -10, -5 and 0 dB where K is the ratio of the power of the Rayleigh fading path to the direct path power.

The simulation results are shown in Figure 3.7 for the two series of tests. One should note that the degradation of differential detection with respect to coherent detection under no multipath conditions is approximately 3 dB. This agrees with the results obtained in [2] and to a large part is caused by the tradeoff between noise and ISI made with the choice of a finite BT product. (The degradation caused by ideal differential detection relative to coherent detection is on the order of 1 dB on the indicated range.)

Comparing performance with and without the nonlinearity present, there is no noticeable degradation due to the nonlinearity. This is to be expected because of the constant envelope property (nearly constant envelope with transmit filtering) of MSK modulation.

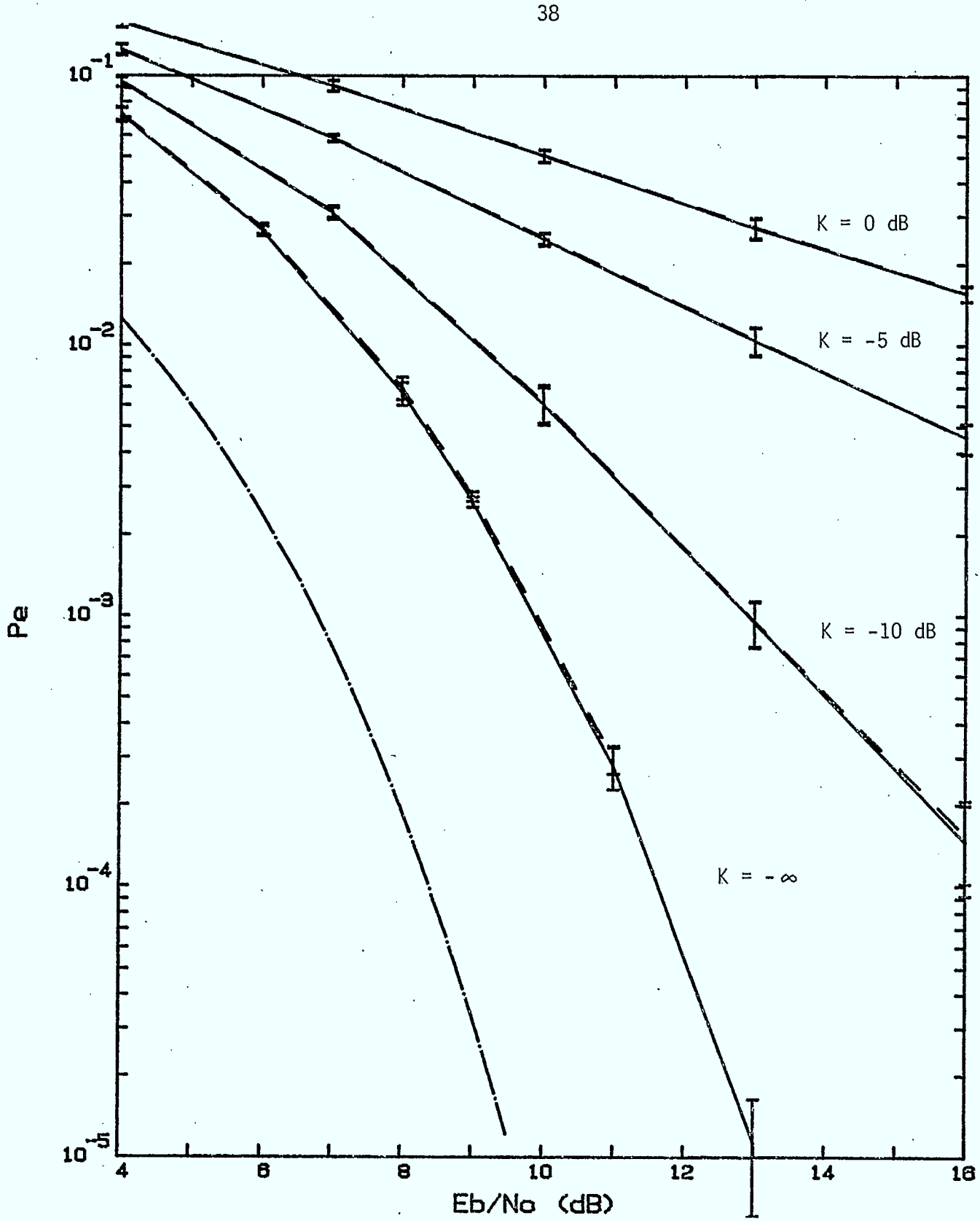

Performance of conventional DMSK

——————— without nonlinearity

— — — — with nonlinearity

—·—·—·— Ideal Coherent Performance

Figure 3.7

With increasing amounts of multipath the performance deteriorates as expected, flattening out as the Rician channel factor is increased.

3.5.2 DMSK With Single Error Correction

The same series of tests described in Section 3.5.1 were also done including a single error correction (SEC) circuit. These results are shown in Figure 3.8. These curves repeat the same trends shown in Figure 3.7 except that the average bit error rate has been reduced.

To determine the enhancement in performance obtained by using the SEC circuit, one should look at Figure 3.9 which compares conventional and SEC DMSK performance without the nonlinearity. Similar relationships are obtained with the nonlinearity present. In Figure 3.9, an approximate 1 dB improvement in performance is obtained with SEC in the case of no multipath. As the level of the multipath, K, is increased the gain obtained with SEC becomes less and less. This would indicate that more of the errors are occurring in bursts (a case which the SEC can't handle) as the multipath is increased. This is to be expected because of the slow fading rate relative to the bit rate.

3.5.3 MSK Spectrum After Nonlinearity

Besides BER performance, other features of the MSK modulation scheme are of interest. In particular, its spectral shape after a nonlinear amplifier is of importance because of the possibility of causing adjacent channel interference. Theoretically since the MSK signal has a constant envelope, the nonlinearity should have no effect. However in practice, both a digital implementation and a transmit filter may cause some amplitude variations.

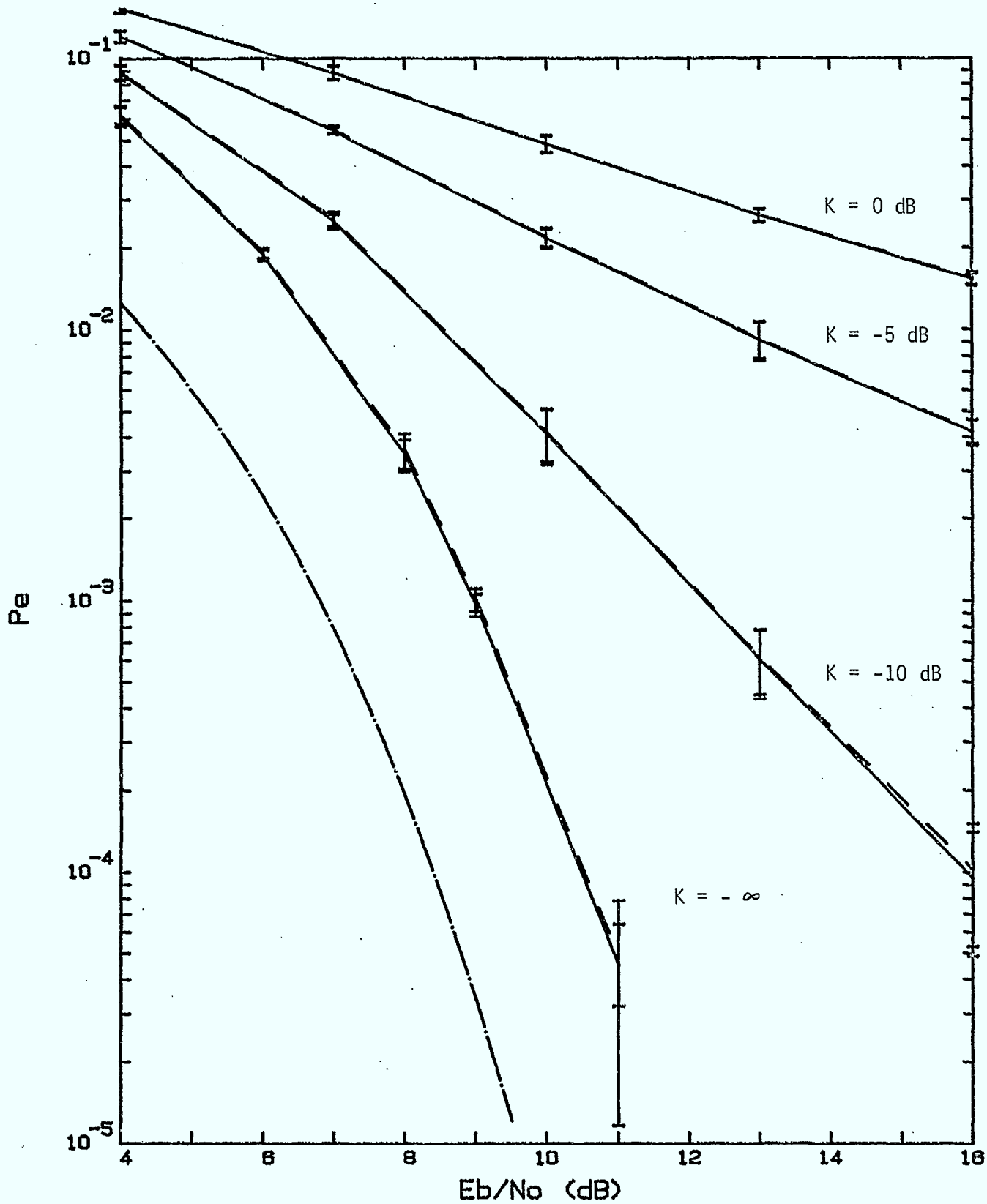

Performance of DMSK with Single Error Correction

——————— without nonlinearity

— — — — with nonlinearity

—·—·—·— Ideal Coherent Performance

Figure 3.8

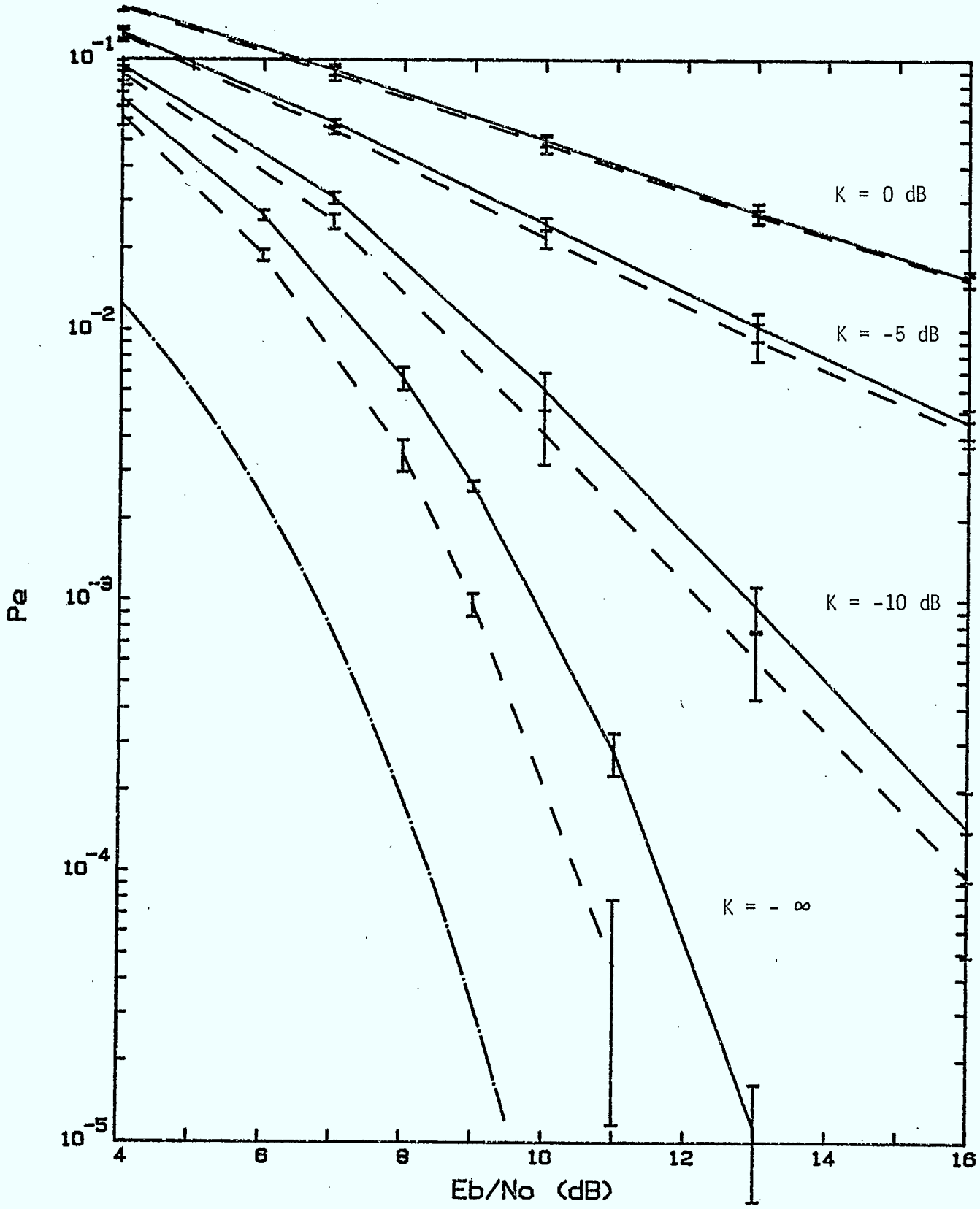

Comparison of conventional and SEC DMSK without nonlinearity

——————— conventional

— — — — SEC

—·—·—·— Ideal Coherent Performance

Figure 3.9

The simulated MSK signal spectrum before and after the nonlinearity, as shown in Figures 3.10 and 3.11, illustrate that the distortion caused by the transmit filter and digital implementation are negligible in terms of the change of sidelobe levels after the nonlinearity.*

*Due to aliasing at the Nyquist frequency, the actual spectrum after the (analog) nonlinearity may be slightly different than that illustrated in Figure 3.11 near the Nyquist frequency. (see Appendix B).

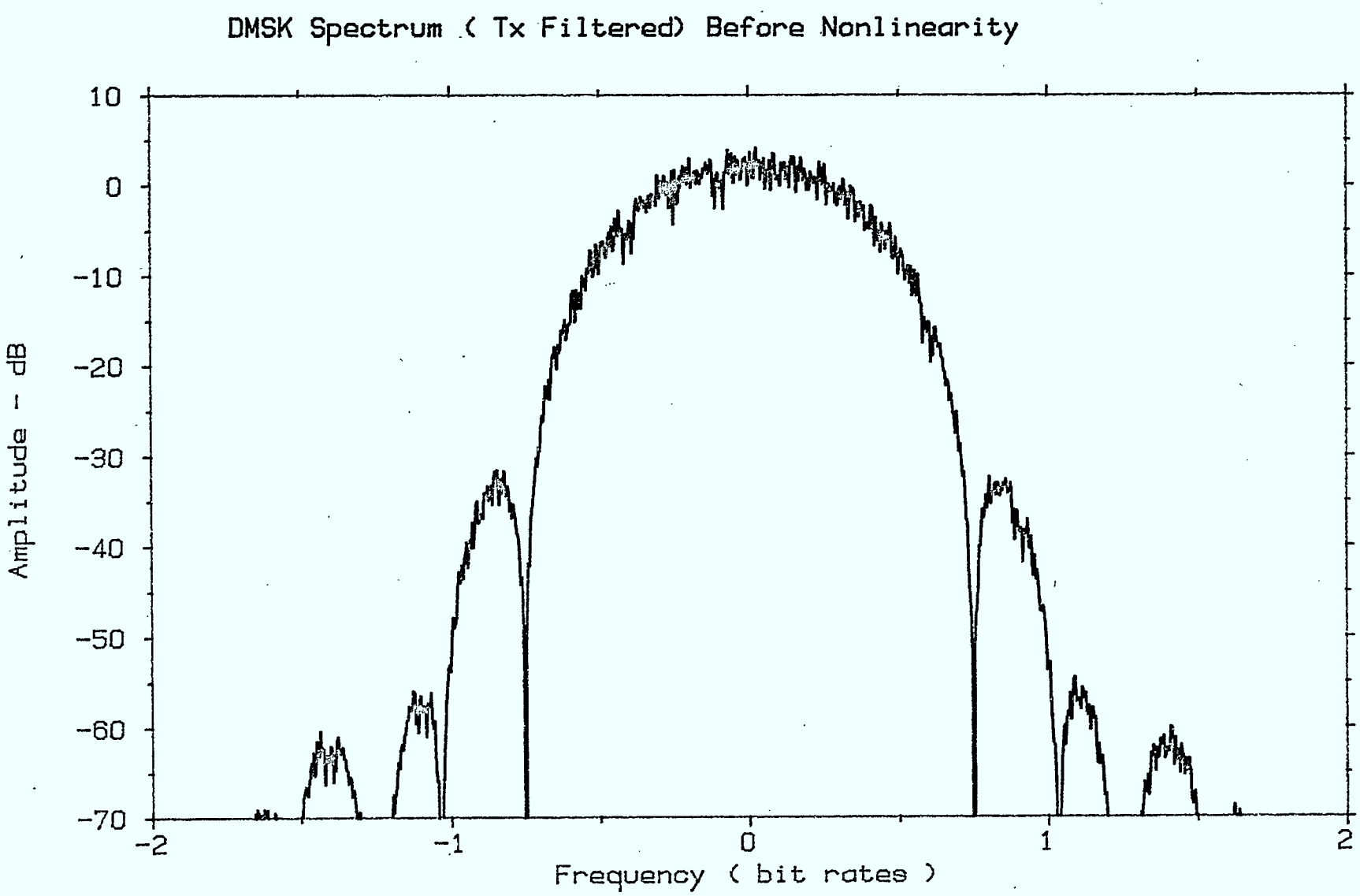
DMSK Spectrum (Tx Filtered) Before Nonlinearity
Amplitude - dB
10
0
-10
-20
-30
-40
-50
-60
-70
-2
-1
0
1
2
Frequency (bit rates)

Figure 3.10

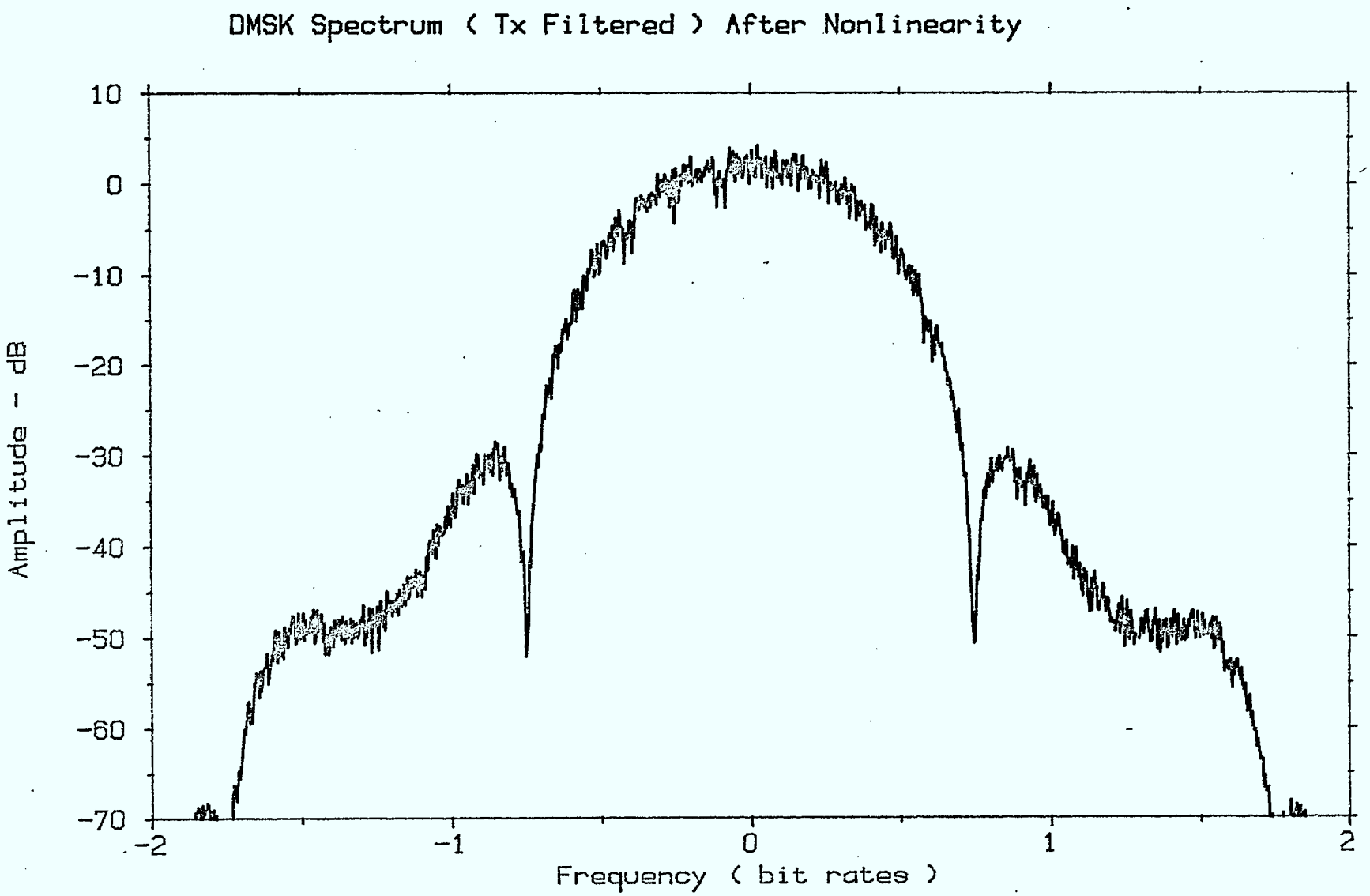
DMSK Spectrum (Tx Filtered) After Nonlinearity
Amplitude - dB
10
0
-10
-20
-30
-40
-50
-60
-70
-2
-1
0
1
2
Frequency (bit rates)

Figure 3.11

4.0 DOQPSK STUDY

This task was to study through simulation the performance of 2.4 kbps differentially detected OQPSK in the channel described in Section 2.0. In fact, DMSK which was described in Section 3.0, is one form of DOQPSK with a particular pulse shape. The DMSK pulse shape results in a constant envelope signal which was shown to result in very little degradation in nonlinear channels. There is, however, a significant degradation due to intersymbol interference.

Alternatively, Nyquist pulse shapes will eliminate the degradation due to intersymbol interference but will cause envelope variations which could degrade performance in nonlinear channels.

4.1 Pulse Shape

The pulse shape suggested for the simulation of DOQPSK was the Nyquist pulse shape corresponding to a 50% raised cosine spectral response with a 3 dB bandwidth of 2400 Hz. To achieve this pulse shape with matched filtering, root raised cosine filters were used for pulse shaping and receive filtering.

In the simulation a 40 point FIR approximation to the root raised cosine pulse shape was used. A comparison of the ideal root raised cosine filter and the approximation is made in Figure 4.1. Note the sidelobes which appear due to the approximation but are not present in the ideal filter.

4.2 DOQPSK Simulation Results

The system described in Section 2.0 was simulated using the DOQPSK modulation strategy and the pulse shape described in 4.1. The results shown in Figure 4.2 are for various

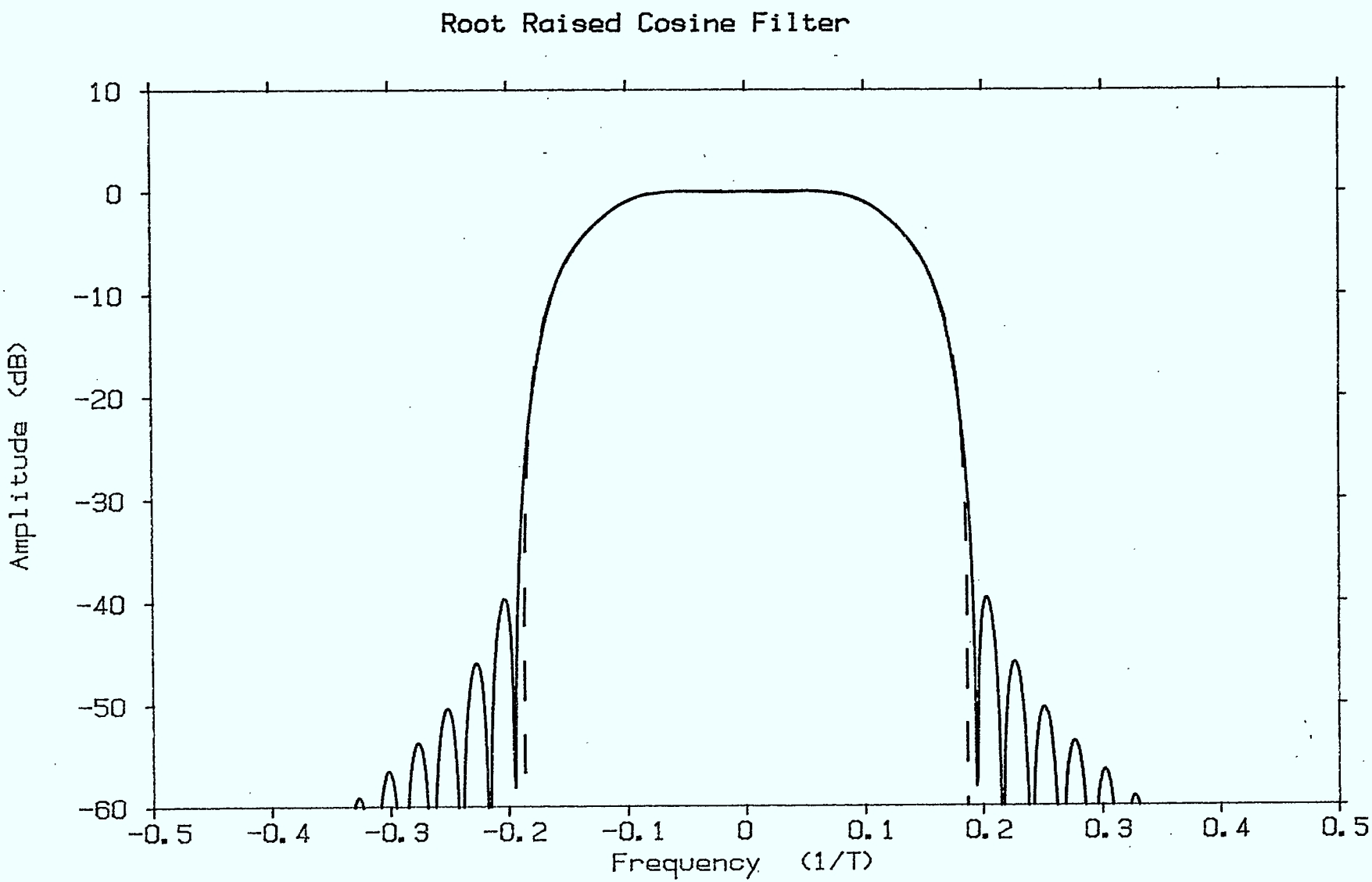

(50% rolloff. B.W. = .25)

Analytic Response ——— ———

40 pt. FIR Approx. ———————

Figure 4.1

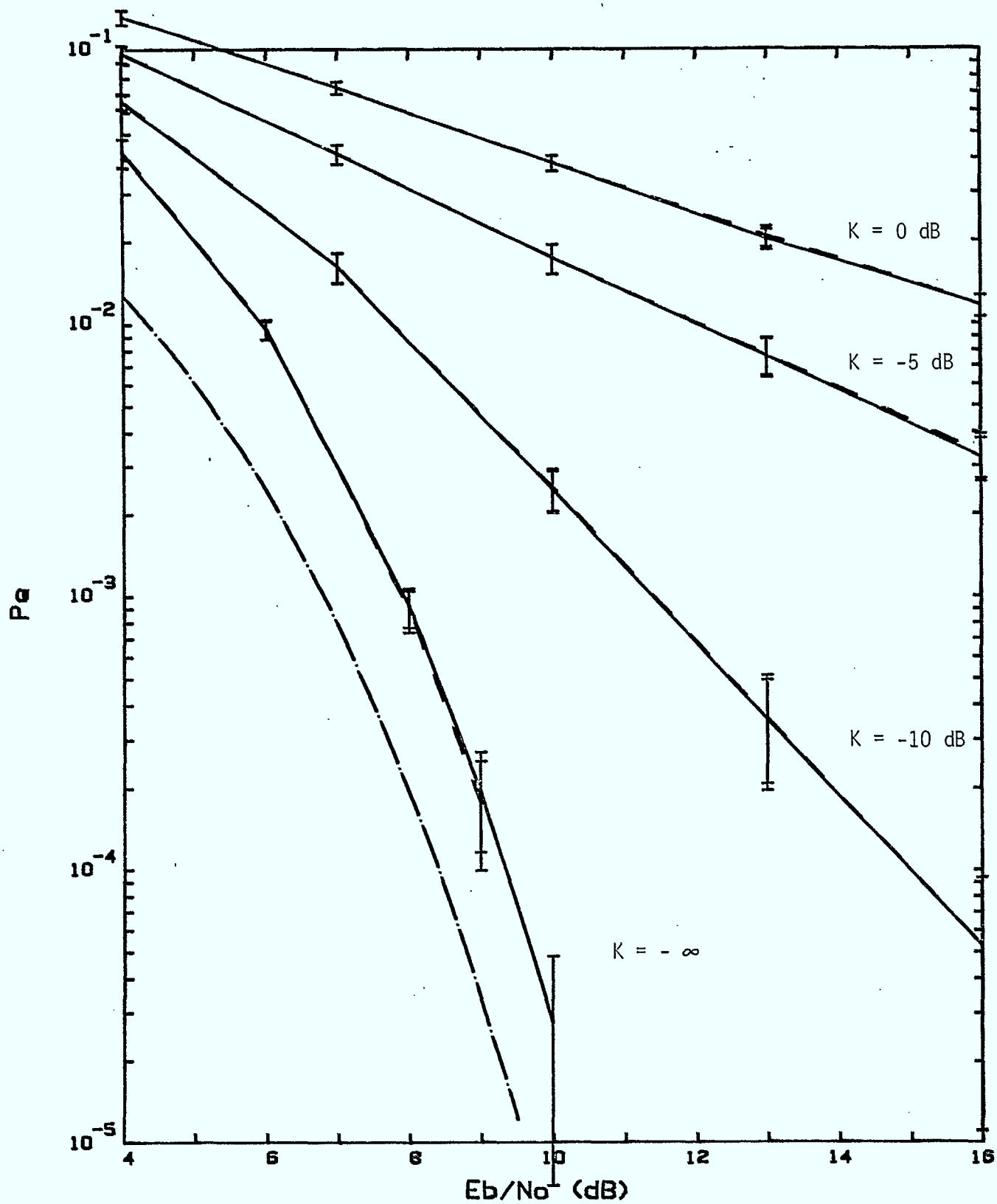

BER Performance of DOQPSK in Rician Channel

——————— without Nonlinearity

— — — — with Nonlinearity

—·—·—·— Ideal Coherent Performance

Figure 4.2

Rician channel fading factors, with and without the nonlinearity present. The most striking feature about these results is the negligible degradation caused by the introduction of the nonlinearity. Although not illustrated here, it was found that the nonlinearity did alter the error process (i.e. the location of the errors) but that the average bit error rate remained virtually unchanged.

This negligible degradation caused by the nonlinearity was found to be quite surprising, and motivated the following investigation into the DOQPSK signal characteristics.

4.2.1 DOQPSK Signalling With A Non-Linearity

The previous results have shown that differential offset QPSK (DOQPSK) signalling with 50% rolloff root raised cosine spectrum shaping is an attractive modulation scheme. The reasons thus far are as follows:

(i) The main lobe bandwidth is 1.5 times the data rate, which is the same as for DMSK.

(ii) Under ideal conditions (AWGN channel) matched filtering at the receiver introduces no intersymbol interference (ISI). Thus the attainable bit error rate (BER) is essentially that of ideal differential detection, which is given by [5]

$$\text{BER} = \frac{1}{2} \exp(-E_b/N_o)$$

This performance is typically 2 dB better than that for DMSK at a BER of 10^{-3}.

(iii) BER performance does not degrade significantly when the signal is passed through a non-linear amplifier at the transmitter.

The above 3 observations clearly seem to indicate that DOQPSK is a better modulation candidate than DMSK. The only potential problem is the amount of sidelobe energy introduced by a non-linearity, as adjacent channel interference must be kept to a minimum.

The amount of spectral distortion introduced by a non-linearity is directly related to the signal's amplitude deviations. A constant envelope signal will experience negligible distortion. This is the case for DMSK (without transmit filtering). The DOQPSK signal format does not yield a constant envelope but the envelope deviations can be quite small. A computer program has been used to evaluate the maximum positive, maximum negative, and rms amplitude deviations for a number of root raised cosine spectrum rolloffs. A 2048 bit PN sequence was used, and thus all possible 11-bit patterns were considered. The results are shown in Figure 4.3. One might of expected that the amplitude deviations would generally decrease with increasing rolloff, but this is not the case. In fact there is a clear minimum for the rms deviation and it occurs for a rolloff of approximately 0.45, which is very close to the rolloff of 0.5 examined in the simulation. Note that the minimum rms deviation is only about 12% which is quite good. Even the maximum positive and negative deviations are no more than about 30% in the same region.

Figures 4.4, 4.5, and 4.6 show the signal power spectrums obtained (one-sided) for a root raised cosine rolloff of

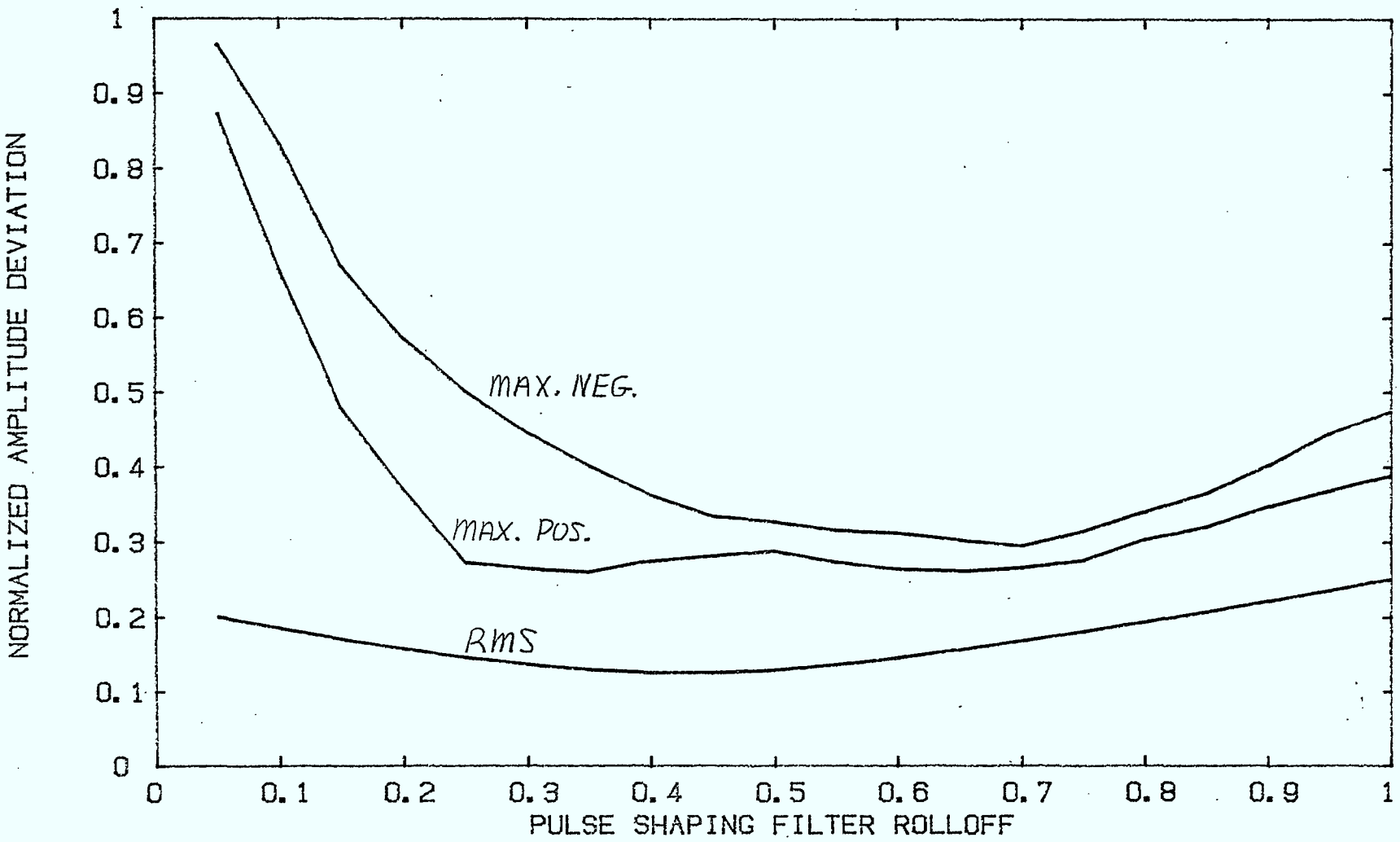

FIGURE 4.3 : RMS AND EXTREME AMPLITUDE DEVIATIONS FOR DOQPSK SIGNALLING WITH ROOT RAISED COSINE SPECTRUM SHAPING

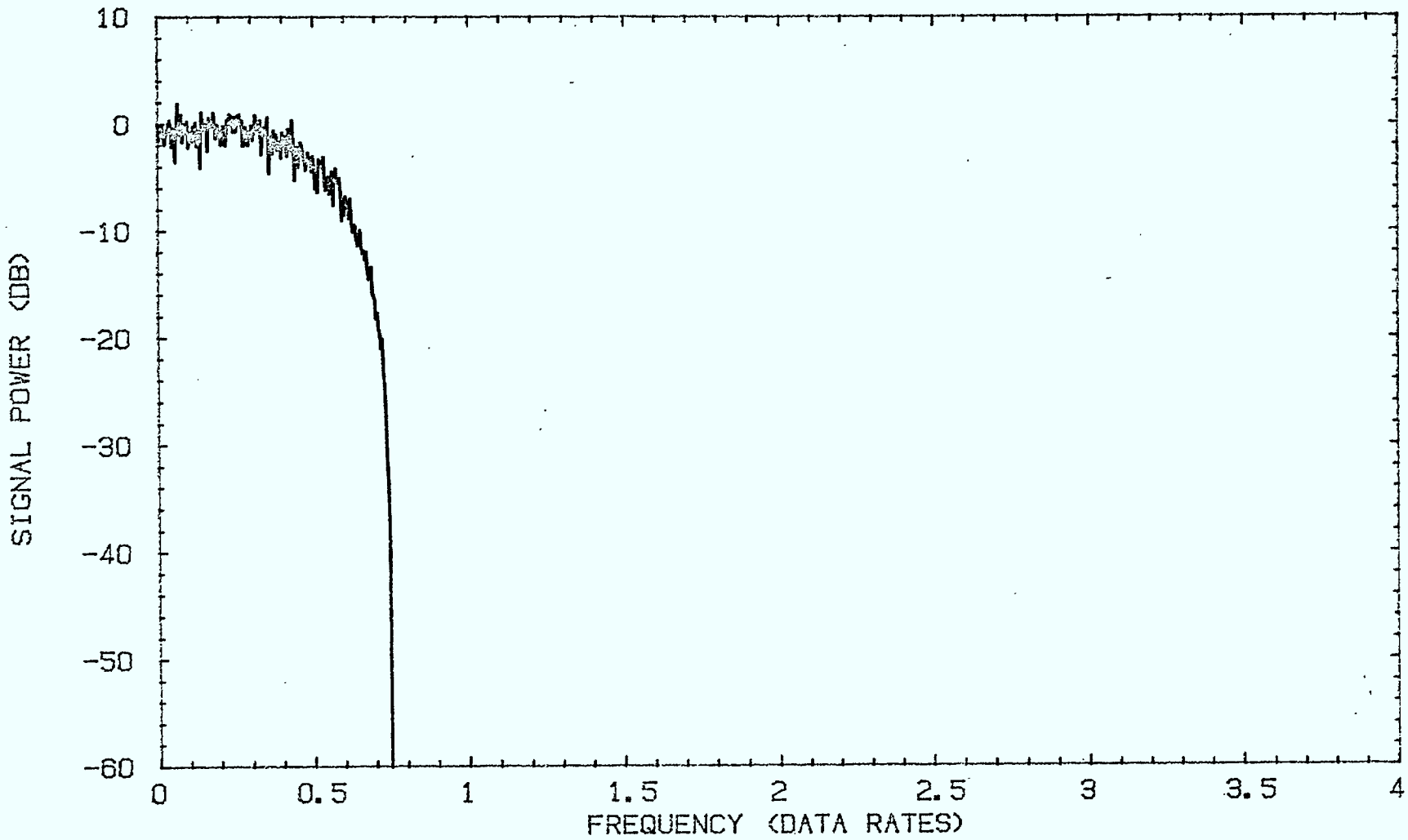

FIGURE 4.4: POWER SPECTRUM OF DOQPSK SIGNAL WITH ROOT RAISED COSINE ROLLOFF OF 0.5 AND NO NON-LINEARITY

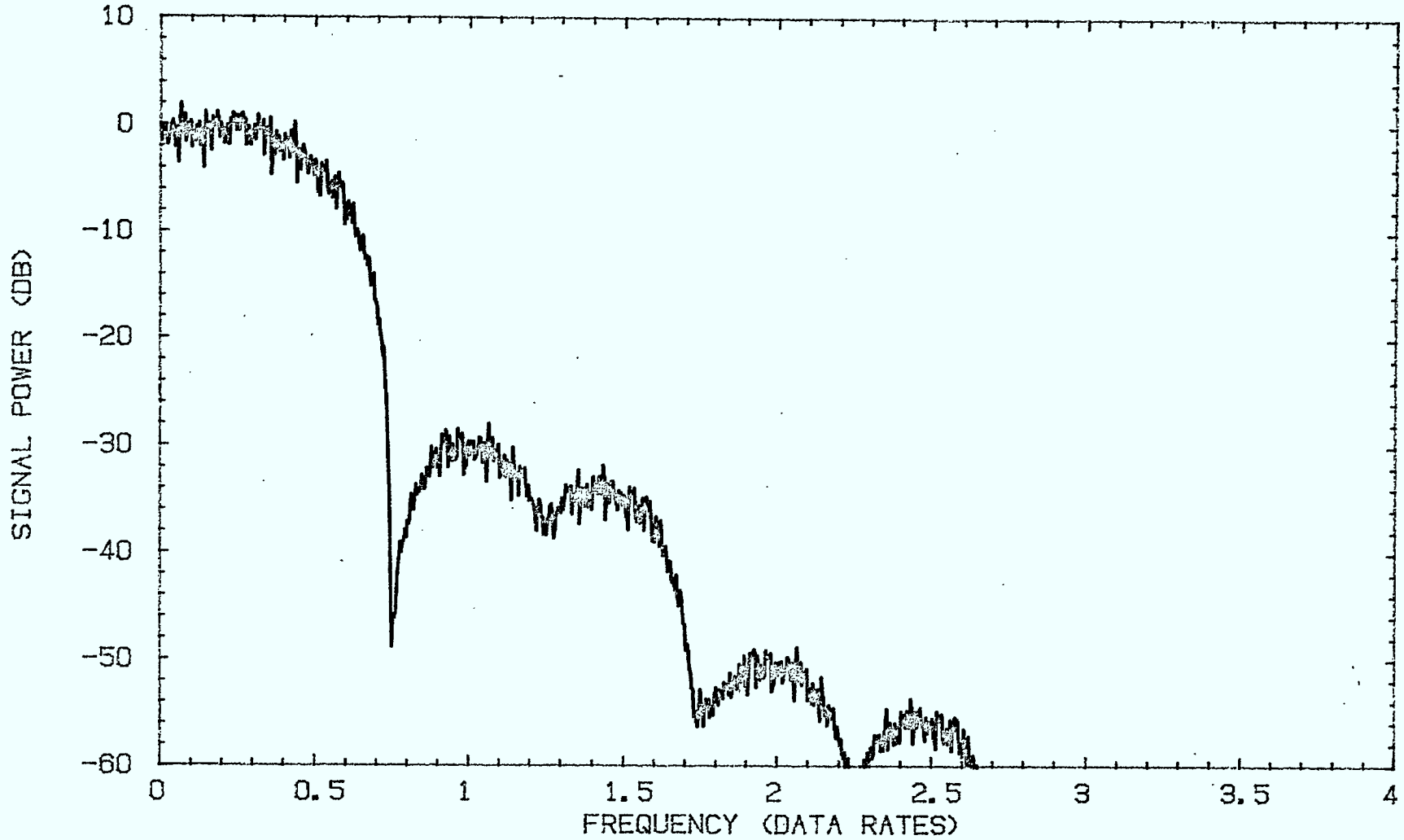

FIGURE 4.5: POWER SPECTRUM OF DOQPSK SIGNAL WITH ROOT RAISED COSINE ROLLOFF OF 0.5 AND NON-LINEARITY

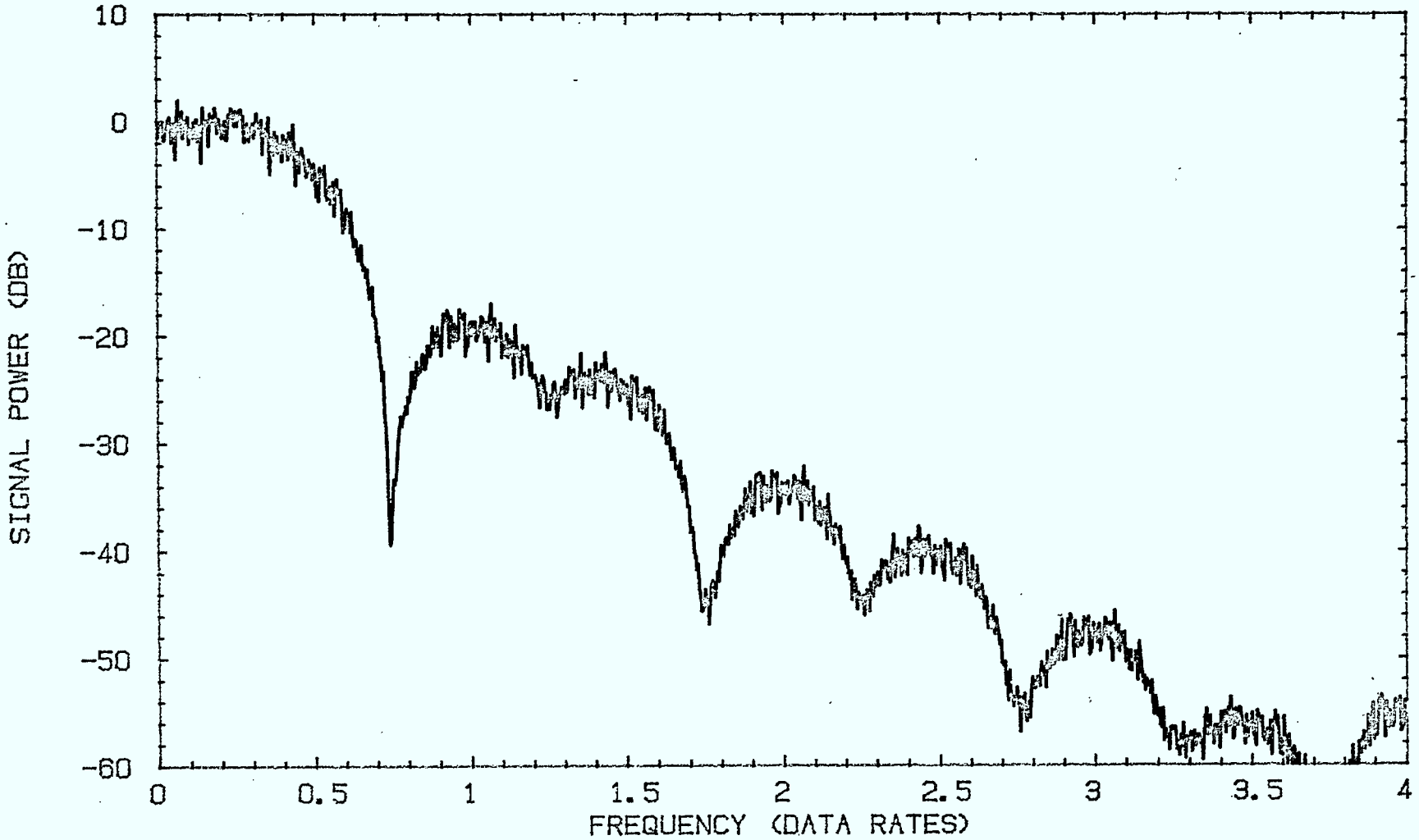

FIGURE 4.6 : POWER SPECTRUM OF DOQPSK SIGNAL WITH ROOT RAISED COSINE ROLLOFF OF 0.5 AND HARD LIMITER

0.5. Figure 4.4 shows the power spectrum before the signal is passed through a non-linearity. As expected the power spectrum is negligible beyond a frequency of 0.75 data rates. Figure 4.5 shows the power spectrum after the signal is passed through the non-linearity specified by the Scientific Authority. The power spectrum is still down 30 dB at a frequency of 1 data rate and is down 50 dB at a frequency of 2 data rates, which is approximately at the centre of the adjacent channel. Note that these sidelobes are well below those of DMSK (with no transmit filtering). As an example, DMSK is only down 36 dB at a frequency of 2 data rates [4]. Figure 4.6 shows the power spectrum after the signal is passed through a hard limiter. Even with a hard limiter the sidelobes are still down 20 dB and 35 dB at frequencies of 1 and 2 data rates respectively, which is about the same as that provided by DMSK.

Figures 4.7, 4.8 and 4.9 show the power spectrums obtained for a root raised cosine rolloff of 0.45. Recall that a rolloff of 0.45 yields the lowest rms amplitude deviation. The sidelobes generated by the non-linearity and hard limiter are typically within 1 dB of those for a rolloff of 0.5.

For comparison purposes, Figures 4.10, 4.11 and 4.12 show the power spectrums obtained for a root raised cosine rolloff of 1.0. Notice that the non-linearity and hard limiter actually narrow the bandwidth of the main lobe significantly. Compared with a rolloff of 0.5 the sidelobe power, after the non-linearity or the hard limiter, is 8 dB higher at a frequency of 2 data rates.

In conclusion DOQPSK signalling with a root raised cosine rolloff of about 0.5 is a very attractive modulation scheme. With the non-linearity specified by the Scientific

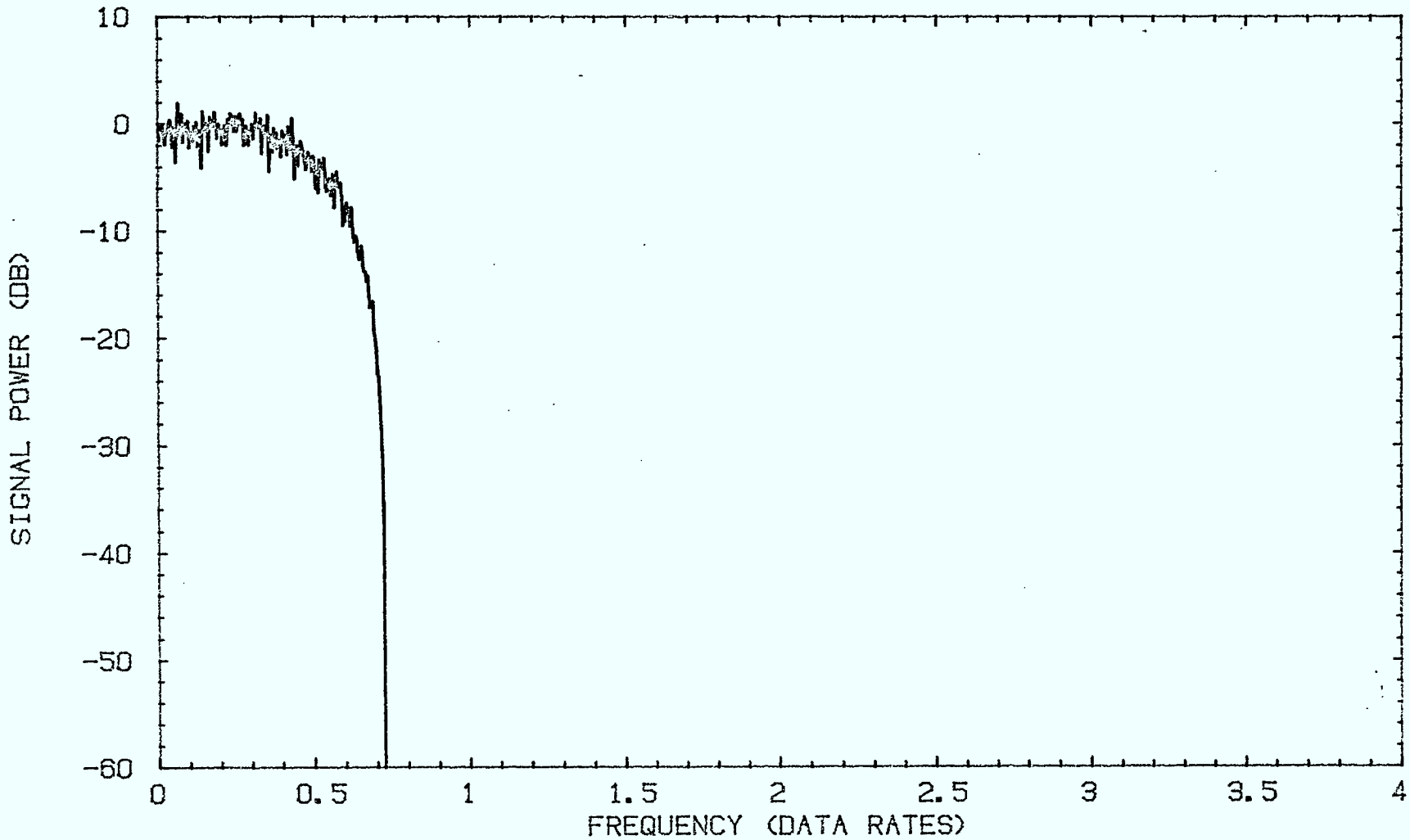

FIGURE 4.7: POWER SPECTRUM OF DOQPSK SIGNAL WITH ROOT RAISED COSINE ROLLOFF OF 0.45 AND NO NON-LINEARITY

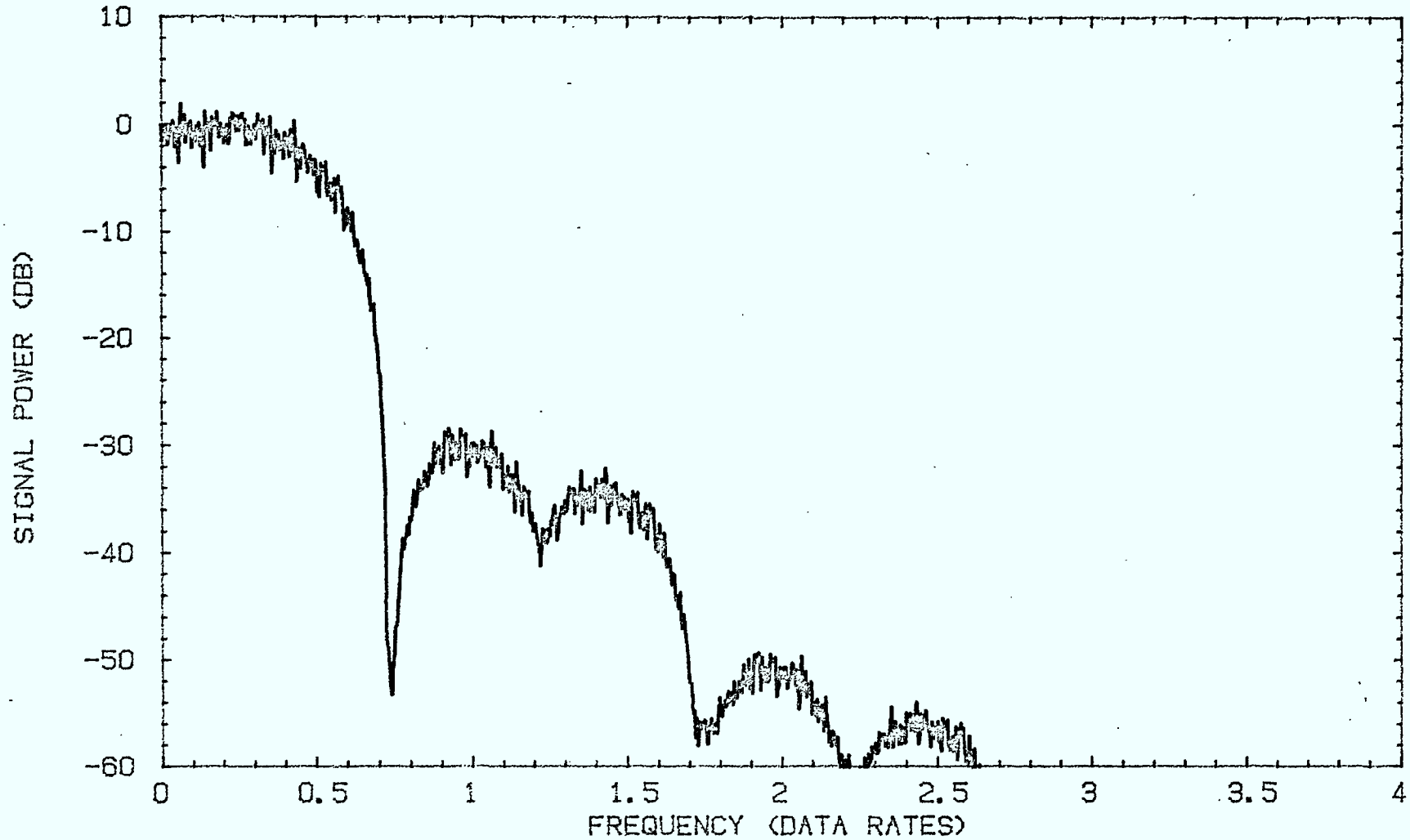

FIGURE 4.8: POWER SPECTRUM OF DOQPSK SIGNAL WITH ROOT RAISED COSINE ROLLOFF OF 0.45 AND NON-LINEARITY

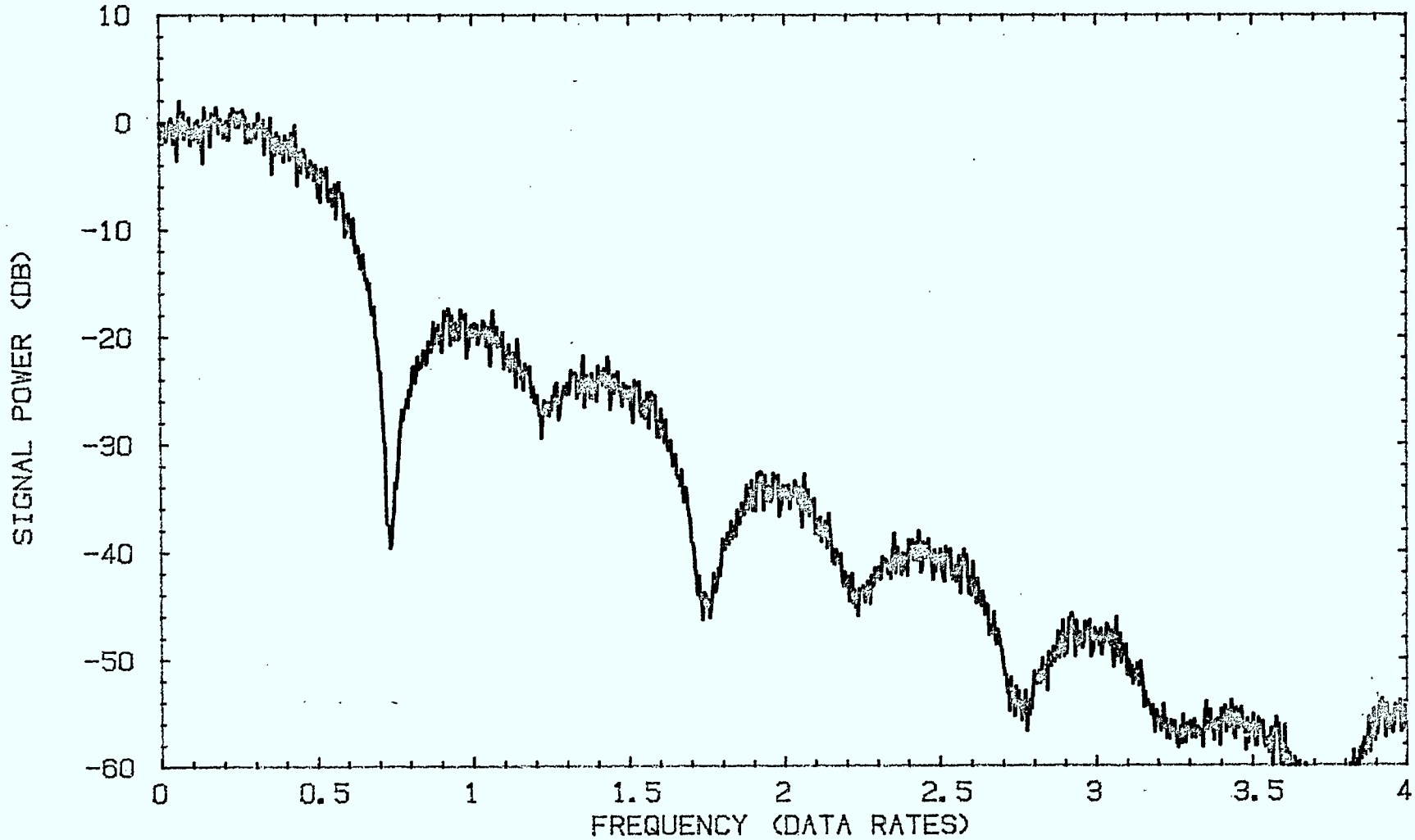

FIGURE 4.9: POWER SPECTRUM OF DOQPSK SIGNAL WITH ROOT RAISED COSINE ROLLOFF OF 0.45 AND HARD LIMITER

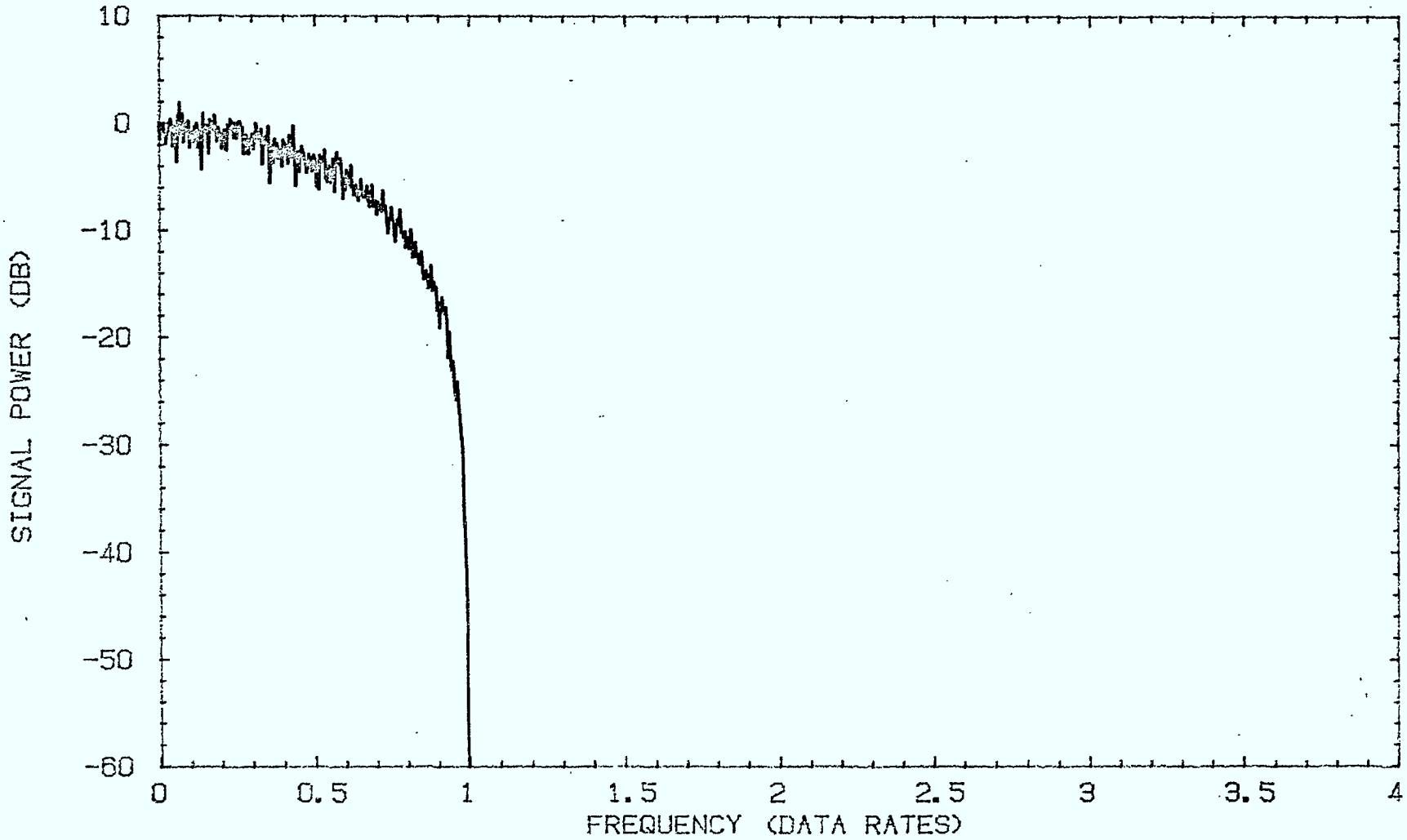

FIGURE 4.10: POWER SPECTRUM OF DOQPSK SIGNAL WITH ROOT RAISED COSINE ROLLOFF OF 1.0 AND NO NON-LINEARITY

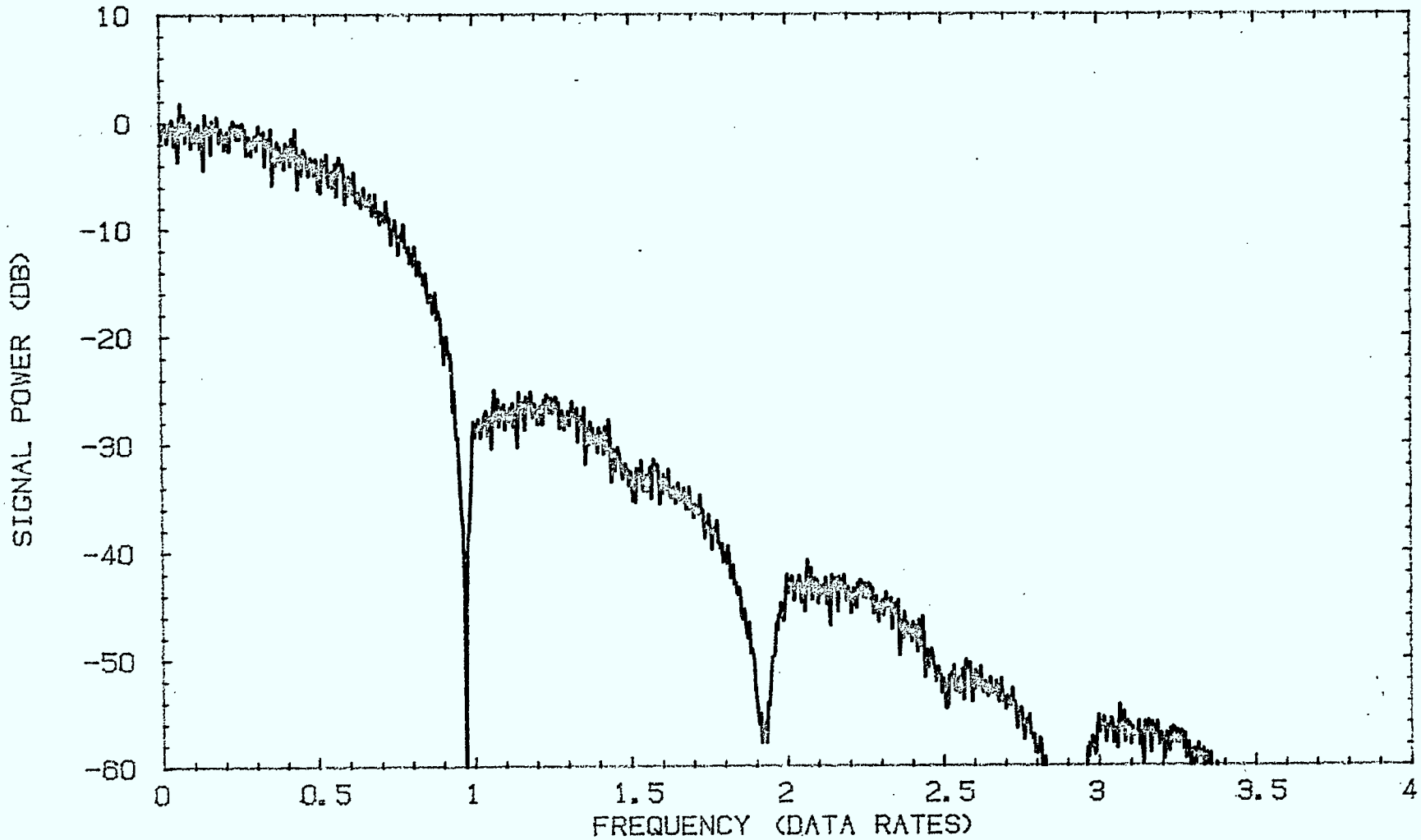

FIGURE 4.11: POWER SPECTRUM OF DOQPSK SIGNAL WITH ROOT RAISED COSINE ROLLOFF OF 1.0 AND NON-LINEARITY

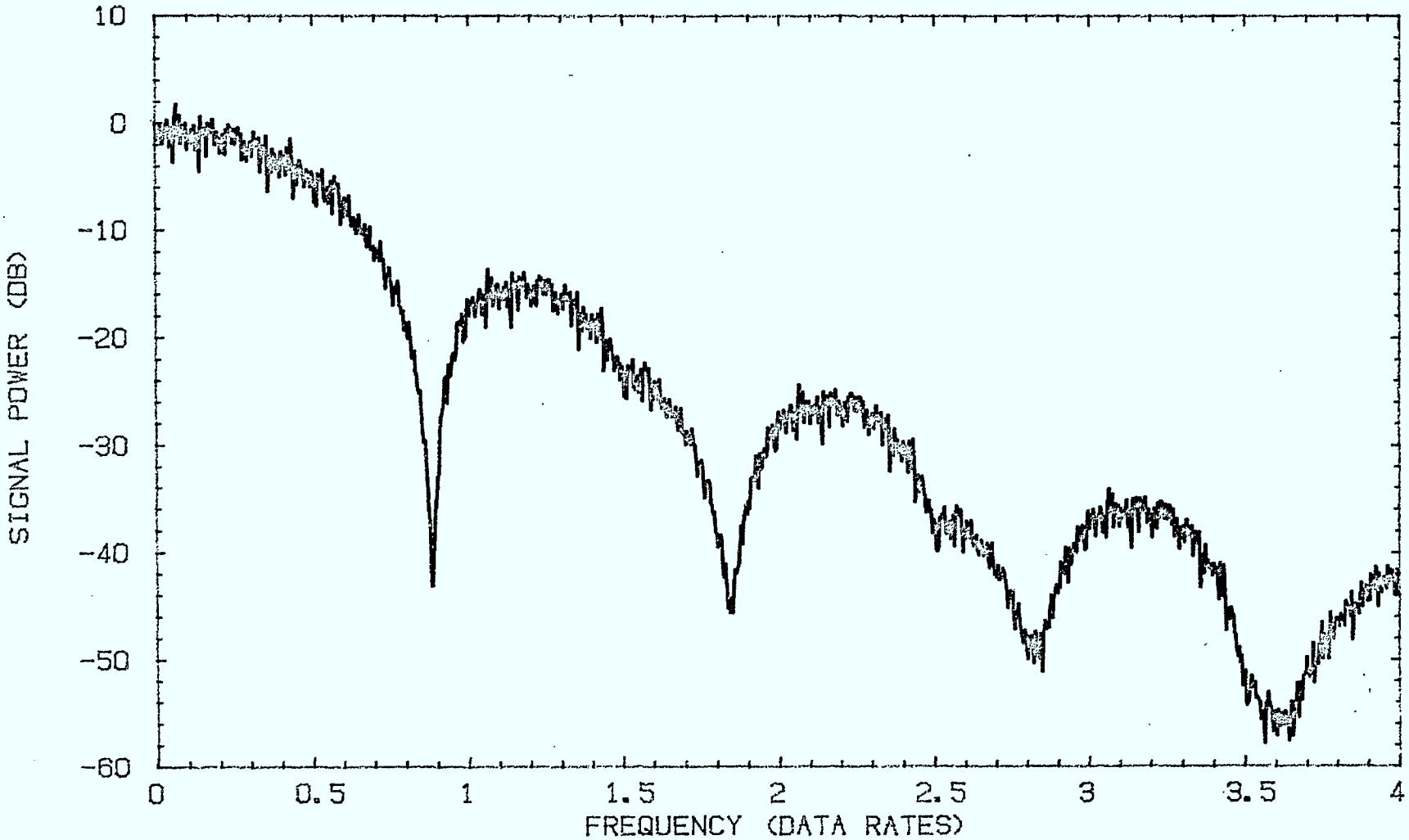

FIGURE 4.12: POWER SPECTRUM OF DOQPSK SIGNAL WITH ROOT RAISED COSINE ROLLOFF OF 1.0 AND HARD LIMITER

Authority the BER performance can be 2 dB better than DMSK, and adjacent channel interference at a centre frequency offset of 2 data rates is 14 dB lower than DMSK (without transmit filtering). In fact, if the adjacent channel interference is acceptable, it may even be desirable to hard limit the DOQPSK signal before the transmit amplifier to minimize any phase distortion which might be introduced by a practical non-linear amplifier. Following the hard-limiter by a bandlimiting filter (e.g. the tx filter used in the previous chapter) that leaves the main lobe unaltered but reduces adjacent channel interference would also be useful, and is recommended as an area for further investigation.

4.2.2 Performance of DOQPSK With Hard Limiting Nonlinearity

The degradation caused by the nonlinearity when DOQPSK modulation was used was expected to be significantly worse than that observed with DMSK or even filtered DMSK because of the larger amplitude fluctuations.

However, the degradation observed was barely 0.1 dB which was quite surprising. The investigation of the DOQPSK waveform in the previous section showed that the rms amplitude fluctuation is approximately 12%, and the peak variation is approximately 30% for a 50% root raised cosine pulse shape. The relatively small rms amplitude fluctuation is likely the reason for the small degradation caused by the nonlinearity.

The results with DOQPSK concerning the effects of the nonlinearity led to the investigation of the performance degradation caused by a hard limiter. A comparison of the BER performance of DOQPSK with and without a hard limiter

is shown in Figure 4.13. As can be seen the degradation caused by the nonlinearity is no more than 0.2 dB over the bit error rates tested.

This insignificant degradation seems incredible but there is a price to pay. As shown in Figure 4.6, with the hard limiter the sidelobes are raised significantly. In fact the adjacent sidelobes are only about 20 dB below the main lobe which may be unacceptable in a practical situation.

4.2.3 Comparison To Theoretical Performance

Appendix C derives the theoretically optimum performance of a signalling scheme which uses matched filtering and differential detection in a Rician fading channel for the case where the fading bandwidth is small (approaches 0) relative to the data rate.

The DOQPSK system under study, which uses a Nyquist pulse shape and has a data rate of 2400 bps relative to a fading bandwidth of 100 Hz, closely approximates the theoretical case studied. Figure 4.14 shows a comparison of theoretical performance and simulated performance on a Rician fading channel for various K factors. (Note that the E_b used in this figure has been adjusted from that derived in Appendix C, to include both direct path and fading path energy). In the case of no fading ($K = -\infty$) and the case of a Rician channel factor of K = -10 dB, the simulated system performs very close to the optimum predicted by theory. With larger fading factors, there is a slight degradation from ideal. This could be expected because with higher fading factors the assumption of constant phase between adjacent bits, used in deriving the theoretical bound, is more likely to be violated.

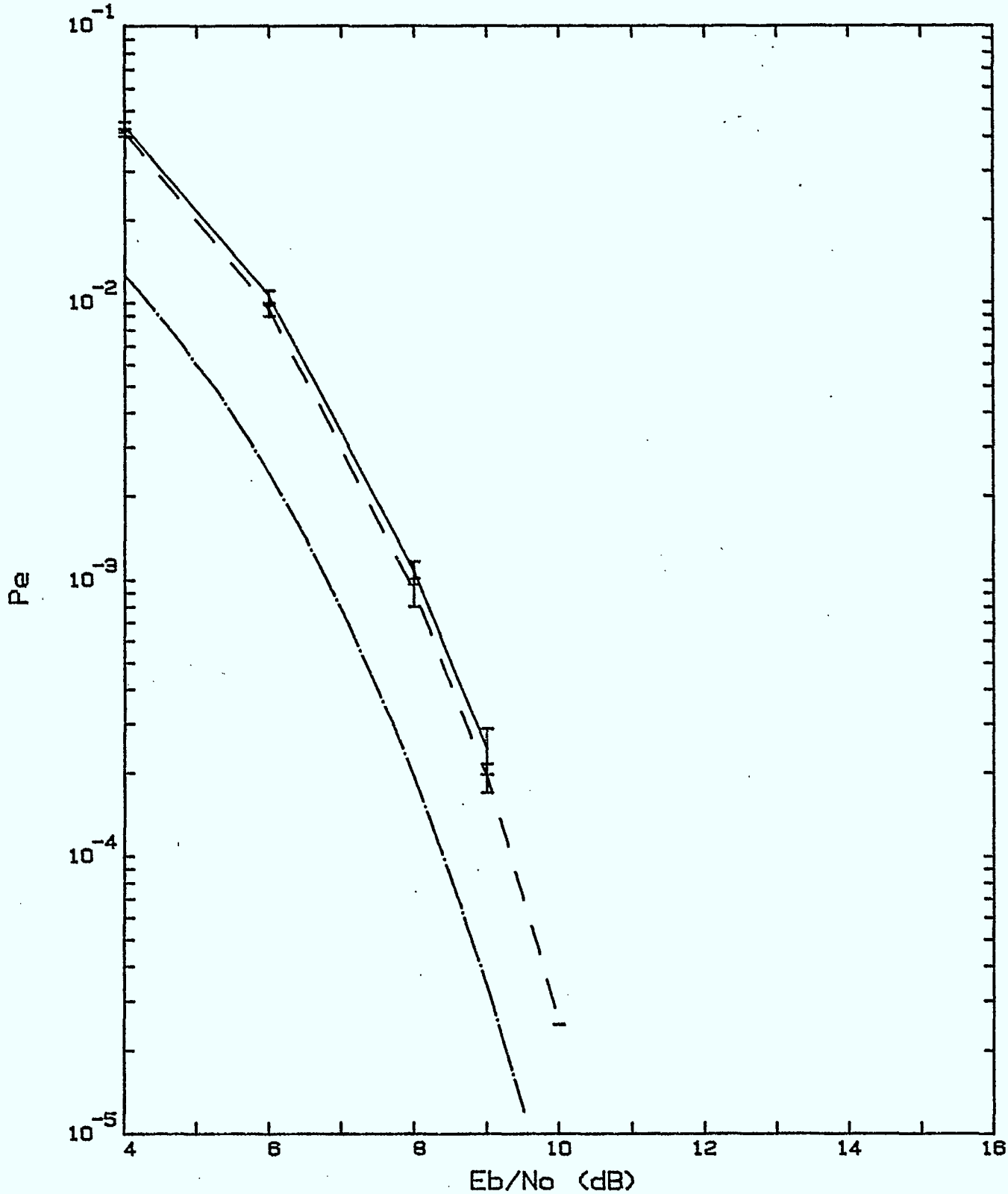

Comparison of Differential OQPSK with hard limiter

——————— Hard Limiter

— — — — No Hard Limiter

—·—·—·— Ideal Coherent Performance

Figure 4.13

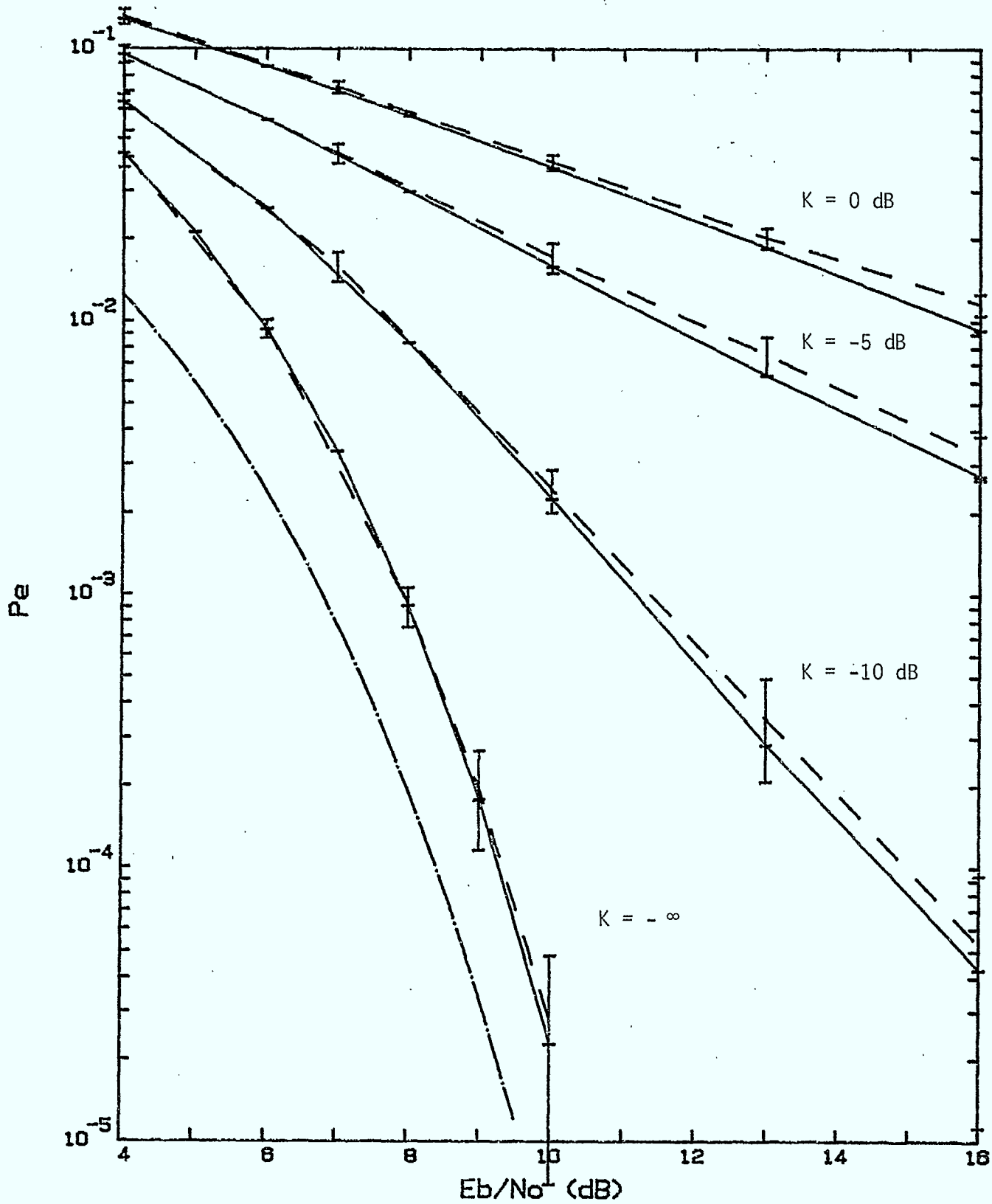

Comparison of Theortical and Simulated DOQPSK BER Performance

——————— Theoretical

— — — — Simulated

—·—·—·— Ideal Coherent Performance

Figure 4.14

On the whole, DOQPSK modulation should provide near optimum performance over a slowly fading channel using differential detection.

4.2.4 Performance of DOQPSK With SEC

The performance of the DOQPSK signalling scheme can be enhanced by using a single error correction (SEC) circuit; the same as that used in the DMSK case, and described in Section 2.8.

The simulated bit error rate performance of DOQPSK with SEC is shown in Figure 4.15. Again, there is virtually no degradation due to the nonlinearity but this might have been expected from the previous results. Figure 4.16 compares the performance with SEC to that without SEC (no-nonlinearity). It is observed that there is an approximate 0.5 dB gain for smaller Rician channel factors ($K=-\infty$ and $K=-10$ dB), but for stronger fading channels there is virtually no gain. This type of behaviour is to be expected because with deep fading bit errors will tend to occur in bursts, a situation for which the SEC technique, which can correct only isolated errors, will offer little advantage.

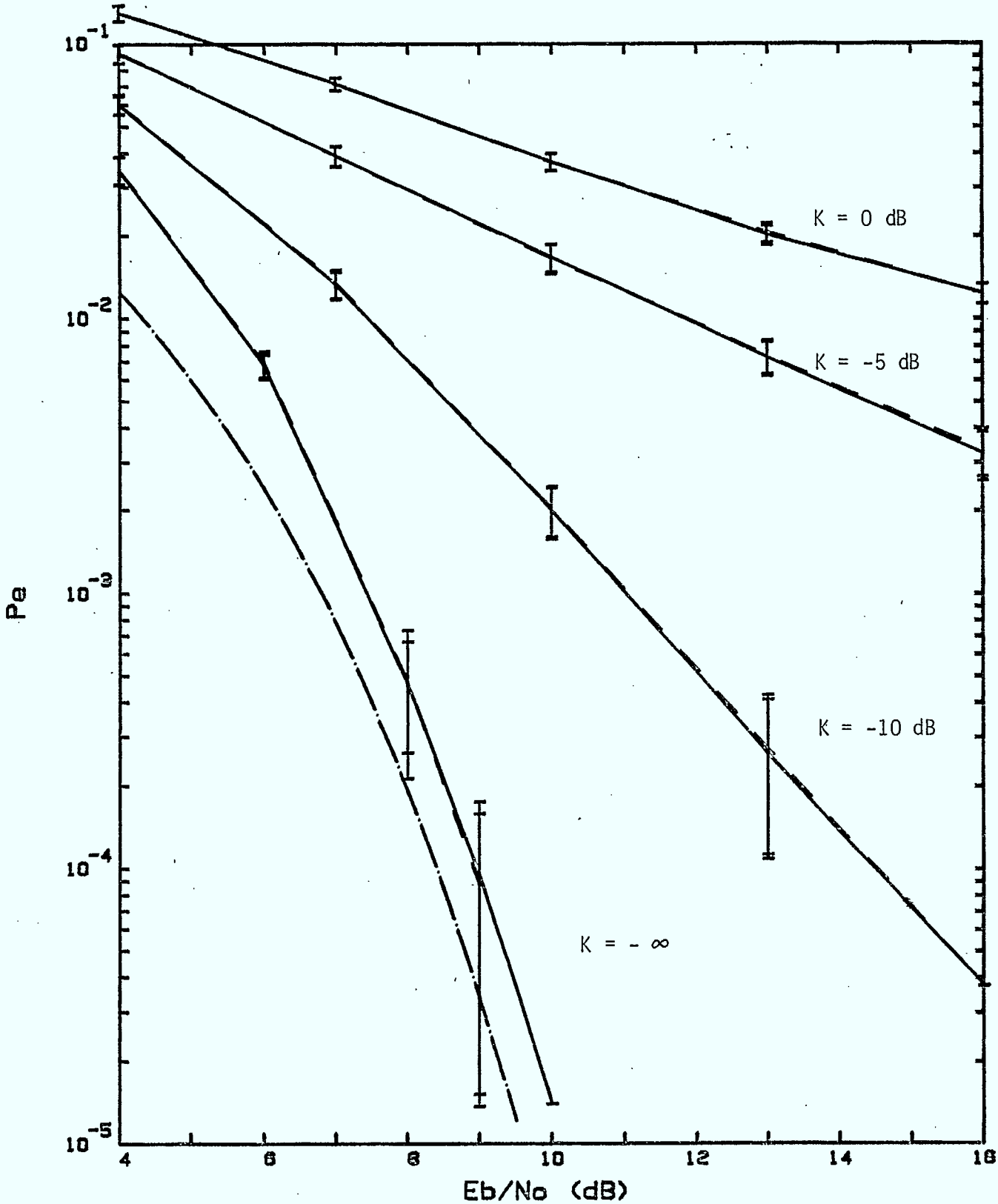

SEC Performance of DOQPSK in Rician Channel

——————— without Nonlinearity

— — — — with Nonlinearity

—·—·— Ideal Coherent Performance

Figure 4.15

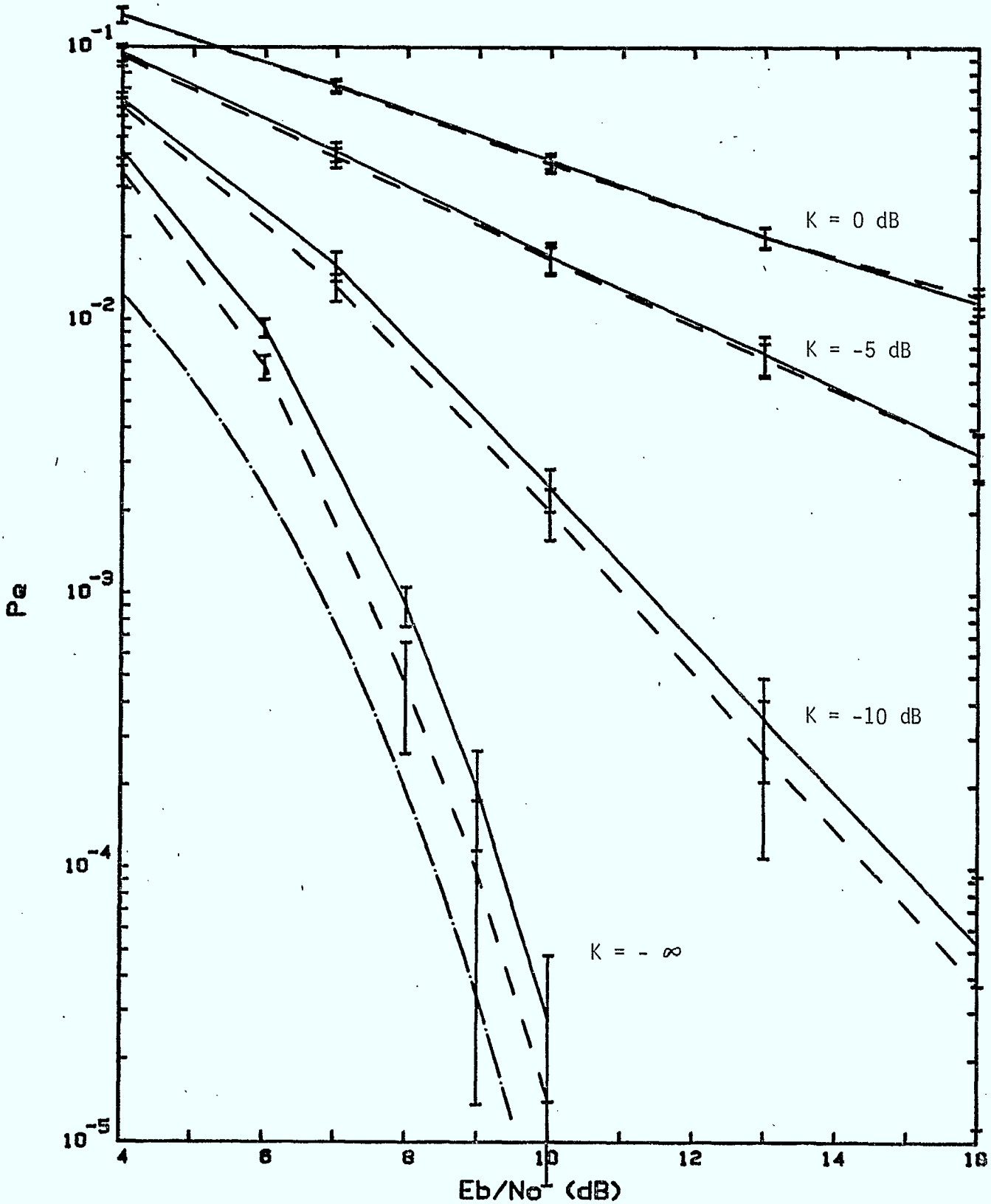

Comparison of DOQPSK BER Performance with and without SEC

——————— **without SEC**

— — — — **with SEC**

—·—·— **Ideal Coherent Performance**

Figure 4.16

5.0 COHERENT BPSK WITH TTIB ACSSB MODEM

As outlined in [8], it may be advantageous to place the data modem in series with an amplitude companded single-sideband (ACSSB) modem, thereby taking advantage of the ACSSB processing. Transparent tone-in-band (TTIB) ACSSB is the approach under consideration. Since an ACSSB modem with TTIB can be used to perform unambiguous carrier recovery [9], coherent modulation strategies are thought to be most appropriate.

5.1 Analysis of the TTIB ACSSB Modem

Figures 5.1 and 5.2 show block diagrams of the complex baseband equivalent modulator and demodulator respectively. The signal spectrums generated at different locations in the system are illustrated in Figure 5.3. These locations (labelled (a) through (j)) are marked on Figures 5.1 and 5.2. The pilot tone is placed at DC and is used for AGC and mitigating the fading perturbations (amplitude and phase) of the channel. The 300 Hz real tone is required for coherent recombining of the subbands at the receiver. Note that the notch or subband spread is 1200 Hz and thus the unspread data signal spectrum must be restricted to approximately 4800-1200 = 3600 Hz. Thus for BPSK and a data rate of 2.4 kbps the spectrum roll-off must be less than or equal to 50%. As agreed to with the Scientific Authority, a 20% root raised cosine spectrum satisfying Nyquist first criterion with matched filtering was used to generate the pulse shape.

The following subsections address some of the modem's components in more detail.

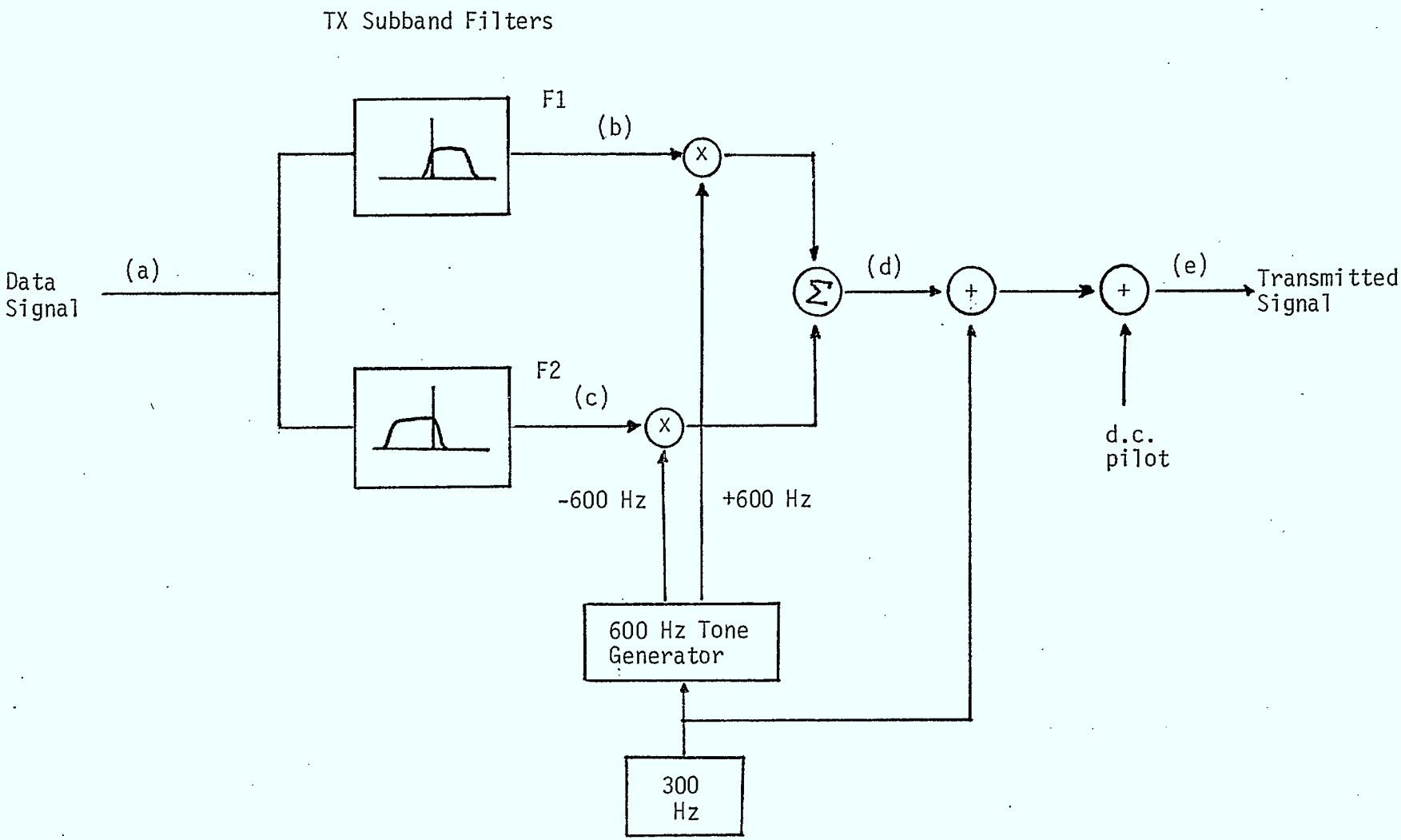

Figure 5.1 Block Diagram of TTIB Modulator

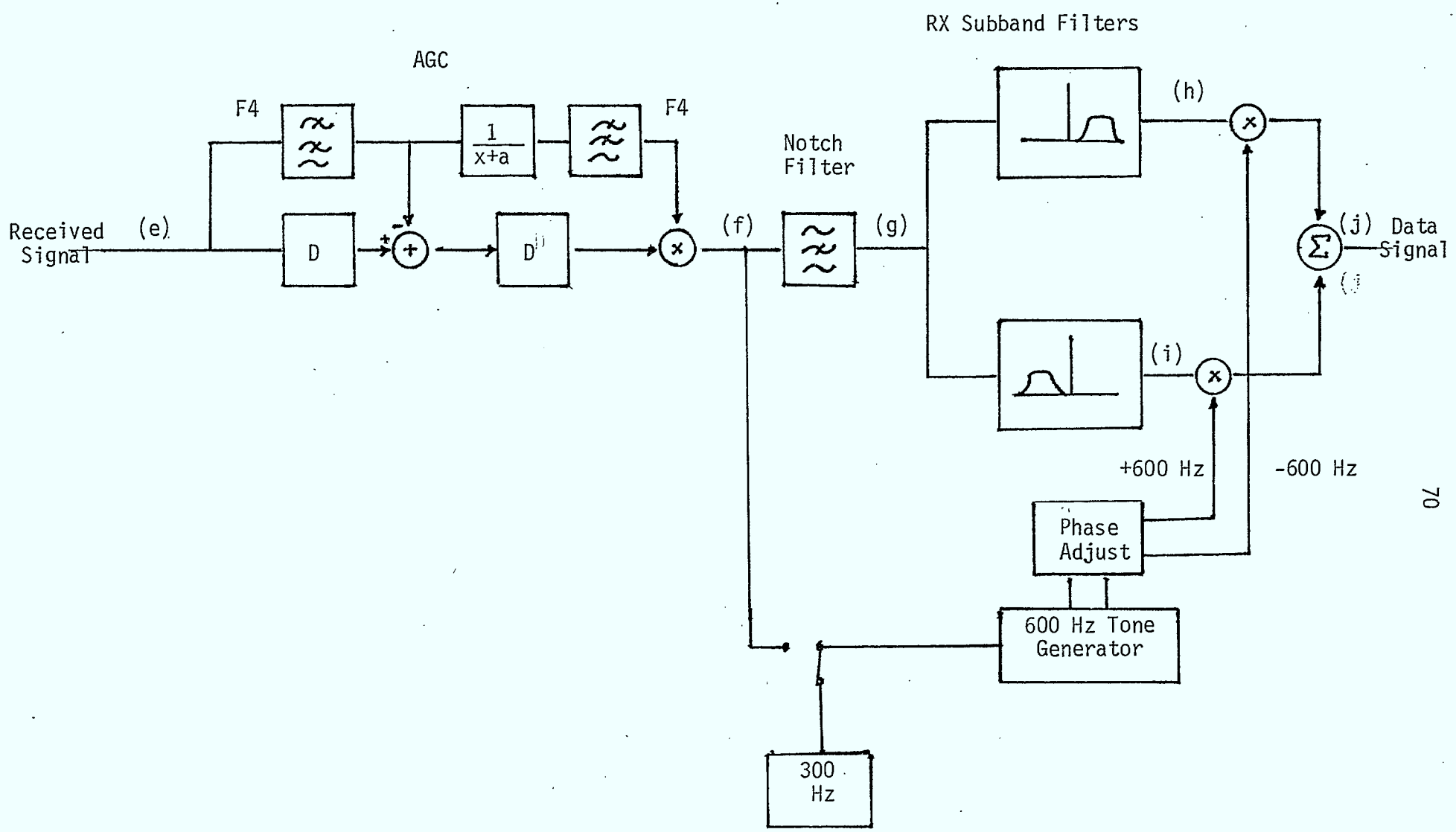

Figure 5.2. Block Diagram of TTIB Demodulator.

Location	Description	Spectrum
(a)	Modulator: input data signal	-2400 0 2400
(b)	upper subband	0 2400
(c)	lower subband	-2400 0
(d)	spread subbands	-2400 -600 0 600 2400
(e)	+ DC pilot+300Hz tone	1 ¼ ¼ -2400 -300 0 300 2400
(f)	Demodulator pilot & fading removed	-2400 0 2400
(g)	300Hz tone removed	-2400 0 2400
(h)	upper subband	0 2400
(i)	lower subband	-2400 0
(j)	coherently recombined subbands	-2400 0 2400

Figure 5.3 : Signal Spectrum for TTIB ACSSB Modem

5.1.1 Delay Requirements for Coherent Subband Recombining

In order for the two subbands to be coherently recombined at the output of the demodulator, certain restrictions must be placed on the implementation delays of the various filters in the modem. The following analysis determines these restrictions.

Let the signal at point (a) at the input to the modulator be modelled as

$$s_a(t) = s_+(t) + s_-(t) \tag{5.1}$$

where $s_+(t)$ and $s_-(t)$ correspond to the upper and lower sideband contributions respectively. Then the signals at points (b) and (c) are just

$$s_b(t) = s_+(t-D_1) \tag{5.2}$$

$$s_c(t) = s_-(t-D_1) \tag{5.3}$$

where D_1 is the implementation delay of the subband filter(s). If the implementation of the second branch is as described in [8] then this delay must be inserted in the second branch to match the delay of the subband filter in the first branch. At this point it suffices to define the complex multiplier signals as

$$e_+(t) = \exp[+j2\pi f_o t + j\theta] \tag{5.4}$$

$$e_-(t) = \exp[-j2\pi f_o t - j\theta] \tag{5.5}$$

Assuming that the complex bandpass filters (BPF's) used to extract the above waveforms are ideal, these waveforms must be the complex conjugate of each other since they are obtained by filtering off the positive and negative

spectral components respectively of a real 300 Hz reference. The value of f_o is 600 Hz in the above expressions and θ is an arbitrary phase shift. It is not necessary to include the delays of the filters used to generate these complex multipliers since they are generated in exactly the same manner at the demodulator. The signal at point (d) is then given by

$$s_d(t) = s_b(t)\ e_+(t) + s_c(t)\ e_-(t) \qquad (5.6)$$

Note that the 300 Hz reference and DC pilot tones are added and transmitted with the signal, without delay.

The front end of the demodulator, from point (e) to point (f), is assumed to remove the DC component, and the amplitude and phase variations introduced by the fading channel. Again, the implementation delay of the low-pass filter(s) must be incorporated into the lower branch of the demodulator front-end. If D_2 is the total delay introduced by the channel and the demodulator front-end, and we assume that the demodulator front-end works ideally, then the effect is just to delay the remaining signal components at point (f) by D_2. In particular the real 300 Hz reference tone is delayed by D_2. Since the generation of the complex multiplier signals, from the 300 Hz reference, is performed exactly the same in the modulator and demodulator, the only effect is to introduce a delay of D_2 in the complex multipliers of the demodulator. Thus the complex multipliers in the demodulator are given by $e_+(t-D_2)$ and $e_-(t-D_2)$. If the delay of the 2 filters between points (f) and (h) is D_3, and the appropriate delay is introduced in the corresponding lower branch, then the signals at points (h) and (i) are given by

$$s_h(t) = s_b(t-D_2-D_3)\ e_+(t-D_2-D_3) \tag{5.7}$$

$$s_i(t) = s_c(t-D_2-D_3)\ e_-(t-D_2-D_3) \tag{5.8}$$

and the output signal at point (j) is given by

$$\begin{aligned} s_j(t) &= s_h(t)e_-(t-D_2)+s_i(t)e_+(t-D_2) \\ &= s_+(t-D_1-D_2-D_3)\ \exp(-j2\pi f_o D_3) \\ &\quad + s_-(t-D_1-D_2-D_3)\ \exp(+j2\pi f_o D_3) \end{aligned} \tag{5.9}$$

Output signal $s_j(t)$ can not represent the coherently recombined subbands unless $f_o D_3=k$, where k is an integer.* With f_o =600 Hz, and a sampled signal format with 9600 samples per second, this implies that D_3 must be a multiple of (9600/600) = 16 sample periods. Recall that D_3 is the combined implementation delay of both the notch filter and a subband filter in the demodulator. Note that the other filter delays in the modulator and demodulator only affect the total delay through the system and not whether the subbands are coherently recombined or not.

If D_3 is not a multiple of 16 sample periods then there are several possible solutions. One solution is to up D_3 to the nearest multiple of 16 sample periods. This is easy to do if D_3 is already an integer number of sample periods. This is not the recommended approach, however, as it unnecessarily ups the total delay through the system. A better approach would be to simply rotate the subband signals by the known phase error, that is multiply the positive and negative subband signals by the constants

*Actually $f_o D_3$ = k/2, k an integer, can also be used if a factor of -1 is allowed. This is easily handled by rotating $s_j(t)$ by 180°, that is multiplying by -1 at the output.

$\exp(+j2\pi f_o D_3)$ and $\exp(-j2\pi f_o D_3)$ respectively. This approach has the added advantage that it can handle delays which are not multiples of the sampling period. This still might not be the best approach however, as it may be desirable to have delay D_3 the same as the delay required to generate the complex multipliers, which we will denote as delay D_4. To see why this might be desirable, suppose that the signal fades to a negligible level for a short period of time. If delays D_3 and D_4 are different, then the severely corrupted subbands and severely corrupted complex multiplier signals will affect the output signal at different times. The result is that the output signal is corrupted for a longer period than the fade duration. Forcing $D_3 = D_4$ should minimize the length of time the signal is corrupted at the output. Assuming D_3 is lengthened to accommodate this last requirement, the phase correction terms are still calculated in the same way, using the new value of D_3.

Another reason for matching delays D_3 and D_4 (if D_4 is longer) is that in the case of bursty data transmission, the initial bits of each message could be severely corrupted by the lack of a good estimate of the subcarriers.

5.1.2 Ideal Subband Filters

Subband filters are required in both the modulator and demodulator to separate the upper and lower frequency subbands. As a minimum these filters must have approximately linear phase to minimize the signal distortion at the demodulator output. An FIR implementation (or equivalent) will satisfy this requirement. Other characteristics are also desirable in order to minimize the signal distortion and noise power spectral density in the overlap region.

An ideal type of subband filter is one with a Nyquist roll-off, such as a square-root raised cosine roll-off, in the overlap region with the 3 dB point at the nominal separation point. In the modulator the 3 dB points should be at 0 Hz, and in the demodulator the 3 dB points should be at ±600 Hz. Coherent reconstruction with such filters will keep the signal corruption to a minimum in the overlap region. Other benefits are that the output noise power spectral density is not enhanced in the overlap region and the notch filter is no longer necessary in the demodulator.

Figure 5.4 illustrates the desired characteristics of these ideal subband filters. With a 20% roll-off the overlap region in the modulator is ±180 Hz. In the demodulator this leaves a 120 Hz guard-band between the 300 Hz pilot tone and the signal spectrum. The 3 dB bandwidth of all the subband filters is 1800 Hz, which ensures that the transmitted signal spectrum does not exceed the 5 kHz channel spacing. Additional matched filtering should be performed on the demodulated signal when the ACSSB modem is used with digital data.

5.2 Implementation of TTIB ACSSB Modem

5.2.1 ACSSB Modulator

In Figure 5.1, filters F1 and F2 are referred to as the transmit subband filters and are used to split the data signal into upper and lower subbands with some overlap.

The two filters, F1 and F2, represent the same filter except shifted in frequency. In the initial implementation F1 and F2, were chosen to be 50 point FIR approximations to a 20% root raised cosine spectrum. This type of spectrum

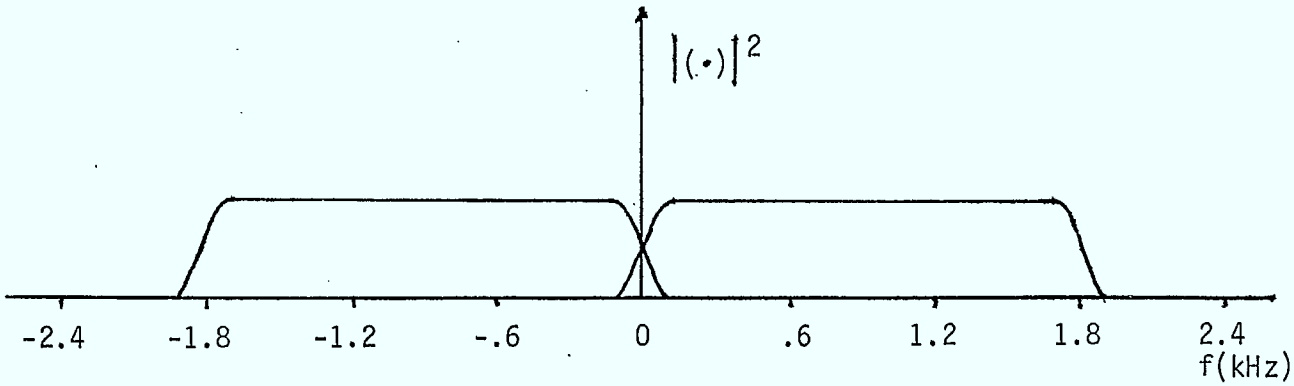

a) Ideal Modulator Subband Filters

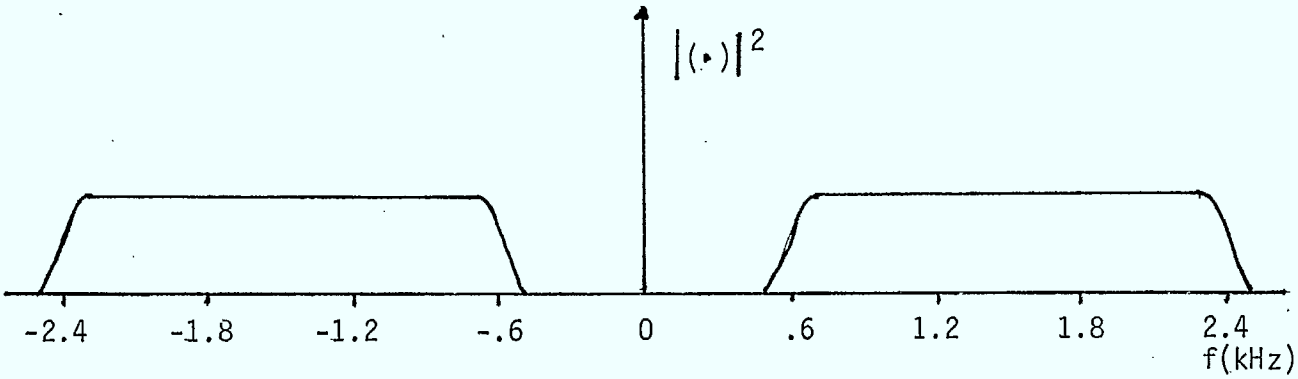

b) Ideal Demodulator Subband Filters

Figure 5.4. Ideal Subband Filters with Root-raised Cosine Roll-off. (e.g. 20% rolloff)

was chosen because if the same filters were used in the ACSSB demodulator, the recombination of the upper and lower sidebands in the demodulator should be perfect (i.e. the combined filter spectrum should be flat across the data signal spectrum). These filters were created with a bandwidth of 1800 Hz, to avoid any distortion of the tails of the signal spectrum, and with a 20% overlap, to reduce the overlap from extending into the region (after splitting) where it is desired to put the 300 Hz subpilot tones. The amplitude response of F1 is shown in Figure 5.5*.

The Scientific Authority suggested an alternative filter which is suited to his implementation. The FIR taps of this filter are listed in Table 5.1, and the corresponding amplitude response is shown in Figure 5.6.

After filtering, the two sidebands are separated using a +600 Hz and -600 Hz tone. In the ideal case these tones are generated analytically (actually done in frequency domain), in the non-ideal case they are generated from an analytic 300 Hz source. The nonideal case will be discussed further later.

After separating the sidebands, the d.c. pilot and ±300 Hz subpilots are added to the signal. At present each subpilot is 6 dB below the d.c. pilot level, and the pilot level is 5 or 10 dB below the signal level.

5.2.2 ACSSB Demodulator

A block diagram of the software simulation of the ACSSB demodulator is shown in Figure 5.2. There are three main

*Note that there are sidelobes present in this figure because of the FIR approximation to the root raised cosine impulse response.

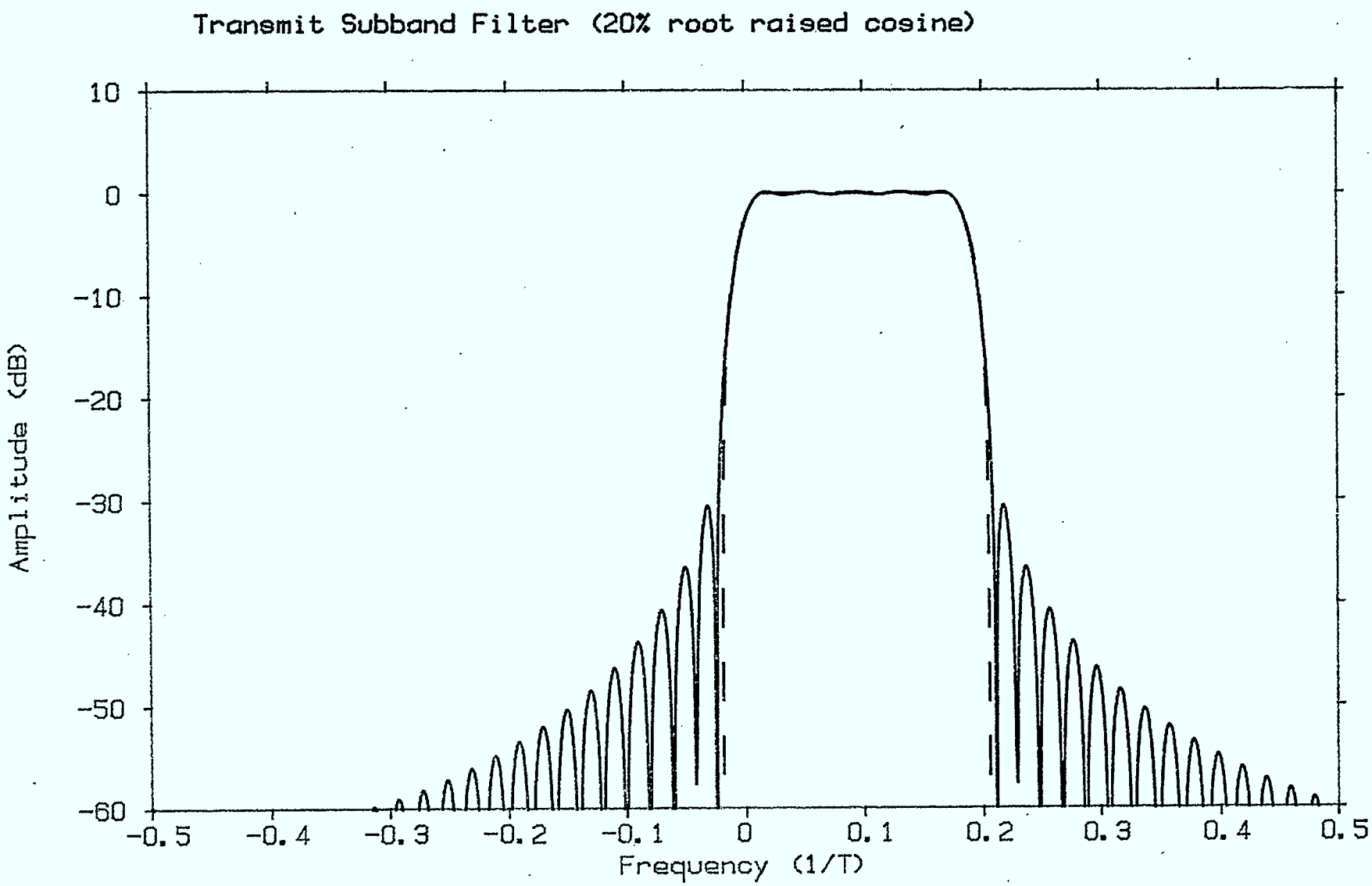

Bandwidth = 1800 Hz (.1875/T) Center Frequency = 900 Hz

Analytic Response

50 pt. FIR Approx.

Figure 5.5

Table 5.1: Transmit Subband Filter

Tap No.	Filter Coefficient
1	-j0.0231
2	0
3	-j0.0154
4	0
5	-j0.0205
6	0
7	-j0.0286
8	0
9	-j0.0397
10	0
11	-j0.0598
12	0
13	-j0.1035
14	0
15	-j0.3176
16	0.5
17	-j0.3176
18	0
19	-j0.1035
20	0
21	-j0.0598
22	0
23	-j0.0397
24	0
25	-j0.0286
26	0
27	-j0.0205
28	0
29	-j0.0154
30	0
31	-j0.0231

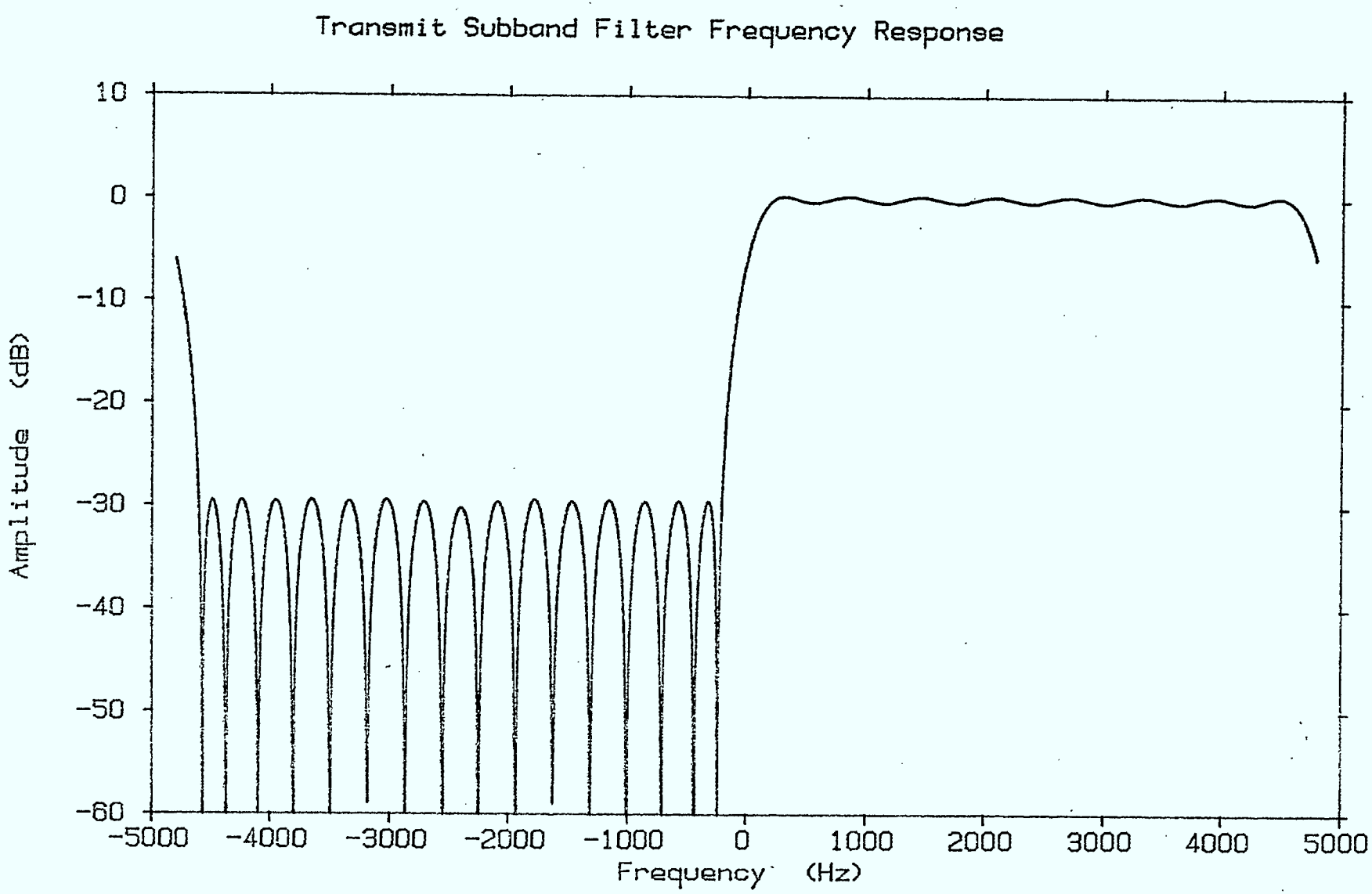
Transmit Subband Filter Frequency Response
Amplitude (dB)
10
0
-10
-20
-30
-40
-50
-60
-5000
-4000
-3000
-2000
-1000
0
1000
2000
3000
4000
5000
Frequency (Hz)

Figure 5.6

sections to the demodulator, the AGC, the subpilot recovery and the subband filtering and recombining. These are discussed separately.

5.2.2.1 The AGC

The first signal processing block of the ACSSB demodulator has been labelled the AGC (often referred to as FFSR in the literature), which is not a misnomer if one realizes that it compensates for the complex gain of the channel. That is, it attempts to correct both the amplitude and phase variations introduced by the channel.

In the implementation, the bandwidth of filter F4 is approximately matched to the expected bandwidth of the fading process. This filter was implemented as a 51 point FIR filter and its amplitude response is shown in Figure 5.7. Note that this filter appears to be equiripple in the stopband and only provides 30 dB attenuation of out of band signals. This may not be optimum if one considers that the data signal may be 10 dB above the pilot level, and thus the pilot estimate may have a background noise of 20 dB due to the data. In fact, the pilot amplitude at the output of the first F4 was observed to vary approximately 10% rms under noiseless conditions, as would be expected from this argument.

The 1/(x+a) operator* in the AGC determines the compensating gain and a small value, a, prevents the possibility of division by zero. The second implementation of F4 is to compensate for any gain effects due to the pilot not being in the centre of the first F4.

The blocks labelled D in the signal path represent delays used to match the corresponding delays in the generation of the complex gain.

*Actually the operator is $1/(x+a\cdot\mathrm{sign}(\mathrm{real}(x)))$.

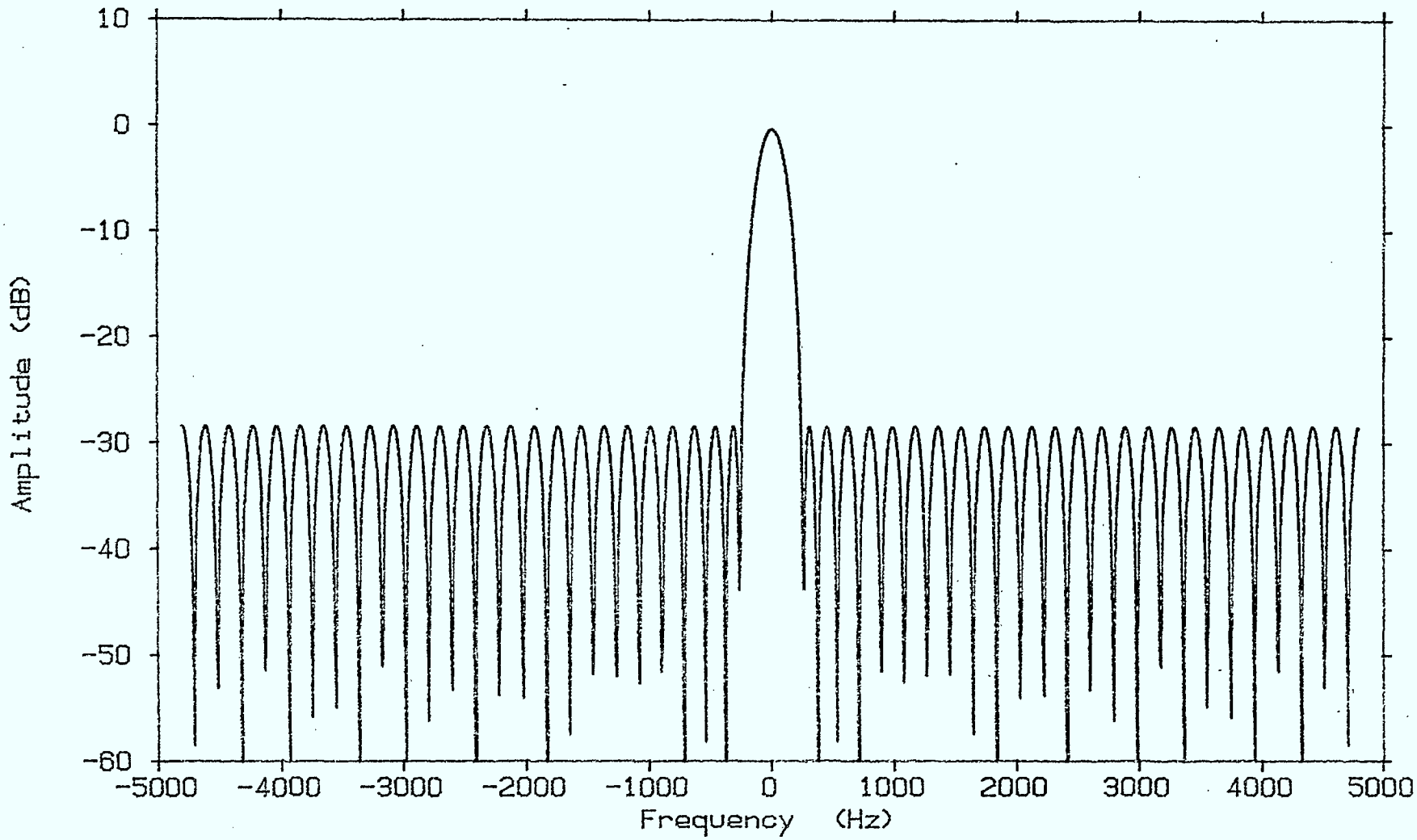

Amplitude Response of ACSSB AGC Filter

Figure 5.7

5.2.2.2 Recombining the Data Signal

This portion of the TTIB ACSSB demodulator coherently recombines the data signal which was split into two subbands during transmission, to produce a signal from which data can be discerned.

The first step in this process is the removal of the ±300 Hz subpilots with a notch filter (the pilot has already been removed by the AGC). This notch filter was implemented as an IIR filter with the following equation

$$H(z) = \frac{1 - 1.9616\ z^{-1} + z^{-2}}{1 - 1.94198\ z^{-1} + .9801\ z^{-2}}$$

The amplitude response of this filter is shown in Figure 5.8.

The ideal subband filters used to separate the two sidebands in the demodulator are the same as described in the TTIB ACSSB modulator except that they have been shifted by ±600 Hz to centre frequencies of ±1500 Hz. This corresponds to the shift of the split data signal.

An alternative subband filter suggested by the Scientific Authority has the FIR coefficients given in Table 5.2, and an amplitude versus frequency response as shown in Figure 5.9. The main advantage of this filter is the ease of implementation. It has the disadvantage that because it includes the noise spectrum from 0 to 600 Hz, upon recombining, the signal (if the received noise is white) will have a noise spectrum which is 3 dB higher over the centre 1200 Hz, as shown in Figure 5.10.

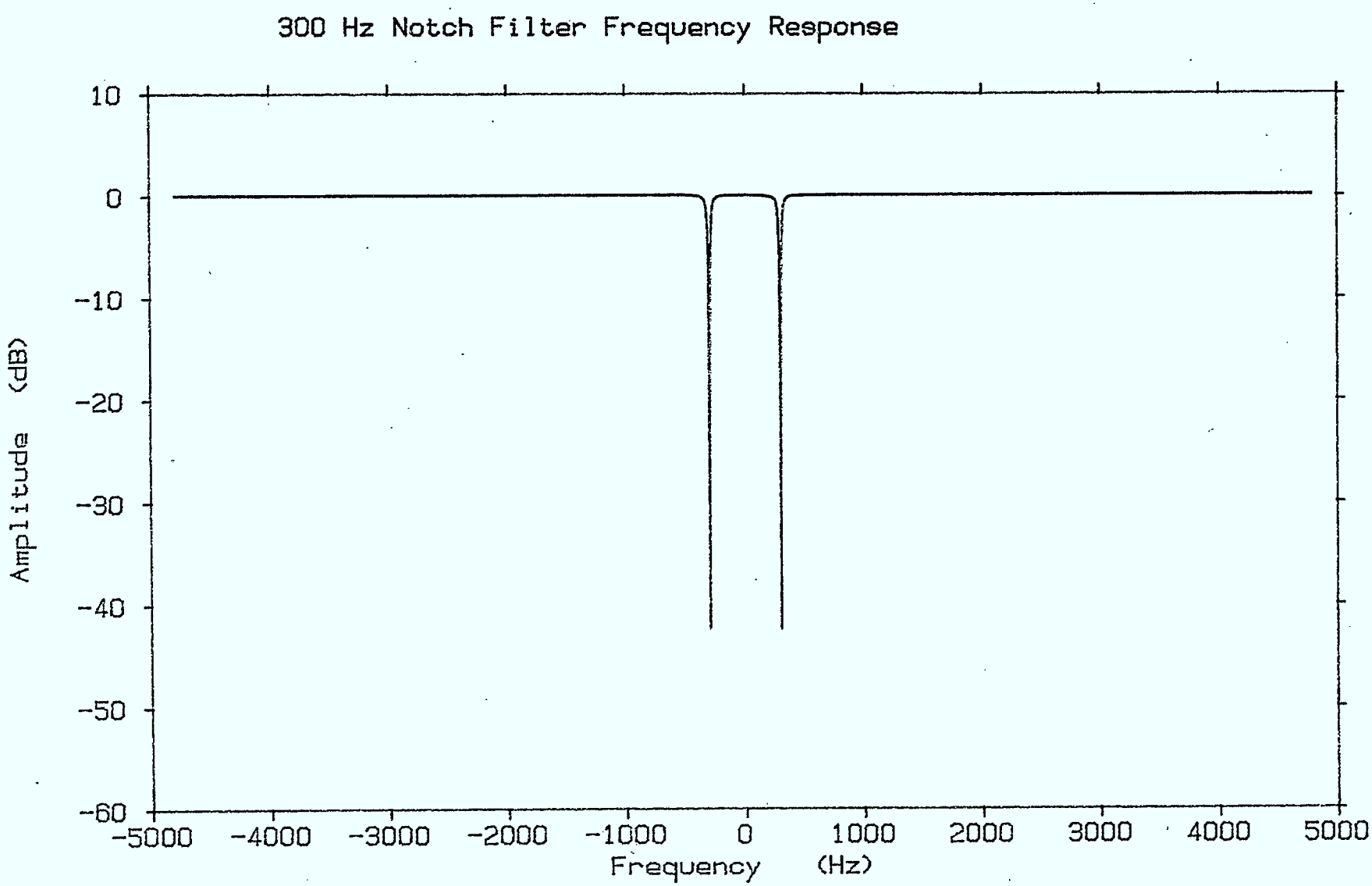
300 Hz Notch Filter Frequency Response
Amplitude (dB)
10
0
-10
-20
-30
-40
-50
-60
-5000
-4000
-3000
-2000
-1000
0
1000
2000
3000
4000
5000
Frequency (Hz)

Figure 5.8

Table 5.2: Receive Subband Filter

Tap No.	Filter Coefficient
1	-j0.0197
2	0
3	-j0.0277
4	0
5	-j0.0497
6	0
7	-j0.0975
8	0
9	-j0.3152
10	0.5
11	-j0.3152
12	0
13	-j0.0975
14	0
15	-j0.0497
16	0
17	-j0.0277
18	0
19	-j0.0197

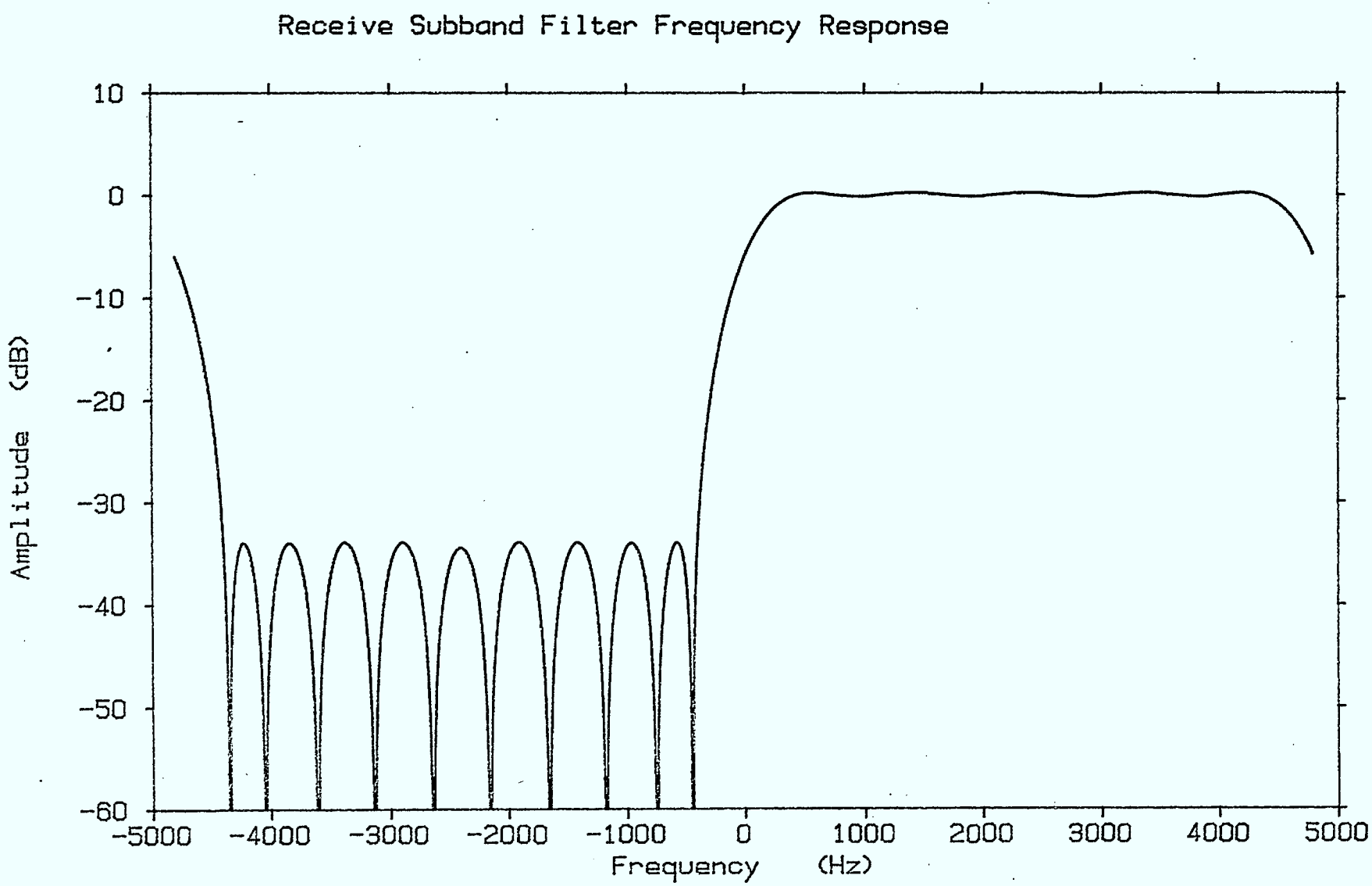
Receive Subband Filter Frequency Response
10
0
-10
-20
-30
-40
-50
-60
Amplitude (dB)
-5000
-4000
-3000
-2000
-1000
0
1000
2000
3000
4000
5000
Frequency (Hz)

Figure 5.9

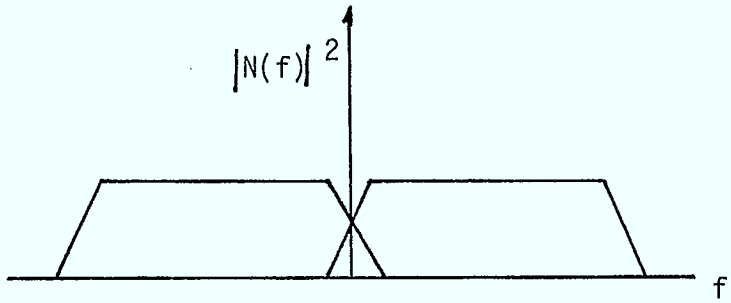

a) Filtered Noise Spectrums before recombining.

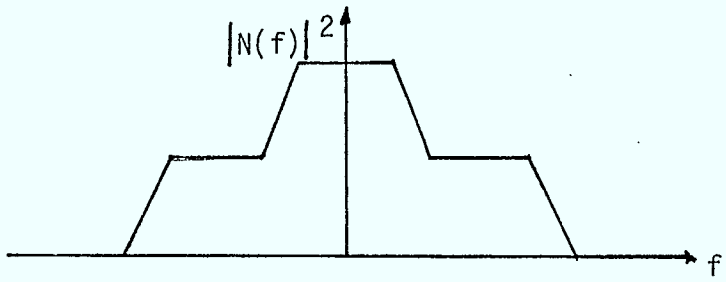

b) Noise Spectrum after recombining.

Figure 5.10

5.2.2.3 Subpilot Recovery

The subpilot recovery refers to the regeneration of the phase coherent plus and minus 600 Hz tones required for coherently recombining the split data subbands. In practice, the ±600 Hz* signals are recovered from the 300 Hz pilot.

In our ideal setup, the ±600 Hz signals are generated ideally (rather than recovered), in the same manner as those used in the transmitter and then the phase is adjusted to account for the delay of the channel, receiver front end (AGC), and the demodulator subband filtering.

The originally suggested method of obtaining the ±600 Hz subcarriers from the ±300 Hz recovered subpilot was to square each of the + and - 300 Hz complex tones, as illustrated in Figure 5.11. However, it was observed that the two tones could be averaged to provide an approximate 3 dB reduction in the effects of noise.

In fact, three different ways of averaging the tones were proposed, and if s_{+300}, s_{-300}, s_{+600} and s_{-600} represent the ±300 Hz and ±600 Hz tones respectively, then the different alternatives can be expressed mathematically as ($\overline{(\cdot)}$ represents complex conjugation)

(i) $$s_{+600} = \left\{\frac{1}{2}\left(s_{+300} + \overline{s_{-300}}\right)\right\}^2$$

(ii) $$s_{+600} = s_{+300}\,\overline{s_{-300}}$$

---

*There is a slight abuse of notation here, in that, +600 Hz means $e^{+j\omega_c t}$ with $\omega_c = 2\pi 600$ and similarly for -600 Hz.

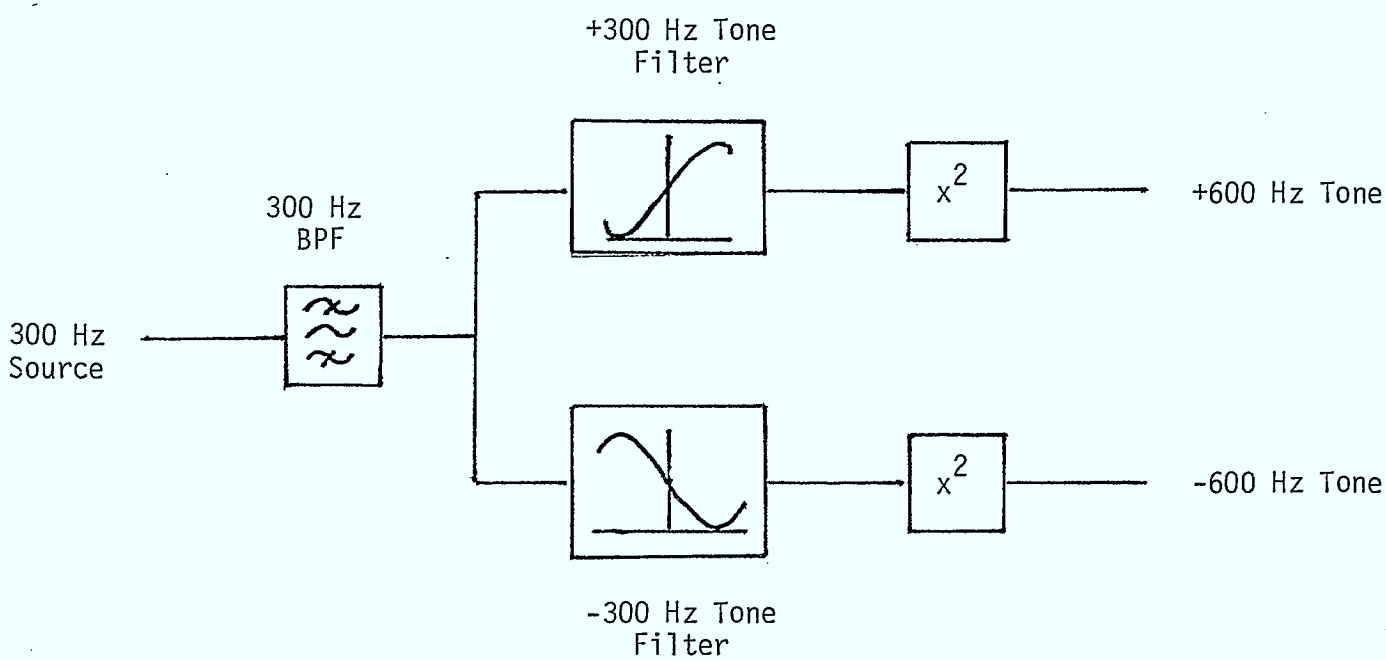

Figure 5.11 . 600 Hz Tone Generator.

(iii) $s_{+600} = \frac{1}{2}(\{s_{+300}\}^2 + \overline{\{s_{-300}\}^2})$

with $s_{-600} = \overline{s_{+600}}$ in all cases. In the limited number of cases tested all of these methods performed approximately the same, and reduced the error rate by a factor of between 2 and 3 over the originally suggested method. Method (ii) was implemented in the following tests because of its computational simplicity. In fact this same circuit is used in both the modulator and demodulator. In the modulator, the 300 Hz input comes from a local oscillator; in the demodulator, the 300 Hz input is the subpilot tones which are stripped off the received signal. The same scheme is used in the modulator as the demodulator to ensure that the regenerated ±600 Hz tones have the same phase relationship to the ±300 Hz subpilots in both instances. As a result, the only phase adjustment required in this case is to account for the delay of the demodulator subband filtering which is controlled by the receiver.

The 300 Hz bandpass filter which is used to strip the ±300 Hz subpilots from the received signal is implemented as a digital IIR filter with the following transfer function

$$H(z) = \frac{.01}{1 - 1.94198\ z^{-1} + .9801\ z^{-2}}$$

The amplitude versus frequency response of this filter is shown in Figure 5.12. The filter used to separate the +300 Hz and -300 Hz complex tones has a sinusoidal amplitude response with a peak at +300 Hz and a null at -300 Hz and was implemented as the FIR filter described by

$$H(z) = -.25\ j + 0.5\ z^{-8} + .25\ j\ z^{-16}$$

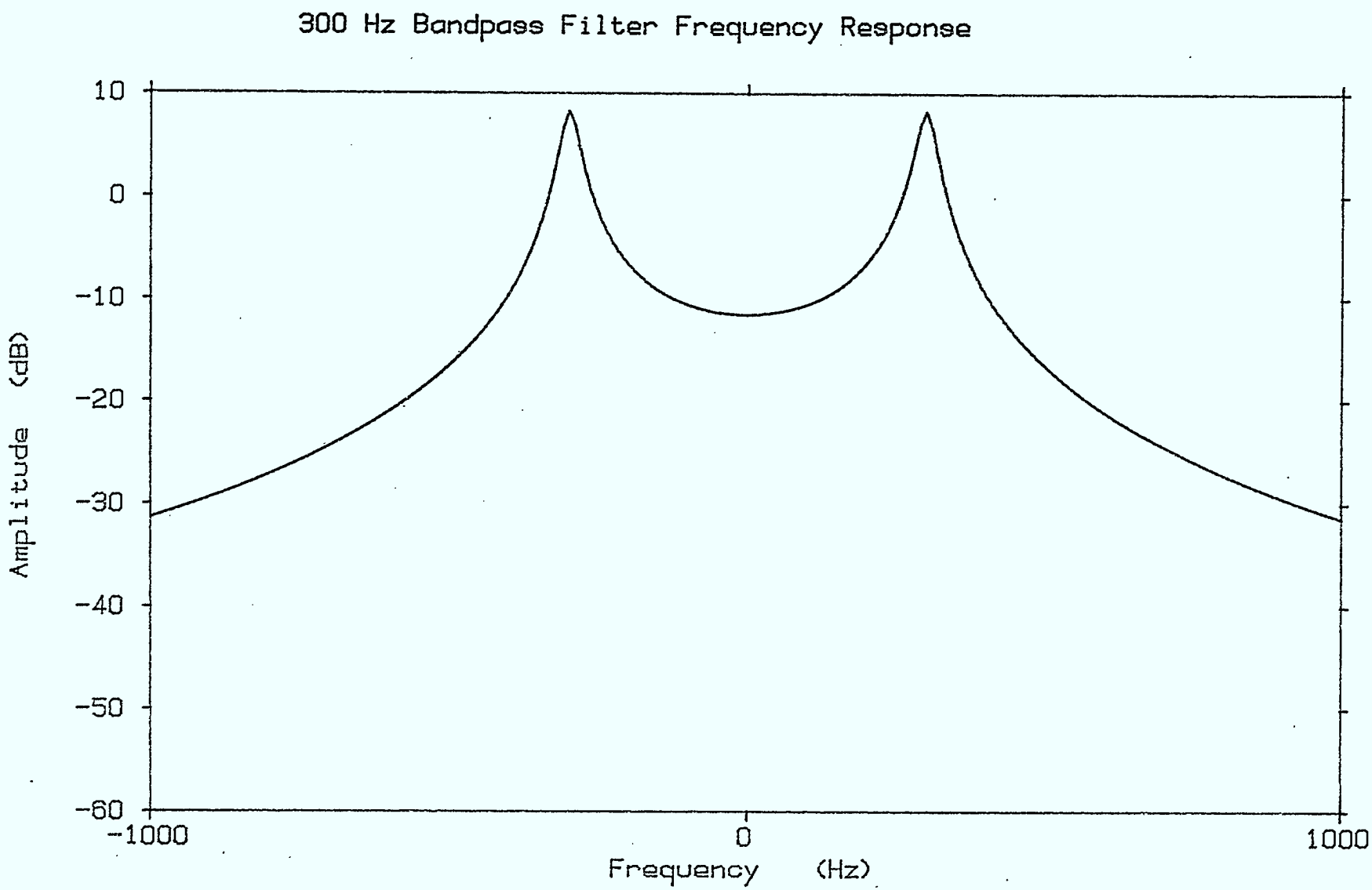
300 Hz Bandpass Filter Frequency Response
10
0
-10
-20
-30
-40
-50
-60
Amplitude (dB)
-1000
0
1000
Frequency (Hz)

Figure 5.12

5.3 BER Performance With Ideal Recombining

The initial performance results using an ACSSB modem with a 2.4 kbps BPSK signal format, and with ideal subband recombining are shown in Figure 5.13 for various Rician channel K factors.

In the case of no multipath ($K=-\infty$) there is a significant degradation of performance from ideal. This degradation is slightly less than 2 dB over the range of bit error rates tested. Note however that the energy per bit, E_b, used in determining the horizontal axis includes the average pilot and subpilot energy per bit as well as the "data" energy per bit. For the test results shown in Figure 5.13 the pilot was 5 dB below the data signal and the two subpilots were each 6 dB below the pilot. This implies a 1.7 dB increase in the "usual" energy per bit. This accounts for most of the degradation seen between the ideal case and that using the ACSSB modem under no multipath conditions. The degradation caused by the AGC under no multipath conditions is thus a small fraction of a dB.

Under multipath conditions, (K= -10 dB, -5 dB, 0 dB), the performance of the ideal TTIB ACSSB modem is very similar to that obtained for DOQPSK under similar multipath conditions.

5.4 BER Performance With Nonideal Subpilot Recovery

Nonideal subpilot recovery refers to the recovery of the ±600 Hz subcarriers from the received ±300 Hz subpilot, and then using these subcarriers to recombine the split data signal; in other words, the practical situation.

In the previous section, it was shown that the degradation in performance caused by the TTIB ACSSB modem with ideal

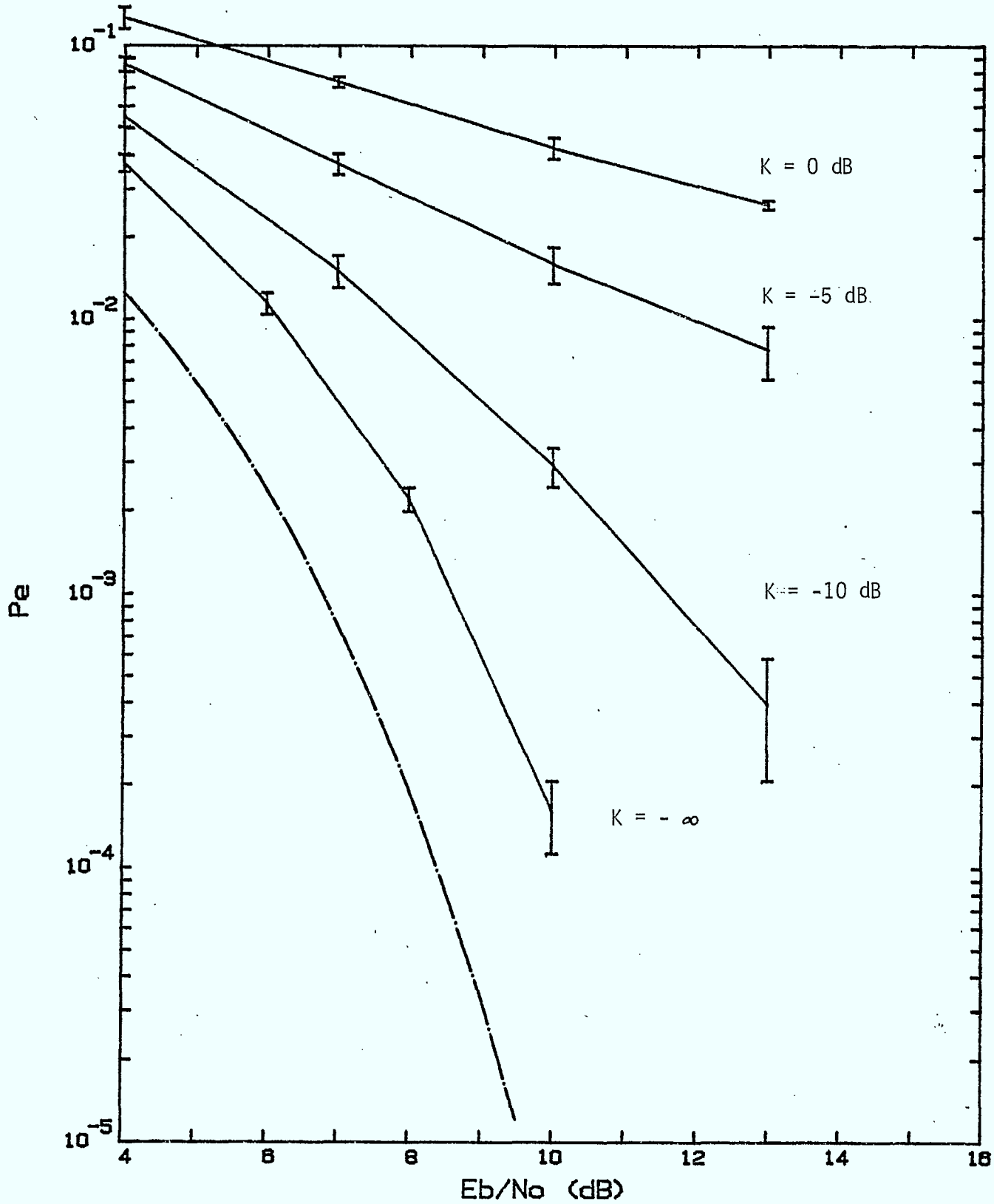

BPSK BER Performance of ACSSB Modem with Ideal Carrier Recovery

——————— K = - ∞, -10, - 5 and 0 dB

—·—·—·— Ideal Coherent Performance

Figure 5.13

subpilot recovery was mainly that due to the power lost in the pilots. However, if we look at typical eye diagrams, we see some degradation that apparently did not significantly affect the performance. In particular, Figure 5.14 shows the eye diagram obtained using BPSK modulation, a 20% root raised cosine pulse shape and no ACSSB modem under noiseless conditions. Figure 5.15 shows the eye diagram of the same (nearly) bit sequence but with the TTIB ACSSB modem and ideal subpilot recovery, under similar conditions. The degradation is definitely noticeable, but it does not significantly alter the eye width and only slightly decreases the eye height . The degradation seen is due mainly to two factors, the nonideal action of the AGC portion of the modem (the data signal appears as a background noise signal on the pilot), and the not quite ideal implementation of the subband filters.

Figures 5.16 and 5.17 are repetitions of 5.14 and 5.15 except that the E_b/N_o ratio is 15 dB.

Figures 5.18 and 5.19, are the eye diagrams using the TTIB ACSSB modem and nonideal subpilot recovery at an E_b/N_o of infinity (noiseless) and 15 dB respectively. The degradation in the non-ideal case relative to the previous examples is quite noticeable, both the eye width and eye height are noticeably smaller.

The bit error rate performance of BPSK with the TTIB ACSSB modem and non-ideal subpilot recovery is shown in Figure 5.20. In this case the d.c. pilot was 5 dB below the data signal and each of the ±300 Hz subpilots were 6 dB below the d.c. pilot. This implies that the pilots add an additional 1.7 dB to the total transmitted power and this is included in the calculation of E_b/N_o.

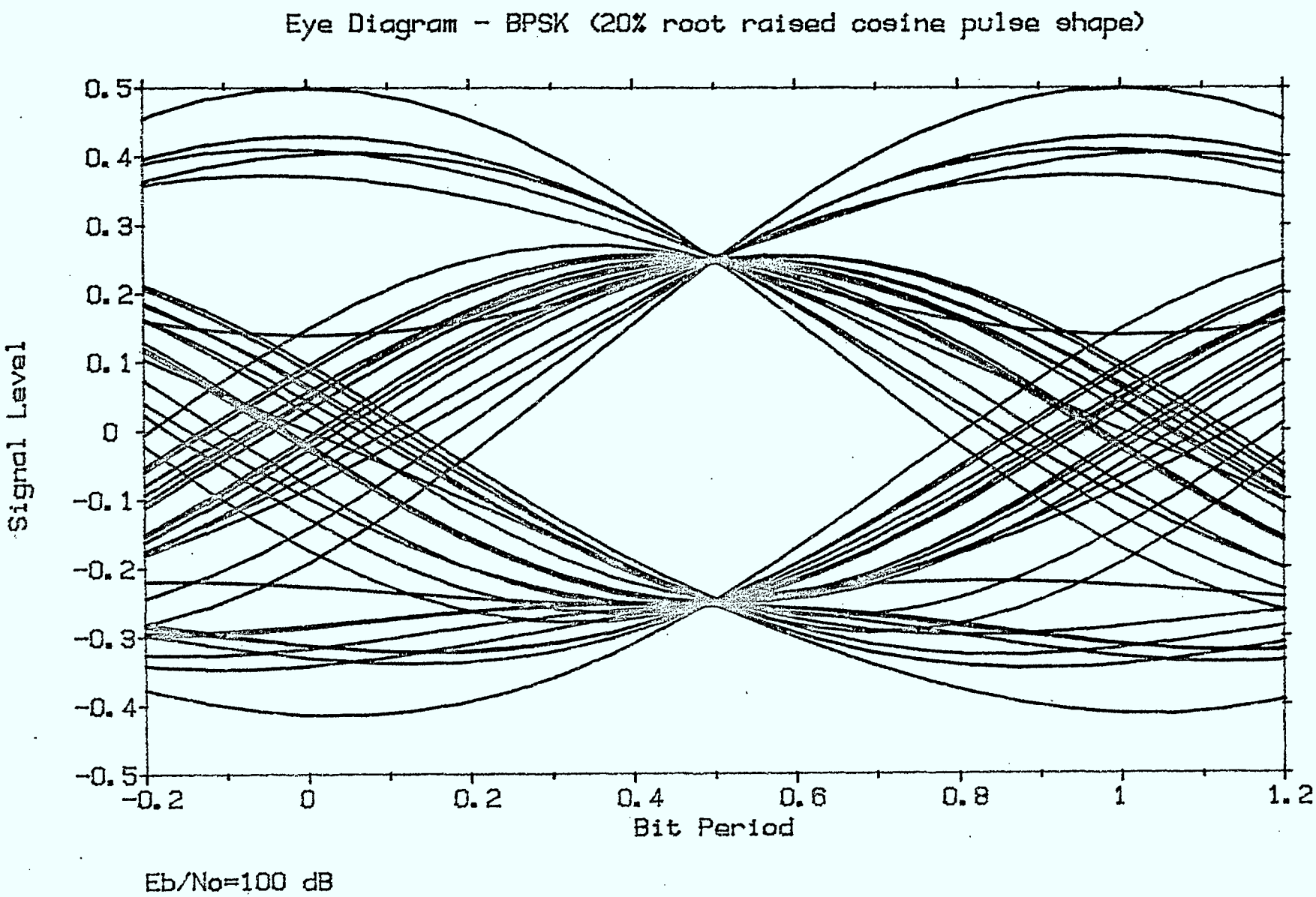
Eye Diagram - BPSK (20% root raised cosine pulse shape)
Signal Level
0.5
0.4
0.3
0.2
0.1
0
-0.1
-0.2
-0.3
-0.4
-0.5
-0.2
0
0.2
0.4
0.6
0.8
1
1.2
Bit Period
Eb/No=100 dB

Figure 5.14

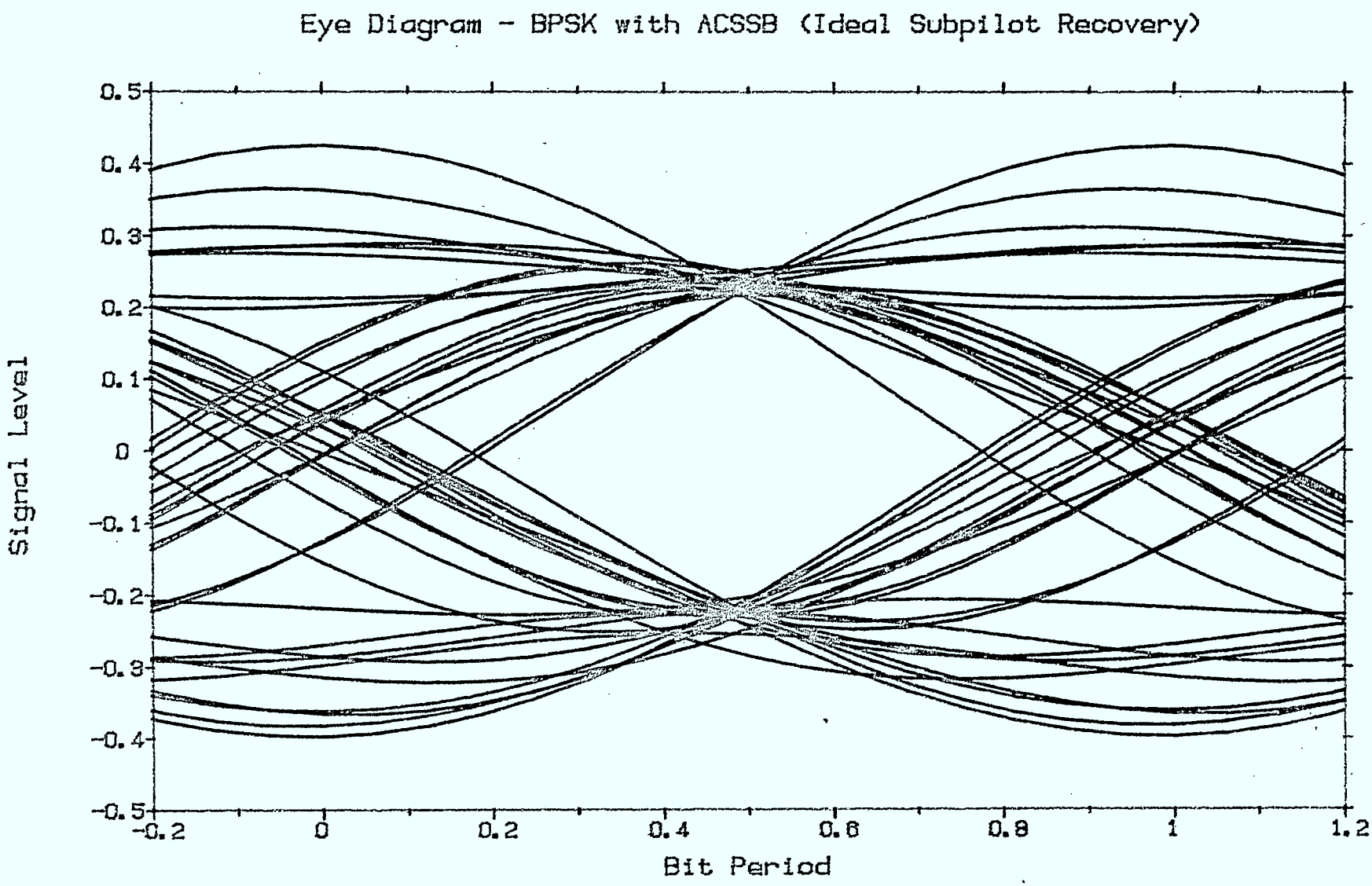

Eb/No = 100 dB

20% root raised cosine pulse shape

Root raised cosine subband filters

Figure 5.15

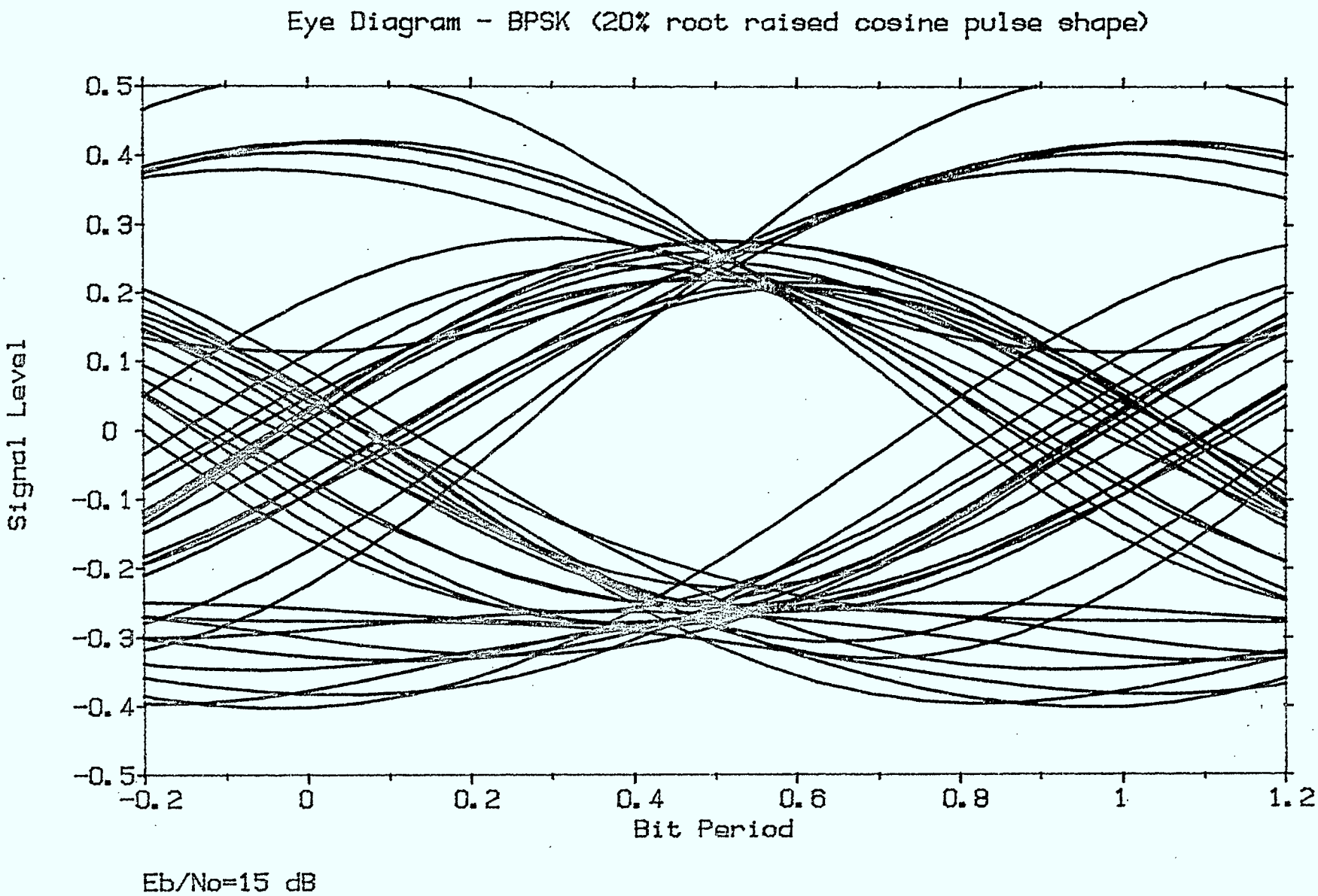
Eye Diagram - BPSK (20% root raised cosine pulse shape)
Signal Level
0.5
0.4
0.3
0.2
0.1
0
-0.1
-0.2
-0.3
-0.4
-0.5
-0.2
0
0.2
0.4
0.6
0.8
1
1.2
Bit Period
Eb/No=15 dB

Figure 5.16

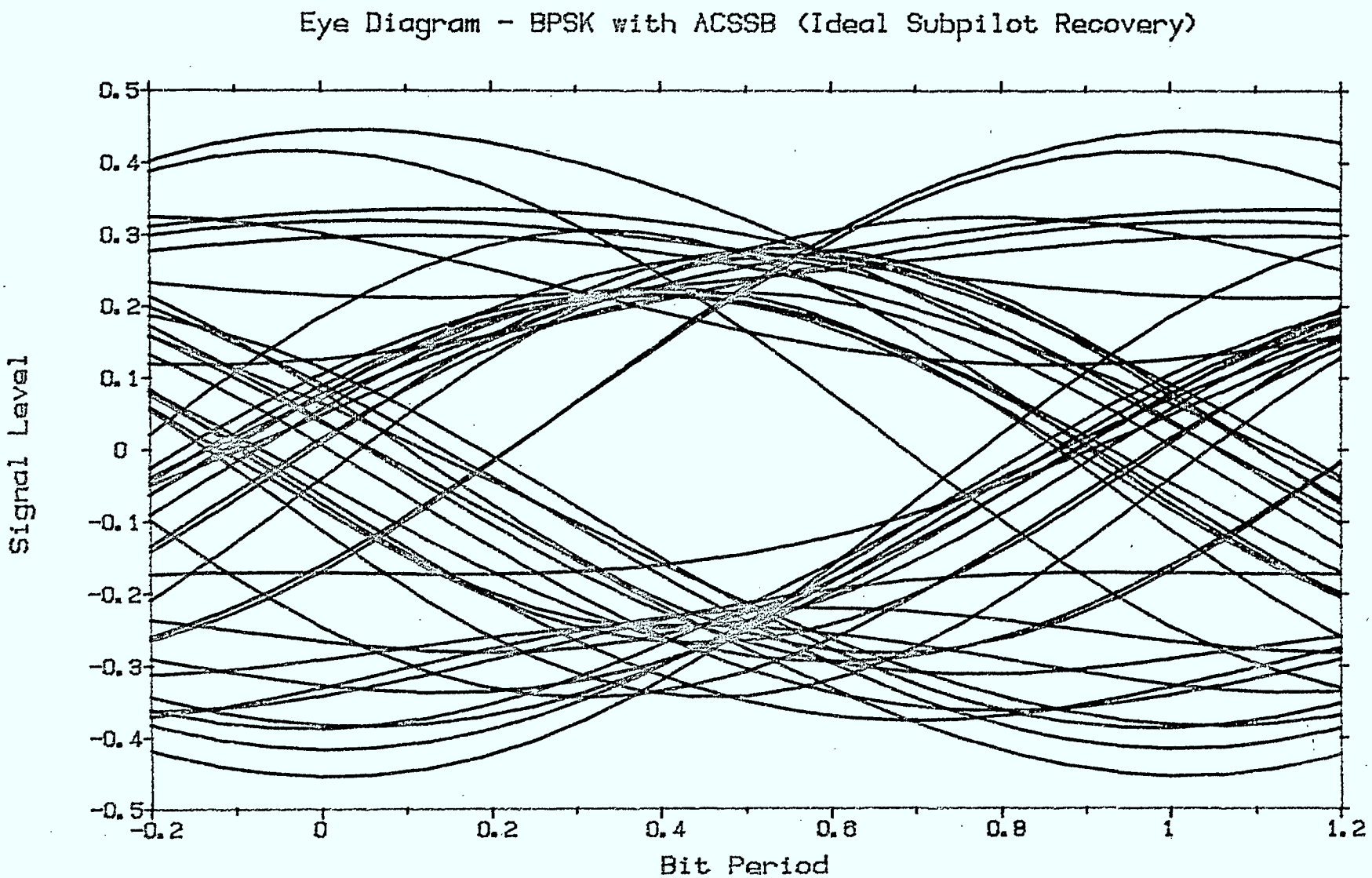

Eb/No = 15 dB

20% root raised cosine pulse shape

Root raised cosine subband filters

Figure 5.17

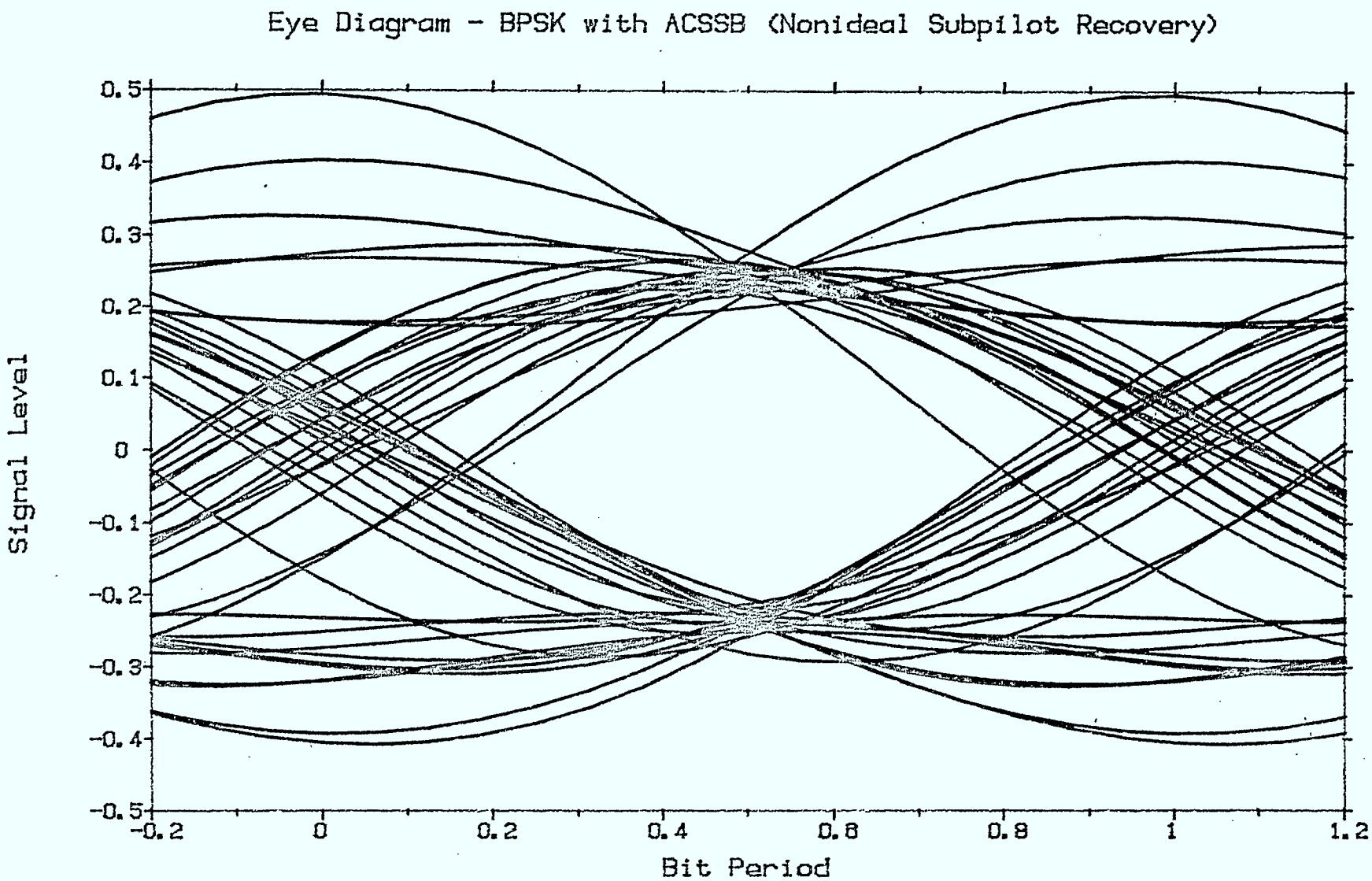

Eb/No = 100 dB

20% root raised cosine pulse shape

Specified subband filters

Figure 5.18

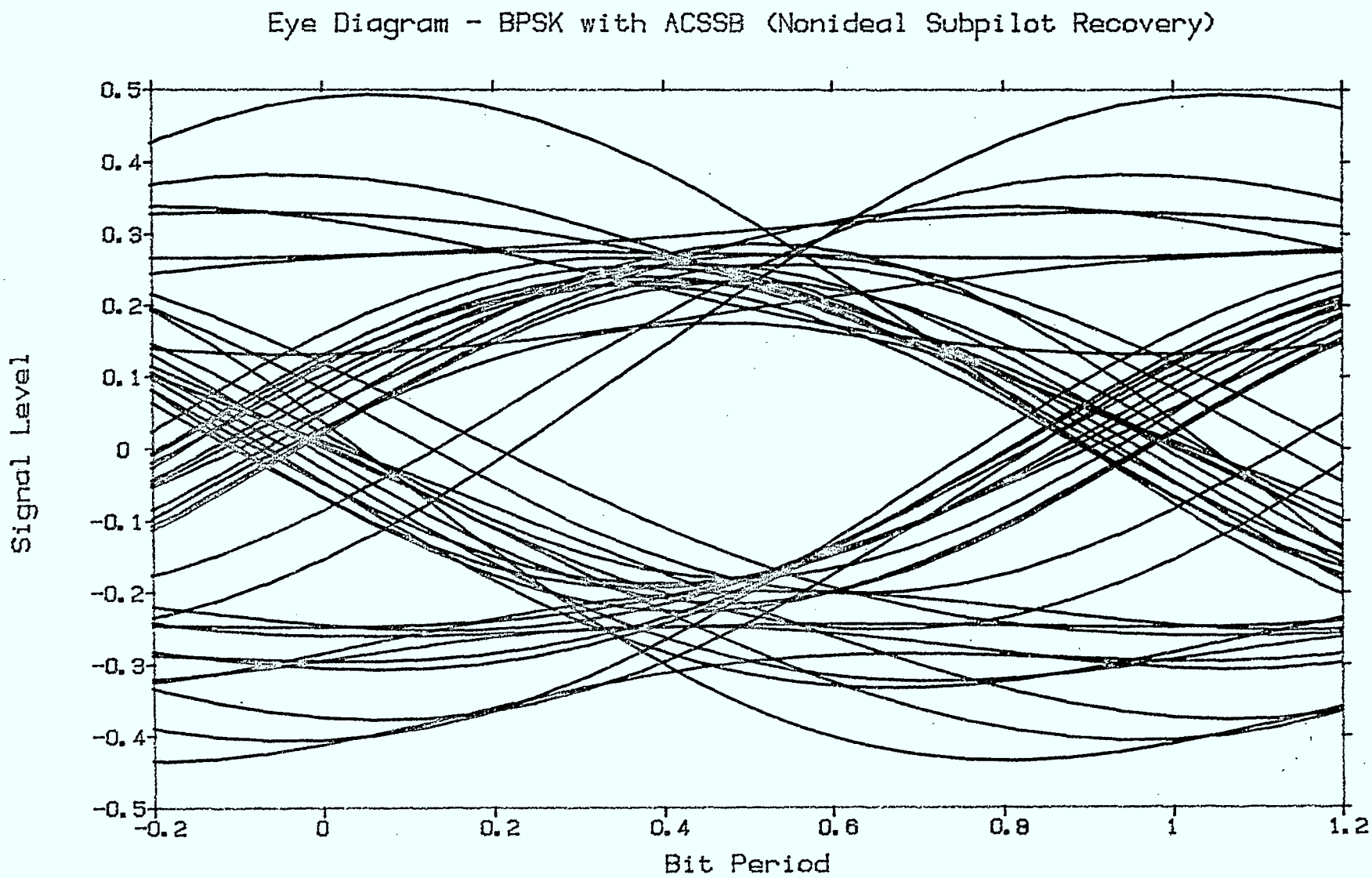

Eb/No = 15 dB

20% root raised cosine pulse shape

Specified subband filters

Figure 5.19

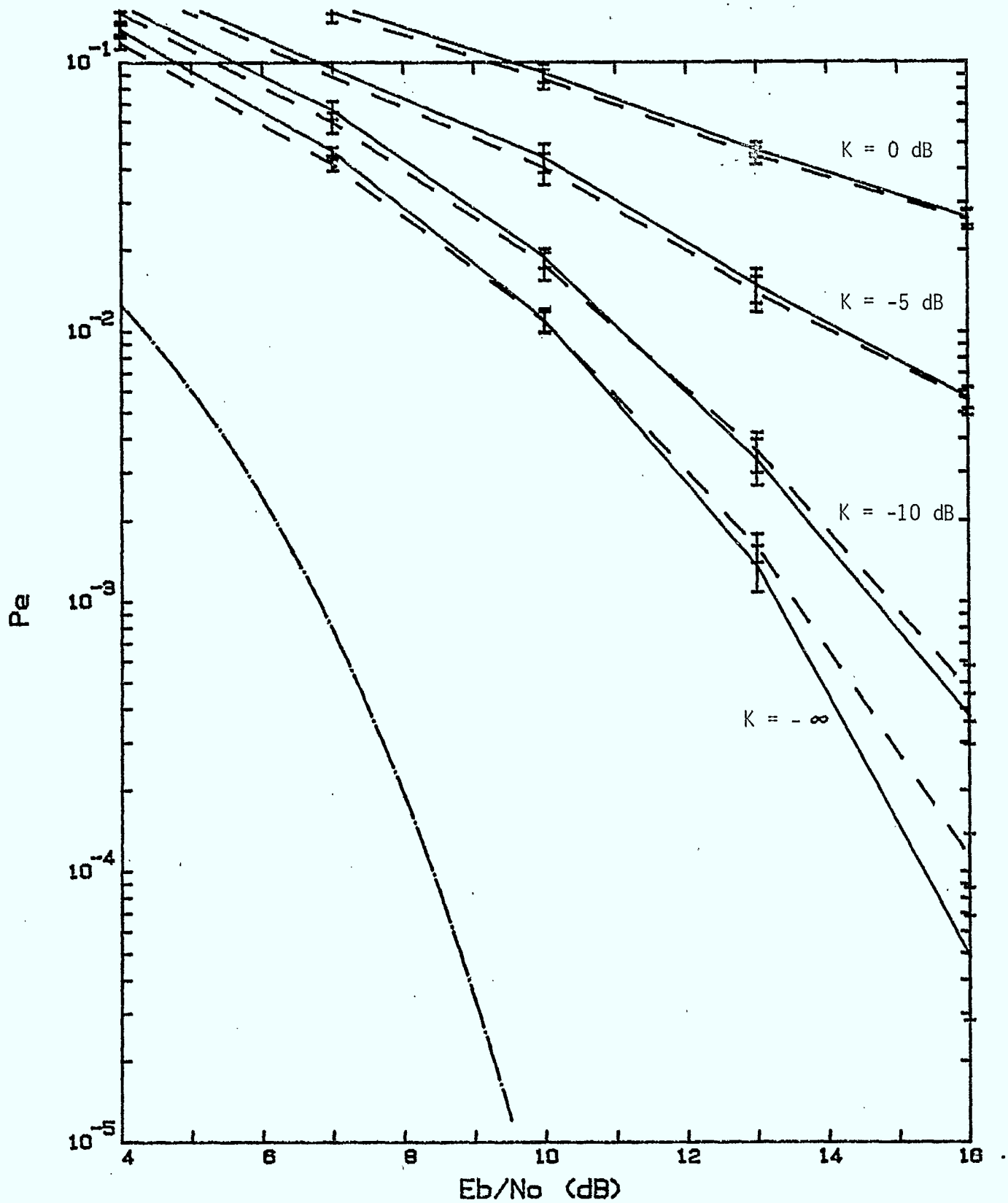

BER Performance of BPSK with ACSSB (nonideal pilot recovery)

——————— without nonlinearity (-5dB pilot)

— — — — with nonlinearity (-5dB pilot)

—·—·—·— Ideal Coherent Performance

Figure 5.20

The performance of coherent BPSK in conjunction with the TTIB ACSSB modem is very poor. In the case of no multipath ($K=-\infty$), performance is degraded at least 6 dB over the range of E_b/N_o tested. The previous tests indicated that only about 2 dB of this degradation can be attributed to the AGC and the power in the pilots, the remaining 4 dB is caused by the non-ideal coherent recombining of the data subbands. The method is apparently very sensitive to noise on the recovered ±600 Hz sub-carriers.

Under multipath conditions, comparing the BPSK/ACSSB results to those obtained with DOQPSK, the degradation is not as large as in the case of no multipath but there is clearly a significant degradation in performance. Again, this is due to the poor performance of the coherent recombining.

In Figure 5.21, there is a similar set of curves for the case when the d.c. pilot is 10 dB below the data signal. Once again, the subpilots are each 6 dB below the d.c. pilot. In this case performance is even worse, as would be expected with lowering the subpilot power levels.

In general, the increased complexity and poor performance of the scheme makes it a very poor candidate for the modulation strategy to be used on a mobile satellite communications channel.

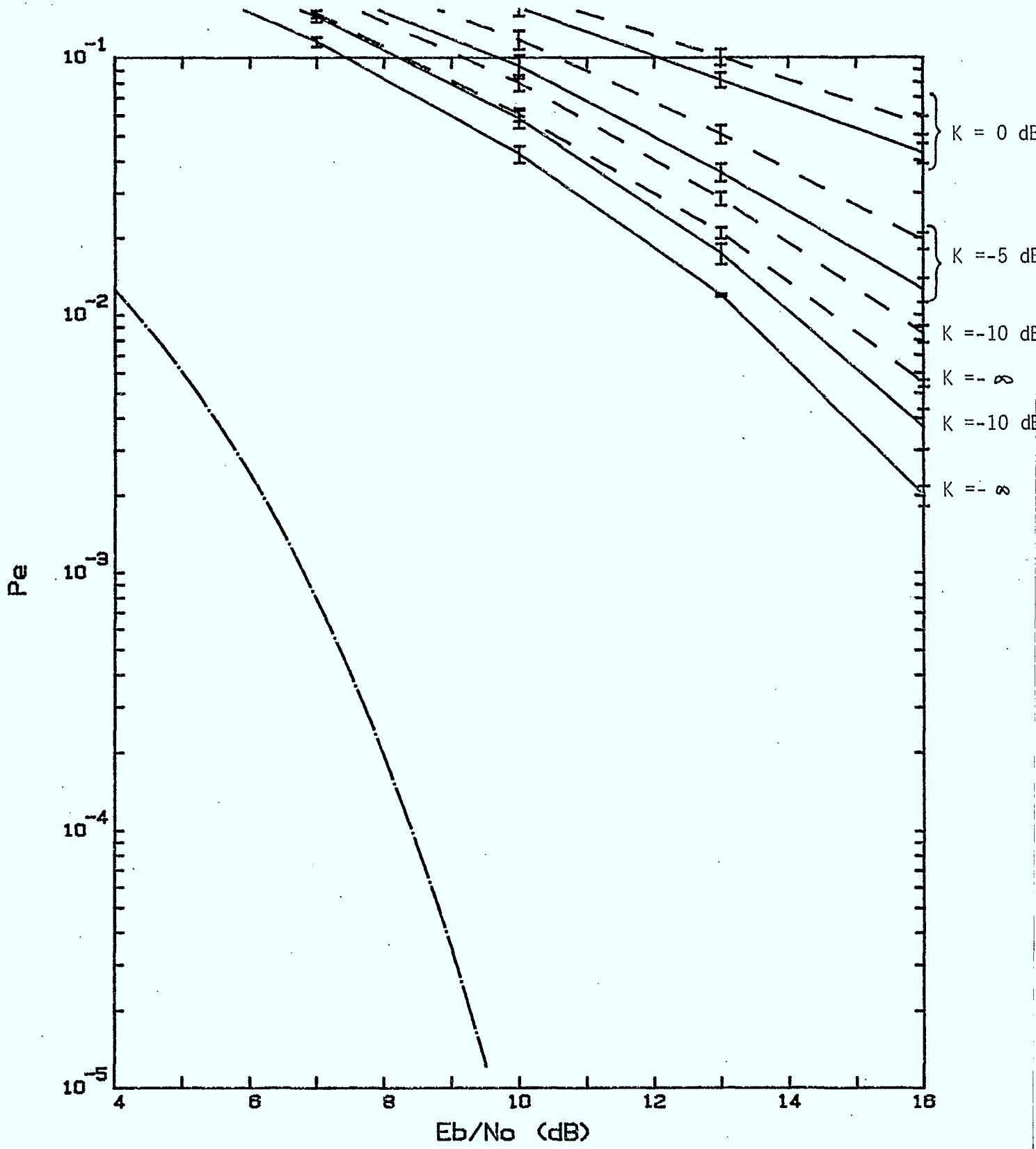

BER Performance of BPSK with ACSSB (nonideal pilot recovery)

——————— without nonlinearity (-10 dB pilot)

— — — — with nonlinearity (-10 dB pilot)

—·—·—·— Ideal Coherent Performance

Figure 5.21

6.0 CONCLUSIONS AND RECOMMENDATIONS

In this study we have evaluated three modulation strategies with respect to a simulated mobile satellite communications channel.

The three modulation strategies evaluated were differentially detected MSK (DMSK), differentially detected OQPSK (DOQPSK), and coherent BPSK in conjunction with an ACSSB modem with transparent tone in band (TTIB) signalling.

The main advantages of DMSK are that

(i) 99.5% of the energy is contained within an IF bandwidth of 1.5 times the data rate, and

(ii) the signal envelope is essentially constant, and as a result DMSK was demonstrated to have negligible degradation when used over a nonlinear channel.

The main disadvantages of differentially detected MSK are that

(i) there is a theoretical E_b/N_o penalty arising from the use of an essentially noisier reference signal in differential detection, and

(ii) receive filtering of the MSK signal, when using differential detection, introduces intersymbol interference (ISI).

The first results in a penalty of approximately 1 dB in SNR for bit error rates in the range 10^{-3} to 10^{-4}, when compared to ideal coherent detection. And for the near

optimum receive filter tested, the second disadvantage was shown to result in an additional penalty of 2 dB in SNR. However, this penalty can be reduced by approximately 1 dB by employing a parity detector with a single error correction (SEC) circuit in the demodulator. (No additional coding is required in the modulator.)

In this study differential offset QPSK (DOQPSK) signalling with 50% rolloff root raised cosine spectrum shaping surfaced as a very attractive modulation scheme. The reasons are as follows:

(i) The main lobe bandwidth is 1.5 times the data rate, which is the same as for DMSK.

(ii) Under ideal conditions (AWGN channel) matched filtering at the receiver introduces no intersymbol interference (ISI). Thus the attainable bit error rate (BER) is essentially that of ideal differential detection, which is given by [5]

$$\text{BER} = \frac{1}{2} \exp(-E_b/N_o)$$

This performance is typically 2 dB better than that for DMSK for bit error rates in the range 10^{-3} to 10^{-4}.

(iii) BER performance does not degrade significantly when the signal is passed through a non-linear amplifier at the transmitter (less than 0.1 dB with the nominal nonlinearity, and 0.2 dB with a hard limiter).

The only disadvantages of DOQPSK are:

(i) approximately a 1 dB penalty associated with differential detection, relative to ideal coherent detection for bit error rates in the range 10^{-3} to 10^{-4}, and

(ii) the amount of sidelobe energy introduced by the nonlinearity, as adjacent channel interference must be kept to a minimum.

These disadvantages are not major however, as some of the differential detection loss can again be recovered using a single error correction circuit, and the adjacent channel interference can still be quite low when a nonlinear amplifier is employed. Simulation results show that for the nominal nonlinearity given, the sidelobes are down 30 dB at the band edge and down 50 dB at the centre of the adjacent channel. One of the reasons for selecting a rolloff of 50% is because it results in close to the minimum RMS amplitude fluctuation attainable (only 12%) for this modulation scheme.

The third modulation strategy studied was coherent BPSK in conjunction with a TTIB ACSSB modem. The main advantages of this approach are:

(i) the ability to employ a coherent detection scheme, namely BPSK, and thus the potential to achieve ideal coherent bit error rate performance (neglecting the additional power required for the pilot tones), and

(ii) the AGC which compensates for the amplitude and phase perturbations introduced by the fading channel.

The major drawbacks of this approach are:

(i) the wider bandwidth required to transmit both data and pilot tones,

(ii) the degradation in performance due to nonideal subband recombining, and

(iii) the additional E_b/N_o penalty due to the transmitted power which must be devoted to the pilot tones.

There is little that can be done to mitigate these disadvantages. As a result, this modulation scheme faces some large penalties in performance. In fact under otherwise ideal conditions, the third disadvantage alone results in poorer performance than the DOQPSK scheme.

As the previous observations would tend to indicate, DOQPSK is the recommended modulation strategy, at least for low K factor fading channels. Figure 6.1 shows the performance of the best of the three modulation strategies examined under no multipath conditions. These strategies are:

(i) DMSK with single error correction (SEC)

(ii) DOQPSK with SEC

(iii) BPSK in conjunction with a TTIB ACSSB modem (the d.c. pilot is 5 dB below the data, and each subpilot is 6 dB below the d.c. pilot)

As quantitatively indicated by this figure, DOQPSK is clearly the superior modulation strategy. The curves shown do not include a nonlinearity in the channel; with the nominal nonlinearity present, the only curve which shows a significant degradation is that for the TTIB ACSSB modem. The performance indicated for the TTIB ACSSB modem is for

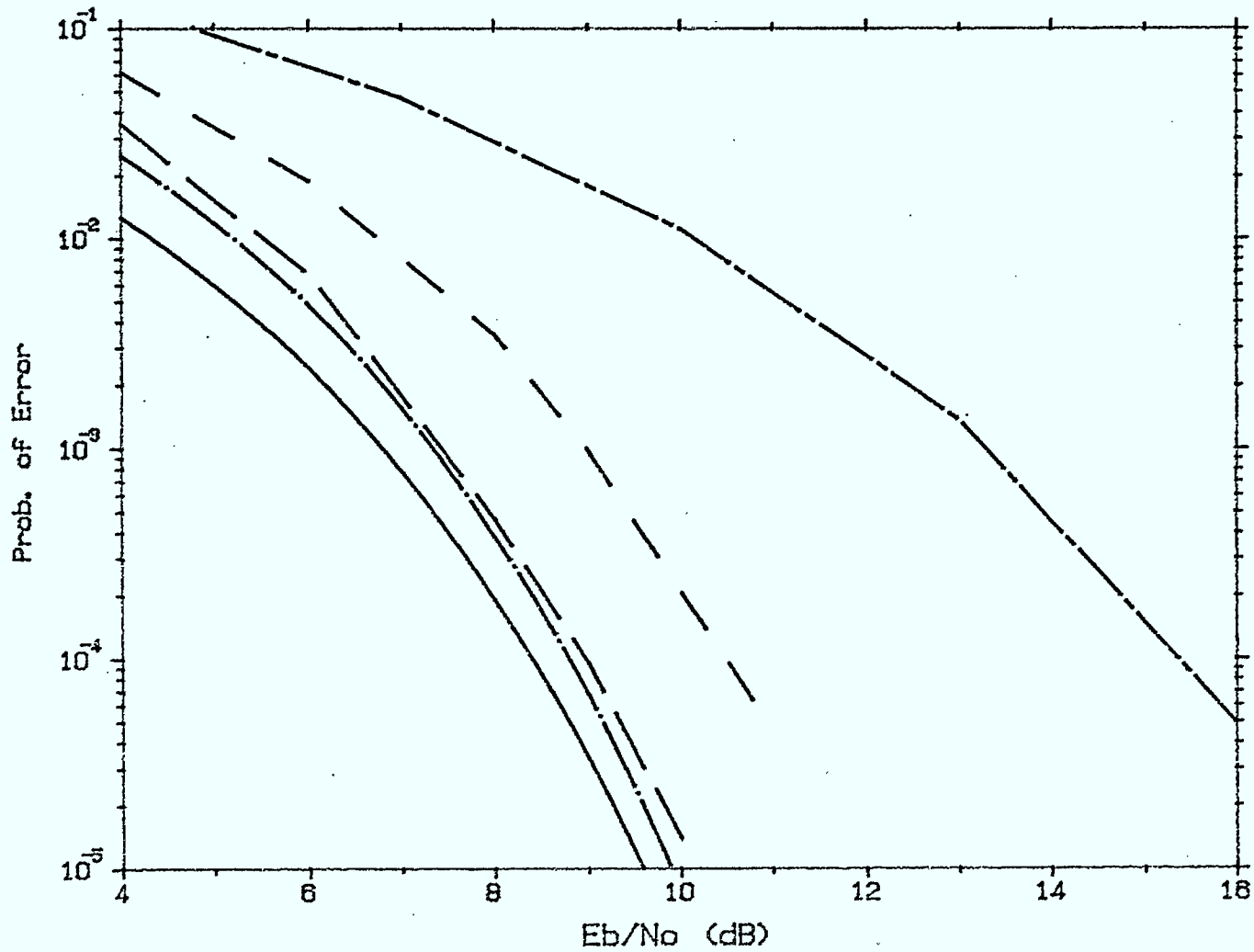

Comparison of DMSK(SEC), DOQPSK(SEC) and BPSK with ACSSB

DMSK (SEC) DOQPSK (SEC)

BPSK with ACSSB (-5 dB pilot)

Ideal Coherent Ideal D.E. Coherent

Figure 6.1

non-ideal subband recombining. With ideal subband recombining the performance is still only about the same as that for DMSK with SEC. Also shown in this figure is ideal coherent bit error rate performance with differential encoding. Differential encoding is often used with coherent modulation techniques to resolve the 180° phase ambiguity problem associated with carrier recovery at the receiver*. Note that DOQPSK with SEC is very near this theoretical lower bound.

To this point, we have mainly compared the modulation strategies in terms of their performance in a non-multipath channel. Figure 6.2 shows the performance of the best three modulation strategies of each type (as described above) under fading conditions. These results clearly indicate that DOQPSK is superior under fading conditions as well. In all three cases, performance degrades considerably with increased fading (channel K-factor). Similar performance is obtained when the nonlinearity is introduced, although the TTIB ACSSB case degrades somewhat more than the other two cases. Again performance has been presented for the non-ideal TTIB ACSSB modem. With ideal subband recombining, the performance under multipath conditions ($K > -10$ dB) is very similar to that obtained for DOQPSK. Thus, while pilot-oriented techniques may have an advantage over differential techniques at high SNR's (e.g. land mobile), they do not at the low to moderate SNR's typical of mobile-satellite links.

In summary, a very useful software tool has been developed which can be used to analyze a wide range of modulation schemes under numerous time varying multipath channel scenarios. Of the three modulation strategies considered,

*A preamble could also be used to resolve the phase ambiguity at the receiver, but is not very practical for a fading channel.

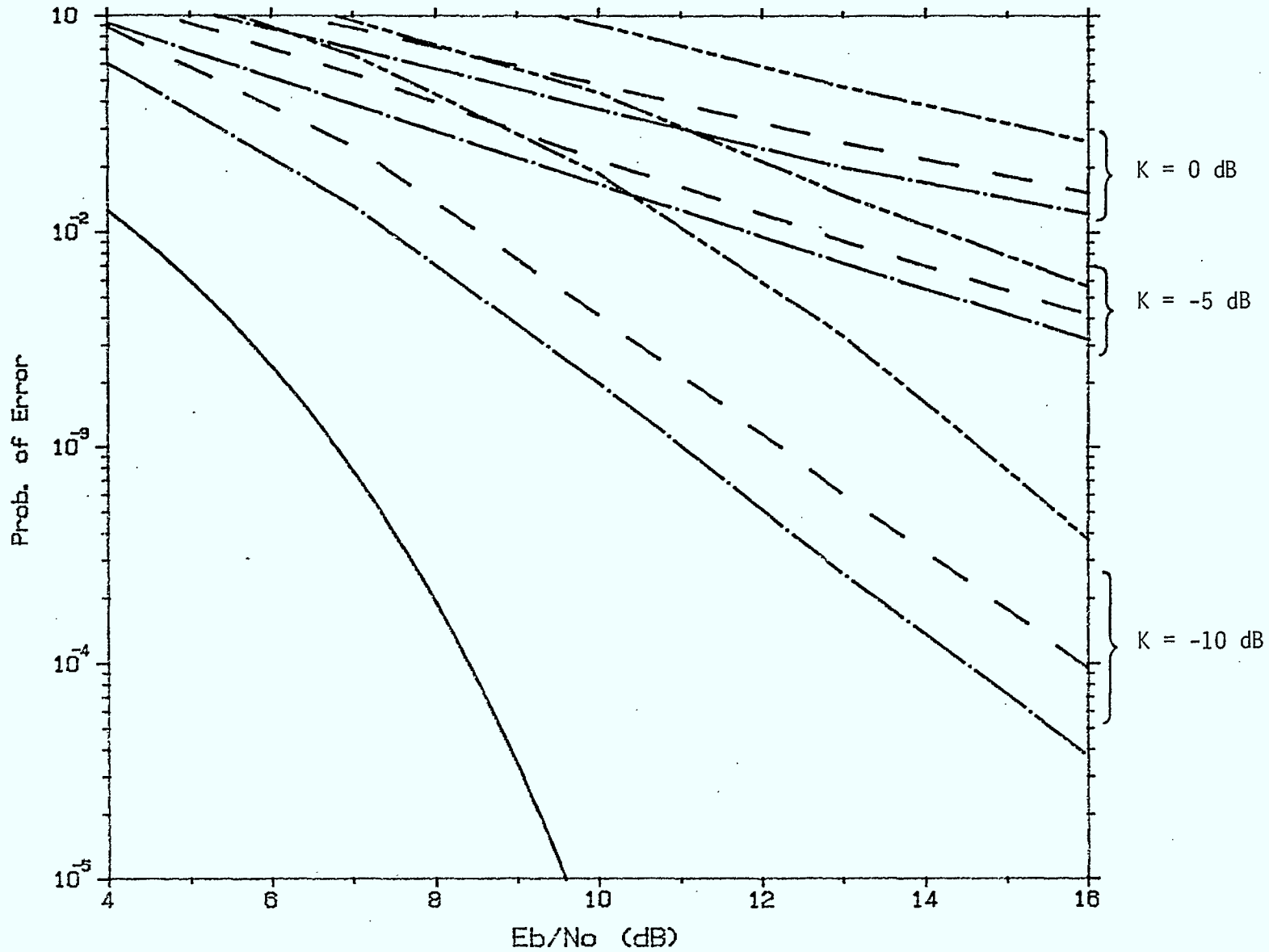

Comparison of DMSK(SEC), DOQPSK(SEC) and BPSK with ACSSB

DMSK (SEC) DOQPSK (SEC)

BPSK with ACSSB (-5 dB pilot)

Ideal Coherent

Figure 6.2

differentially detected offset QPSK, with 50% rolloff root raised cosine spectral shaping, is clearly superior for both the forward and return link of a mobile-satellite communications channel. This scheme performs very close to ideal and has a significant advantage over both DMSK and BPSK in conjunction with a TTIB ACSSB modem. The former suffers from degraded performance due to significant intersymbol interference caused by receive filtering. The latter is degraded because of the poor performance of the coherent subband recombining over the range of signal-to-noise ratios of interest.

The simple structure of the specific DOQPSK scheme considered suggests that a fairly inexpensive digital/software modem could easily be developed. With the superior performance indicated above, such a modem should have good market potential, especially for low power, mobile-satellite applications.

6.1 Recommendations For Further Work

A number of areas merit further investigation. These include:

(a) DOQPSK signalling with filtering after a hard limiter. This scheme should yield a close to constant signal envelope with reduced adjacent channel interference.

(b) Multiple parity branches to improve the performance with non-redundant error correction.

(c) Forward error correction coding with interleaving (time diversity) to combat fading. Both soft and hard decision coding should be considered.

Interleaving is very important to obtain the time diversity required to improve performance with fading channels.

(d) Channel estimation. With multilevel signalling and/or soft decision decoding it is important to have an estimate of the channel state or quality, especially for time-varying channels.

(e) Non-linearity estimation from either the transmit or receive end. This may be required if multilevel signalling schemes are employed.

REFERENCES

[1] J. R. Ball, A Real-Time Fading Simulator for Mobile Radio, The Radio and Electronic Engineer, Vol. 52, No. 10, pp 475-478, October 1982.

[2] S. Crozier et al., Phase I of the Development of the Demodulator Portion of a JTIDS Receive Terminal, Final Report, Miller Communications Systems Report, SSC File No: 21ST.36001-1-1401, MCS File No. 8231, April 1982.

[3] K. W. Moreland et al., Definition Study to Determine the Technical Requirements and Develop Cost Estimates For MSAT Data Services Final Report, Miller Communications Systems Report, DSS File No: 01SM.36001-3200, MCS File No: 8418-A, July 1984.

[4] S. A. Gronemeyer and A. L. McBride, MSK and Offset QPSK Modulation, IEEE Trans. on Comm., Vol-COM-24, No. 8, August 1976.

[5] W. Bennett and J. Salz, "Binary Data Transmission by FM Over a Real Channel", BSTS, September 1963, pp. 2387-2426.

[6] T. Masamura et al., "Differential Detection of MSK with Nonredundant Error Correction", IEEE Trans. on Comm., Vol. COM-27, No. 6, June 1979.

[7] R. K. Tiedemann and S. Crozier, Proposal for Modulation and Coding Study of Data Transmission from the Gateway Station to the Mobile and Vice Versa, MCS File No: 85063, January 10, 1985.

[8] Appendix "A", Statement of Work, DSS File No. 29ST.36001-4-2612 (Subject RFP).

[9] J. P. McGeehan and A. J. Bateman, "Phase-Locked Transparent Tone-in-Band (TTIB): A New Spectrum Configuration Particularly Suited to the Transmission of Data Over SSB Mobile Radio Networks", IEEE Trans. Commun., vol. COM-32, pp. 81-86, January 1984.

[10] L. Rabiner and B. Gold, Theory and Application of Digital Signal Processing, Prentice-Hall, Englewood Cliffs, New Jersey, 1975.

[11] P. R. K. Chow and D. H. S. Ko, "Improving DCPSK Transmission by Means of Error Control", IEEE Trans. Commun., vol. COM-19, p. 715, October 1971.

[12] J. G. Proakis, Digital Communications, McGraw-Hill, 1983.

[13] M. Abramowitz and I. Stegun, eds, Handbook of Mathematical Functions, Dover Publications, New York, 1972.

[14] C. Loo, "A Statistical Model for a Land Mobile Satellite Link", ICC'84.

[15] J. Butterworth and E. Matt, "The Characterization of Propagation Effects For Land Mobile Satellite Services", IEE Conference Publications No. 222: Satellite Systems for Mobile Communications and Navigation, London, June 1983.

[16] R. de Buda, "Coherent Demodulation of Frequency-Shift Keying with Low Deviation Ratio", IEEE Trans. Commun. (concise paper), Vol. COM-20, pp. 429-435, June 1972.

[17] M. L. Doelz et al, "Minimum-Shift Data Communication System", U.S. Patent Number 2 977 417, March 1961.

[18] H. R. Mathwich, J. F. Balcewicz, M. Hecht, "The effect of tandem band and amplitude limiting on the E_b/N_o performance of minimum (frequency) shift keying (MSK)", IEEE Trans. Commun., vol. COM-22, October 1974.

[19] R. Matyas, S. Sunter, C. Jagger, P. Jeans, "An LSI FFSK (MSK) Modem", Proc. NTC '81, New Orleans, November 30 - December 4.

[20] H. Suzuki, "Optimum Gaussian Filter for Differential Detection of MSK", IEEE Trans. Commun, Vol. COM-29, June 1981.

[21] S. Crozier, B. Mazur, R. Matyas, "Performance Evaluation of Differential Detection of MSK", Global Telecommunications Conference, Miami, November, 1982, pp. A5.1.1-.5.

[22] H. C. Chan, D. P. Taylor, S. S. Haykin, "A comparative study of digital modulation techniques for single-carrier satellite communications", presented at the 3rd Int. Conf. Digital Satellite Communications, Kyoto, Japan, November 1975, Paper B2.

[23] F. M. Gardner, "Carrier and Clock Synchronization for TDMA Digital Communication", European Space Research Organization, ESTEC Report 744976, Noordwijk, Netherlands; June 1974.

[24] A. V. Oppenheim and R. W. Schafer, Digital Signal Processing, Prentice Hall, 1975.

APPENDIX A

DERIVATION of E_b/N_o

A.0 DERIVATION OF RF EQUIVALENT E_b/N_o AT COMPLEX BASEBAND

In the real world signals are "real". (Profound isn't it!) The problem, when modelling RF systems using complex baseband equivalent techniques, is to come up with the correct model for the complex baseband noise process which corresponds to the proper RF definition of E_b/N_o.

Consider the real RF signal and real RF noise processes depicted in Figure A.1(a). These signal and noise processes are assumed to be centred at a carrier frequency of f_o with their bandwidths restricted to B Hz. The two-sided noise power spectral density is defined as $N_o/2$ watts/Hz.

The total received RF waveform is given by

$$r_{RF}(t) = s_{RF}(t) + n_{RF}(t) \tag{A.1}$$

The RF signal and noise contributions can be modelled as

$$\begin{aligned} s_{RF}(t) &= d_c(t)\cos(2\pi f_o t) - d_s(t)\sin(2\pi f_o t) \\ &= \mathrm{Re}\left[d(t)\exp(2\pi f_o t)\right] \end{aligned} \tag{A.2}$$

and

$$\begin{aligned} n_{RF}(t) &= n_c(t)\cos(2\pi f_o t) - n_s(t)\sin(2\pi f_o t) \\ &= \mathrm{Re}\left[n(t)\exp(2\pi f_o t)\right] \end{aligned} \tag{A.3}$$

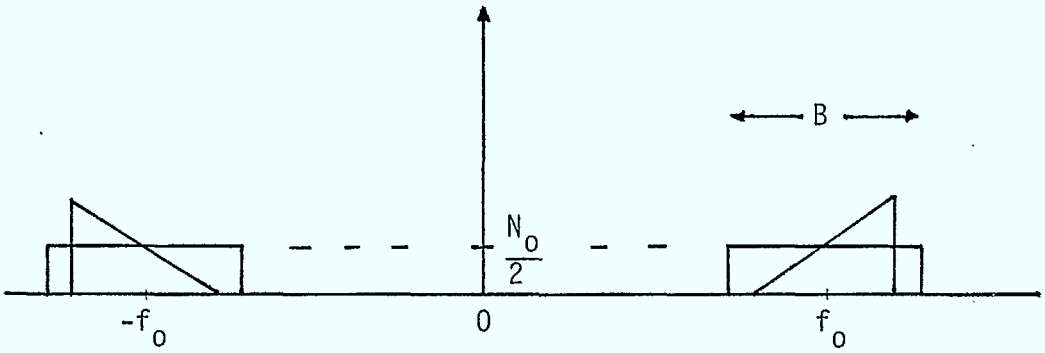

a) RF Signal and Noise Power Spectrum

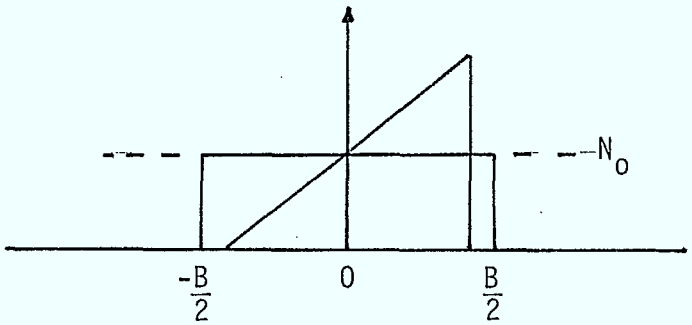

b) Complex Baseband Equivalent Signal and Noise Power Spectrums (scaled so that the baseband signal power is equal to the RF signal power).

Figure A.1 RF and Complex Baseband Equivalent Power Spectrums

respectively, where by definition the complex baseband equivalent signal and noise envelope waveforms are given by

$$d(t) \triangleq d_c(t) + j\, d_s(t) \tag{A.4}$$

$$n(t) \triangleq n_c(t) + j\, n_s(t) \tag{A.5}$$

If we let d(t) be a single (real or complex) data pulse corresponding to a single bit of information, then the received energy per bit is simply given by

$$\begin{aligned} E_b &= \int s_{RF}^2(t)\, dt \\ &= \frac{1}{2} \int |d(t)|^2 dt \\ &\triangleq \frac{1}{2} E_d \end{aligned} \tag{A.6}$$

where by definition E_d is the baseband energy in d(t).

The average noise power in bandwidth B is given by

$$\begin{aligned} P_n &= \lim_{T\to\infty} \frac{1}{T} \int_0^T n_{RF}^2(t)dt \\ &= \frac{1}{2} E[n_c^2(t)] + \frac{1}{2} E[n_s^2(t)] \\ &= \frac{1}{2} \sigma_c^2 + \frac{1}{2} \sigma_s^2 \\ &= N_o B \end{aligned} \tag{A.7}$$

where σ_c^2 and σ_s^2 are the variances of real baseband noise processes $n_c(t)$ and $n_s(t)$ respectively. Letting $\sigma_c^2 = \sigma_s^2 = \sigma^2$, as is the case for normal white Gaussian noise (WGN), we have

$$\sigma^2 = N_o B \tag{A.8}$$

Note that both real baseband noise processes have variance σ^2, and thus the total power or variance of $n(t)$ is $2\sigma^2$. Combining results (A.6) and (A.8) yields

$$\frac{E_b}{N_o} = \frac{B\ E_d}{2\sigma^2} \tag{A.9}$$

Thus far we have not addressed the implications of a discrete signal model. The complex baseband equivalent signal and noise processes are bandlimited to the interval $[-B/2,\ B/2]$, as shown in Figure A.1(b). Thus the Nyquist sampling frequency is B and the sampling period is $\tau = 1/B$. Then, by using Nyquist's theorem, it can be shown that

$$\begin{aligned} E_d &= \int \left|d(t)\right|^2 dt \\ &= \tau \sum_k \left|d_k\right|^2 \\ &\triangleq \tau\ S \end{aligned} \tag{A.10}$$

where d_k is defined as $d(k\tau)$, that is the k-th Nyquist sample of $d(t)$. If complex noise samples $n_k = n(k\tau)$ are also taken at the Nyquist sampling rate, then from (A.8) the real and imaginary noise components will each have variance

$$\sigma^2 = \frac{N_o}{\tau} \tag{A.11}$$

Combining results (A.6), (A.10) and (A.11) yields

$$\frac{E_b}{N_o} = \frac{S}{2\sigma^2} \tag{A.12}$$

where S is the discrete sum computed as defined in (A.10). Typically E_b/N_o is an input to a simulation program and the variance of the discrete complex baseband noise process is to be calculated. Rearranging (A.12) gives the desired result as

$$\mathrm{Var}[n_k] = 2\sigma^2 = \frac{S}{(E_b/N_o)} \tag{A.13}$$

The above result was derived for an isolated data pulse, d(t). It can be shown that the result still holds true for continuous data streams (real or complex) provided the channel bits are uncorrelated or the data pulses are orthogonal. The average energy per bit can be different, however, when dealing with intersymbol interference (ISI) and correlated channel bits.

APPENDIX B

CONSTRUCTIVE AND DESTRUCTIVE ALIASING

B.0 CONSTRUCTIVE AND DESTRUCTIVE ALIASING

Many of the generated power spectrums have displayed some peculiar behaviour near the "assumed Nyquist" frequency. In particular, if a symmetric impulse response is sampled at its peak then the spectrum is close to 6 dB higher than expected at plus and minus half the sampling rate (R_s). But, if the impulse response is shifted half a sample period then the spectrum tends to fall off very rapidly near the assumed Nyquist frequency. The suspected cause was some sort of constructive or destructive aliasing. This is indeed the case as is discussed below.

Let h(t) be a real impulse response symmetric about t=0. Then the Fourier transform of h(t), H(f), is also real and symmetric about f=0. Now consider a sampled version of h(t), namely

$$s(t) = h(t) \cdot \delta_T(t) \tag{B.1}$$

where $\delta_T(t)$ is a train of sampling impulses spaced at T intervals, and is given by

$$\delta_T(t) \triangleq T \sum_n \delta(t-nT) \tag{B.2}$$

The Fourier transform of $\delta_T(t)$ is a train of impulse in the frequency domain, given by

$$\delta_{1/T}(f) = \sum_k \delta(f-k\frac{1}{T}) \tag{B.3}$$

Thus the spectrum of s(t), S(f), is given by

$$S(f) = H(f) * \delta_{1/T}(f) \tag{B.4}$$

where * is the convolution operator. If the one-sided bandwidth of H(f) is greater than half the sampling rate, $R_s/2$, then aliasing will occur. If H(f) falls off fairly quickly beyond $R_s/2$, then S(f), in the vicinity of $R_s/2$, is given by

$$S(\frac{R_s}{2} + \Delta) = H(\frac{R_s}{2} + \Delta) + H(-\frac{R_s}{2} + \Delta)$$

$$= H(\frac{R_s}{2} + \Delta) + H(\frac{R_s}{2} - \Delta) \qquad (B.5)$$

Thus S(f) is approximately 6 dB higher than H(f) in the vicinity around $R_s/2$ provided H(f) does not change too quickly with small frequency offset Δ. In fact S(f) is exactly 6 dB higher at the assumed Nyquist frequency of $R_s/2$. This is due to perfect coherent aliasing.

Delaying h(t) by τ, which results in the time samples being offset by τ, introduces a phase ramp to H(f). The new H(f) is given by

$$H'(f) = H(f)\ \exp(-j2\pi\tau f) \qquad (B.6)$$

The corresponding new S(f), in the vicinity of $R_s/2$, is given by

$$S'(\frac{R_s}{2} + \Delta) = H(\frac{R_s}{2} + \Delta)\ \exp(-j\ \frac{\pi\tau}{T} - j2\pi\tau\Delta)$$

$$+H(\frac{R_s}{2} - \Delta)\ \exp(+j\ \frac{\pi\tau}{T} - j2\pi\tau\Delta) \qquad (B.7)$$

When $\tau = nT$, n an integer, the aliasing is in phase and the power of S'(f) is approximately 6 dB higher than that of

$H'(f)$ in the vicinity of $R_s/2$. When $\tau = T/2+nT$ the aliasing is 180° out of phase and $S'(f)$ is forced to roll off to zero at $R_s/2$. Thus we see that the aliasing can be forced to be constructive or destructive depending on the delay of $h(t)$ when sampled.

When implementing digital filters it is often desirable to have the filter roll-off sharply to zero at the Nyquist frequency. From the above analysis we see that any symmetric (about $t=0$) impulse response will have this desired frequency characteristic if it is sampled with a $T/2 + nT$ delay, n an integer.

APPENDIX C

A THEORETICAL BOUND ON BER PERFORMANCE OVER RICIAN FADING CHANNELS

C.0 INTRODUCTION

This appendix derives some theoretical performance curves for ideal differential detection in a Rician fading channel when the fading bandwidth is much narrower than the data bandwidth.

C.1 The Rician Fading Channel

If the transmitted signal is s(t), then the output of the fading channel model, r(t), is given by

$$r(t) = s(t) + A(t)e^{j\theta(t)}s(t) + n(t) \qquad (C.1)$$

where $A(t)e^{j\theta(t)}$ is a complex gain associated with the Rayleigh fading path and n(t) represents additive white Gaussian noise. In this model it is assumed that the delay of the Rayleigh fading path relative to the direct path is negligible.

The noiseless received signal can be written as

$$r_o(t) = c(t)e^{j\phi(t)}s(t) \qquad (C.2)$$

$$= [1 + A(t)e^{j\theta(t)}]\ s(t)$$

$$= [1 + a_i(t) + ja_q(t)]s(t) \qquad (C.3)$$

where $a_i(t)$ and $a_q(t)$ are orthogonal Gaussian processes with spectral characteristics typical of the fading process being modelled. Thus

$$c(t) = \sqrt{(1 + a_i(t))^2 + a_q^2(t)} \tag{C.4}$$

$$\phi(t) = \tan^{-1} \left\{\frac{a_q(t)}{1+a_i(t)}\right\} \tag{C.5}$$

The fundamental assumption of this analysis is that the fading bandwidth is narrow with respect to the data bandwidth. This is used to claim that in the case of differential detection, the phase change due to the Rician fading between successive bits is small and has negligible affect on detection

With this assumption, it is argued that the effect of the phase term in the received signal is eliminated and can be dropped from further consideration and we only need consider the case

$$r_1(t) = c(t)\ s(t) + n(t) \tag{C.6}$$

where c(t) is given by (C.4).

Under these conditions the received signal to noise ratio is given by

$$\gamma(t) = c^2(t)\ \frac{|s(t)|^2}{|n(t)|^2} \tag{C.7}$$

If we assume that the ratio of the direct path power to noise is relatively constant at γ_o, that is,

$$\gamma_o = \left(\frac{|s(t)|^2}{|n(t)|^2}\right)\Bigg|_{\text{average}} \tag{C.8}$$

then $\gamma(t) = c^2(t)\gamma_o$. thus the received signal has effectively a time varying signal to noise ratio. And from the definition of c(t) in (C.4) and the fact that $a_i(t)$ and $a_q(t)$ are Gaussian processes of zero mean and equal variance, it is obvious that $\gamma(t)$ has a Rician distribution (i.e. non-central Chi-squared of degree 2) and if we define

$$k = E[a_i^2(t)] + E[a_q^2(t)]$$

and also define $2\sigma^2 = k\gamma_o$, then the probability density function of $\gamma(t)$ is given by [12]

$$P_\gamma(\gamma) = \begin{cases} \frac{1}{2\sigma^2} e^{-(\gamma_o+\gamma)/2\sigma^2} I_o\left(\frac{\sqrt{\gamma\gamma_o}}{\sigma^2}\right) & \gamma \geq 0 \\ 0 & \gamma \leq 0 \end{cases} \qquad (C.9)$$

where $I_o(\cdot)$ is the modified Bessel function of order zero. In fact a more convenient form of this is the probability density function of $y = \sqrt{\gamma}$ [12]

$$P_y(y) = \begin{cases} \frac{y}{\sigma^2} e^{-(\gamma_o+y^2)/2\sigma^2} I_o\left(\frac{y\sqrt{\gamma_o}}{\sigma^2}\right) & y \geq 0 \\ 0 & y \leq 0 \end{cases} \qquad (C.10)$$

This will is used in the following calculations.

C.2 Ideal Differential Detection in a Rician Fading Channel

With an ideal signal format, that is matched filtering and a Nyquist pulse shape, the BER performance of a differential detector is given by [12]

$$p^d = \frac{1}{2} e^{-\gamma_b} \tag{C.11}$$

where γ_b is the signal to noise ratio per bit ($\gamma_b = E_b/N_o$) and p^d is the probability of error. This could be rewritten as

$$p^d = P_{e|\gamma} \ (\text{error}|\gamma_b). \tag{C.12}$$

That is, p^d is the probability of error given the signal to noise ratio, γ_b, and if we have a slowly varying signal to noise ratio, one could average this probability of error by the distribution of the signal to noise ratios

$$P_R^d = \int P_{e|\gamma}(\text{error}|\gamma) \ P_\gamma(\gamma) \ d\gamma \tag{C.13}$$

The assumption that the signal to noise is slowly varying is demanded, because (C.11) assumes that the signal to noise ratio is at least constant over the duration of the bit estimation; and depending on the pulse shape, a single bit may be estimated over the information gathered over many adjacent bit intervals and the signal to noise ratio should be constant over this period. If the bandwidth of the fading process is narrow with respect to the data rate, then the requirement should be approximately met.

To evaluate (C.13) we could substitute formulas (C.12), (C.11), and (C.9) but it will be easier to work in terms of $y = \sqrt{\gamma}$ and so equation (C.10) will be used instead.

Thus, the probability of error over a Rician fading channel using ideal differential detection is given by

$$P_R^d = \frac{1}{2\sigma^2} \int_0^\infty y\, e^{-y^2}\, e^{-(\gamma_o+y^2)/2\sigma^2}\, I_o\left(\frac{y\sqrt{\gamma_o}}{\sigma^2}\right) dy \qquad (C.14)$$

$$= \frac{e^{-\gamma_o/2\sigma^2}}{2\sigma^2} \int_o^\infty y\, e^{-\alpha^2 y^2}\, I_o(\beta y)\, dy \qquad (C.15)$$

where $\alpha^2 = (1+\frac{1}{2\sigma^2})$ and $\beta = \sqrt{\gamma_o}/\sigma^2$. And from [13.(11.4.29)],

$$\int_o^\infty y\, e^{-\alpha^2 y^2}\, J_o(\beta y)\, dy = \frac{1}{2\sigma^2}\, e^{-\frac{\beta^2}{4\alpha^2}} \qquad (C.16)$$

where $J_o(y)$ is the ordinary Bessel function of order zero. Note that by [13.(3.6.3)]

$$I_o(\beta y) = J_o(i\beta y) \qquad (C.17)$$

where $i^2 + 1 = 0$. So that applying (C.16) to (C.15) with the appropriate change of variable ($\beta \to i\beta$)

$$P_R^d = \frac{e^{-\gamma_o/2\sigma^2}}{2\sigma^2}\; \frac{e^{\gamma_o/\sigma^4 4\alpha^2}}{2\alpha^2}$$

which upon noting that $2\alpha^2\sigma^2 = (2\sigma^2+1)$, reduces to

$$P_R^d = \frac{1}{2(2\sigma^2+1)}\, e^{-\gamma_o/(2\sigma^2+1)} \qquad (C.18)$$

This provides a simple formula for estimating optimum performance with differential detection under the previously discussed multipath conditions. Using the definition of σ^2 this can be rewritten as

$$P_R^d = \frac{1}{2(k\gamma_o + 1)} e^{-\gamma_o/(k\gamma_o+1)} \tag{C.19}$$

and K = 10 log k is the Rician channel fading factor. Note that γ_o is the signal to noise ratio excluding the multipath signal.

This theoretical bit error rate performance is plotted against E_b/N_o(SNR) for various K factors in Figure C.1.

Note that if $k\gamma_o \gg 1$, then

$$P_R^d \sim \frac{1}{2\,k\gamma_o} e^{-1/k}$$

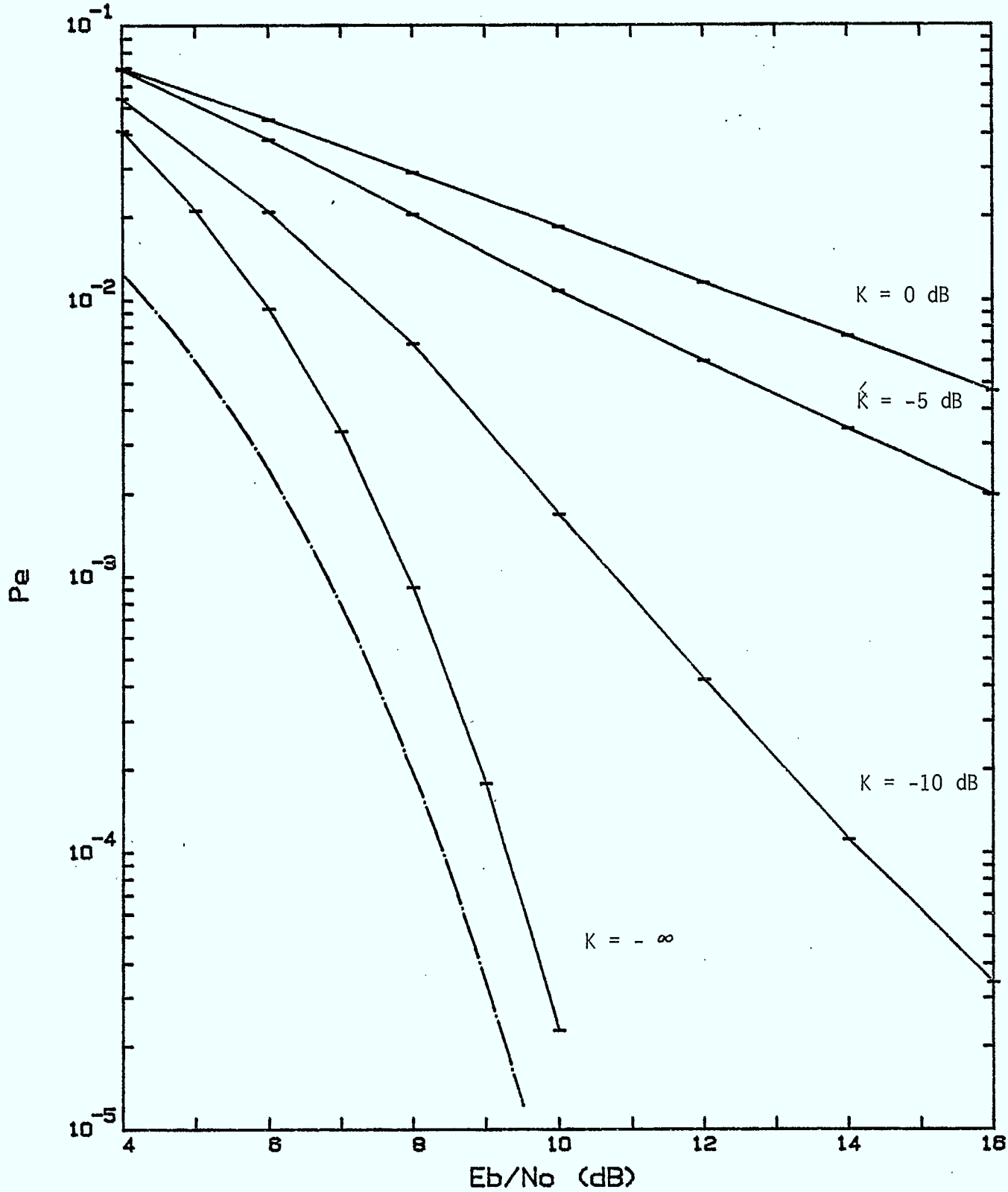

BER Performance of Ideal Differential Detection in Multipath

——————— Rician Channel Factors - K =

—·—·—·— Ideal Coherent Performance

Figure C.1

APPENDIX D

SOFTWARE DOCUMENTATION

TABLE OF CONTENTS

D.0 INTRODUCTION

The software simulation of an MSAT land mobile communications channel was developed using the VAX version of Fortran 77 under the VMS operating system on a VAX 11/750. The main constraint of the simulation under this configuration is the time required to simulate the large amounts of data needed to characterize low bit error rates.

The simulation is a continuous time simulation of both the gateway station to land mobile, and the land mobile to the gateway station links of an MSAT data communications channel. The nominal bit rate is 2.4 kbps but the majority of the simulation calculations are independent of this. (Simulation of other bit rates may require minor adjustments of the software).

The particular model of a mobile satellite communications channel which was simulated is included in Figure D.1. The applicability of this model to the problem being studied is discussed in Section 1.0. The block diagram of Figure D.1 is directly applicable to the simulation program. The simulation includes a data generation module which generates an independent random sequence of data bits. A data encoding module, which may be specified to differential encoding of the data, and one or two (orthogonal) channel signalling must be chosen. This is followed by pulse shaping and transmit filtering of the encoded data sequence. There may (will) be a non-linear amplifier in the (mobile) transmitter.

A Rician statistical model is used to simulate the channel behaviour and there is additive white Gaussian noise at the receiver. There is filtering at the receiver and a choice

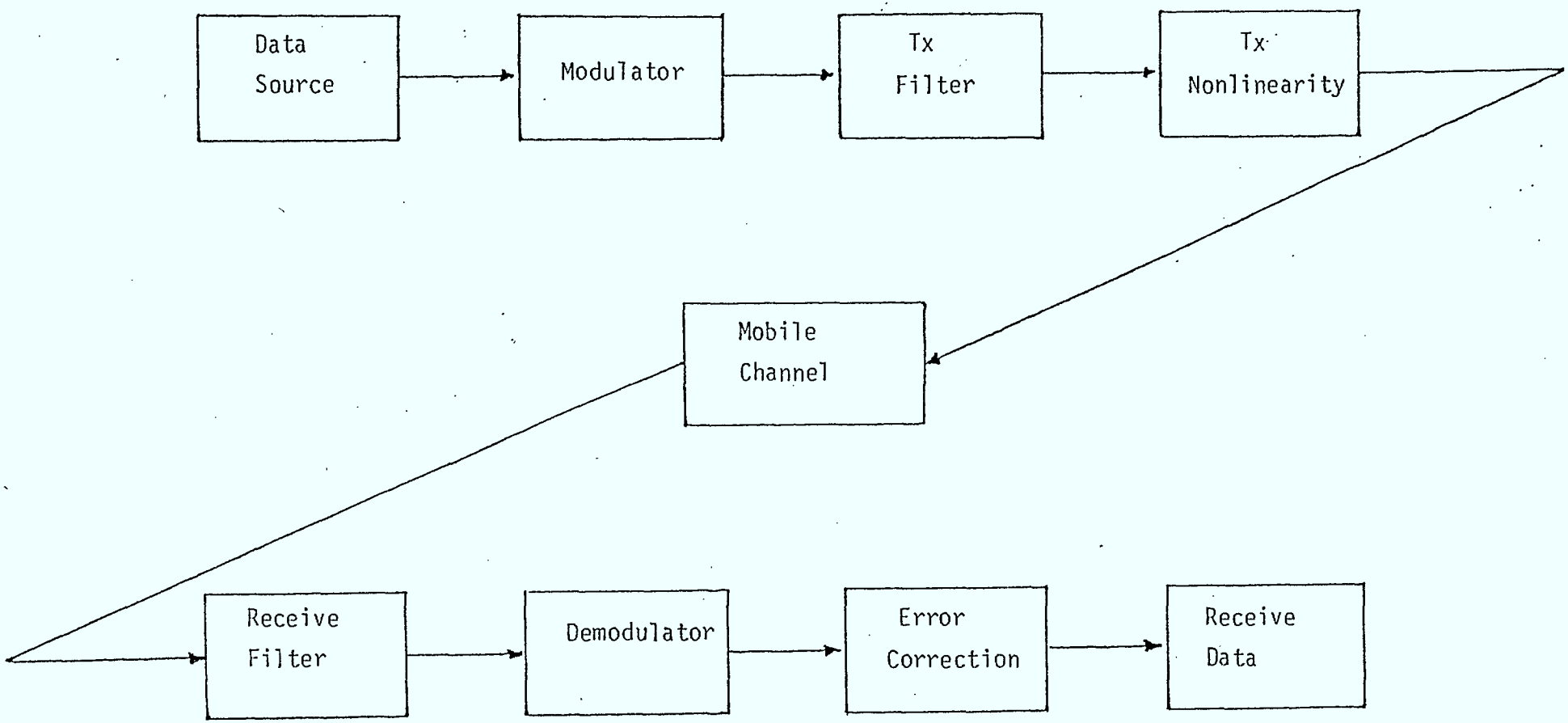

Figure D.1 Simplified Model of Mobile Satellite Communications Channel

of coherent or differential detection. Depending upon the encoding and detection strategy, there is also the possibility of error correction at the receiver. The last step in the simulation is the gauging of performance through the collection of error statistics.

The simulation is carried out in a block processing mode, passing one block of samples completely through the simulation before starting the next. To maintain continuity between blocks, all devices with memory are implemented using the overlap and save technique. All memory devices such as filters are assumed to have finite memory, this limit provides the maximum size of the overlap required.

The main performance criteria produced by the simulation program is the output bit error rate as a function of the input parameters. The entire simulation is performed using a complex baseband representation of the signal.

D.1 Using the Simulation Program

D.1.1 Program Structure

The overall design of the simulation software is drawn from physical considerations of the MSAT communications channel. A block diagram of the MSAT communications channel simulation is shown in Figure D.1. As illustrated in Figure D.1, the communications link consists of the following steps:

- generation of an independent random data sequence

- encoding of the data. This may be specified to be differential encoding and includes the generation of a real or complex impulse train representing the data to be transmitted.

- pulse shaping at complex baseband

- transmit filtering the data to limit adjacent channel interference if required.

- passing the data through an optional non-linearity

- passing the data through the mobile channel which consists of a Rician fading path and additive white noise

- receive filtering the data to limit the noise

- demodulation which corresponds to differential or coherent detection

- performing error correction if possible

- comparing the transmitted and received bit sequences and determining the error statistics.

This system structure is reflected in the software structure which is shown in Figure D.2. For module independence, the vector of signal samples is always in the time domain when in the main procedure. Any subroutine called by the main procedure can assume this, and it also must return the signal vector in the time domain. The input and output details required to run the simulation are discussed in the following two sections. The programming and implementation details are described in Section D.2.

D.1.2 Input Conventions

All of the inputs to the MSATSP program except the run identification label come from files. All information excluding device information comes from the parameter file.

Program MSATSP	-	MSAT Land Mobile Communications Simulation Program
INPUT	-	reads input parameters from a parameter file
INIT	-	initializes all necessary program variables, including filter profiles and overlap vectors
DATAGEN	-	generates a sequence of random bits using the Fortran random number generator
SIGGEN	-	generates a train of impulses corresponding to the data bits (possibly differentially encoded) at spacings appropriate for the sampling rate
FILTER	-	depending on the passed parameters, this program will do any of: the pulse shaping, transmit filtering or receive filtering
TXACSSB	-	modulation portion of ACSSB modem
NONLIN	-	implements a general AM-AM and AM-PM nonlinearity
CHANEL	-	passes the signal through a Rician fading channel and adds Gaussian white noise
RXACSSB	-	demodulation portion of ACSSB modem
DIFFDET	-	implements a differential detection circuit for estimating the data bits
COHDET	-	implements a coherent detection circuit for estimating the data bits (mainly used for bench marking purposes)
ERRCOUNT	-	compares the transmitted and received bit sequences and determines error statistics
OUTPUT	-	saves the collected error statistics on file.

Figure D.2: High Level Structure of MSATSP Simulation Program

For example if the run identification is MSK01, then the program will attempt to obtain further information from the file MSK01.PAR. This includes simulation information such as the number of samples per bit, number of bits to simulate, the random number seeds, the desired E_b/N_o and K, the Rician channel fading factor. A typical input parameter file is shown in Figure D.3. In this file, there is one input per line; as indicated by the comments in the figure, the first line represents the name of the file where the pulse shaping filter can be found. The second line represents the name of the file where the transmit filter may be found. The same file name can be repeated on multiple lines, such as in the case of matched filtering, without causing any difficulty. In the case that a device is not required such as the transmit filter then NONE should be entered as the device name. In cases such as the ACSSB modem where there are a number of input parameters associated with one device, e.g. the transmit and receive subband filters, the type of carrier recovery and the AGC filter, to be safe all device lines should be NONE if the ACSSB modem is not be be included. The program however does do some checking and if only the transmit subband filter is NONE then it ignores other lines relevant to the ACSSB modem. Note that if the ACSSB modem is included, the program does not check that the detector is coherent and the modulation type is BPSK because these are not strictly required although this was the only scenario tested.

Most of the input parameters are self-evident from the comments given in Figure D.3; in some cases the permissible parameter values are stated. In the case of the number of samples of overlap, this refers to the maximum overlap required to accommodate the memory of any device. For example, if the only memory devices included in the

```
TX2MSK.DAT          ! pulse shaping filter
NONE                ! transmit filter
NONE                ! ACSSB transmit subband filter
NONE                ! ACSSB receive subband filter
AGCF4.DAT           ! Rx ACSSB A.G.C. filter
NONIDEAL            ! ACSSB subcarrier recovery (IDEAL or NONIDEAL)
BUT1131.DAT         ! receive filter
DEFAULT.DAT         ! non-linearity name
MUL.DAT             ! multipath filter name
DMSK                ! encoder type e.g.MSK,OQPSK,DMSK,DOQPSK,BPSK
SEC                 ! detector type (DIFF,SEC or COHERENT)
4                   ! samples per bit period
1024                ! block size
10.                 ! signal to noise ratio ( dB )
-10.0               ! Rician channel K factor ( dB )
1.0                 ! non-linearity backoff
0.04166667          ! fading bandwidth to bit rate ratio
40                  ! number of samples of overlap
400                 ! number of bits per subrun
-5.                 ! d.c. pilot level (dB) in ACSSB modem
2345678             ! seed for data generator
3456789             ! seed for multipath channel
4567890             ! seed for channel noise
```

Figure D.3 Typical parameter file.

simulation were FIR filters (this is the usual case) then the number is the maximum length of all of the FIR filters used. Note that the multipath filter is a special case and should not be included in this calculation. And also note that the program may increase this number slightly so that it corresponds to an integer number of bits.

Each simulation run is divided into eight subruns; the bit error rate obtained is the average of all eight subruns, and the subruns are used to estimate the deviation of the bit error rate estimated. This should clarify what the parameter number of bits per subrun means.

The input parameter file can be altered by the user with a text editor. Note that some parameters such as the maximum array size and maximum overlap, are fixed in the program and the user can only use values up to this limit. The limits can be adjusted but it requires re-compiling and re-linking the program.

Further details on the parameter file format can be found in the file PARAMETER.HLP.

The device files are of a specified format and are usually constructed using a utility program which is external to the simulation package. Included with the simulation package are a number of previously created device files which were used in testing the simulation. A list of these files is given in Table D.1, along with comments about the contents of each file. This information is also available on the computer system in the file DEVICEDAT.HLP. To gain immediate familiarity with system the user can use the stated parameter file format and select files from this device file list to construct a complete simulation in a very short time. To create new device files with the proper format, the reader should see the appropriate topic in the detailed software description (Section D.2.1).

ACCF4.DAT - 51 tap FIR lowpass filter with a one-sided bandwidth of approximately 100 Hz. Used in the ACSSB demodulator to recover the d.c. pilot. (see Fig. 5.7 of MSAT Final Report) There are 1024 points at an assumed sampling rate of 9.6 ksps.

BUT1131.DAT - 31 tap FIR approximation to a Butterworth filter with a BT product of 1.1 (bit rate of 2.4 kbps). This is used as the receive filter for the DMSK simulation. (see Fig. 3.5 of MSAT Final Report) There are 1024 points at an assumed sampling rate of 9.6 ksps.

DEFAULT.DAT - this file contains the complex gain coefficients associated with the transmit nonlinearity suggested by the Scientific Authority. (see Fig. 2.2 of MSAT Final Report)

LIMITER.DAT - this file contains the complex gain coefficients associated with a hardlimiting nonlinearity.

MSKPULSE - 8 tap FIR approximation to the MSK pulse shape. This filter is coded directly in the software and no external files are required.

MUL.DAT - 1024 tap FIR approximation to the multipath spectral shaping filter used to simulate a Rician fading channel. It has a one-sided bandwidth of approximately 100 Hz. (see Fig. 2.4 of MSAT Final Report) There are 2048 points at an assumed sampling rate of 9.6 ksps. This is the standard format for the multipath filter; twice the block size of all other filters to account for its long impulse response.

RRC20.DAT - 40 tap FIR approximation to a root 20% rolloff raised cosine spectral shape with a 3 dB bandwidth of 2400 Hz. This file contains 1024 frequency domain samples at a sampling rate of 9.6 ksps.

RRC2015.DAT - 50 tap FIR approximation to a root 20% rolloff raised cosine spectral shape with a 3 dB bandwidth of 1800 Hz centred at 1500 Hz. (see Sec. 5.2.2 of MSAT Final Report) This file contains 1024 frequency domain samples at a sampling rate of 9.6 ksps.

Table D.1a Existing device files.

RRC2090.DAT - 50 tap FIR approximation to a root 20% rolloff raised cosine spectral shape with a 3 dB bandwidth of 1800 Hz centred at 900 Hz. (see Fig. 5.5 of MSAT Final Report) This file contains 1024 frequency domain samples at a sampling rate of 9.6 ksps.

RRC50.DAT - 40 tap FIR approximation to a root 50% rolloff raised cosine spectral shape with a 3 dB bandwidth of 2400 Hz. This file contains 1024 frequency domain samples at a sampling rate of 9.6 ksps.

RXF2.DAT - 19 tap FIR filter suggested by the Scientific Authority to be used as the receive subband filter in the ACSSB demodulator. This filter has a 3 dB bandwidth of 4800 Hz centred at 2400 Hz. (see Fig. 5.9 of MSAT Final Report)
This file contains 1024 frequency domain samples at a sampling rate of 9.6 ksps.

TX2MSK.DAT - 21 tap FIR filter representing the combination of a 8 tap FIR MSK pulse shaping filter and the 13 tap FIR transmit filter suggested by the Scientific Authority. (see Fig. 3.4 of MSAT Final Report)
This file contains 1024 frequency domain samples at a sampling rate of 9.6 ksps.

TXF1.DAT - 31 tap FIR filter suggested by the Scientific Authority to be used as the transmit subband filter in the ACSSB modulator. This filter has a 3 dB bandwidth of 4800 Hz centred at 2400 Hz. (see Fig. 5.6 of MSAT Final Report)
This file contains 1024 frequency domain samples at a sampling rate of 9.6 ksps.

TXFILT2 - 13 tap FIR filter suggested by the Scientific Authority to be used as the transmit filter in the case of MSK modulation. (see Fig. 3.3 of MSAT Final Report)
This file contains 1024 frequency domain samples at a sampling rate of 9.6 ksps.

Table D.1b Existing device files.

D.1.3 Output Conventions

The simulation program produces an output file which echoes most of the information of the input parameter file and provides the error statistics obtained for the given channel configuration. If the run identification is MSK01, then this information is placed in the file MSK01.RES. A typical output file is shown in Figure D.4 (a) and (b). The first section echoes the input parameters and the second section gives the statistics in each of the subruns and the overall statistics. If single error correction decoding was included, then an additional set of statistics would be printed describing these results. Most of the output information is self-evident, but note that the total number of bits simulated may be adjusted to a slightly higher number to reflect the fact that the simulation works with complete blocks of data.

D.1.4 Running The Simulation

To run the MSAT mobile satellite communications channel simulation program (MSATSP), the user must carry out the following steps. Ensure that an executable version of the simulation program exists (if not, one can be created as described in Section D.3). Create an appropriate input parameter file in the format described in Section D.1.2. Ensure that all required device files exist and that the device files and parameter file are in a directory which is accessible to the simulation program.

Once all of this has been done, run the program e.g. RUN MSATSP, and then in response to the request for a run identification type the name of the parameter file excluding the extension, e.g. MSK01, not MSK01.PAR. Note

Results of MSAT Land Mobile Simulation Program

System Characteristics

Pulse Shaping Filter:	TX2MSK.DAT
Transmit Filter:	NONE
ACSSB Tx Filter:	NONE
Nonlinear Device:	DEFAULT.DAT
ACSSB Rx Filter:	NONE
ACSSB AGC Filter:	AGCF4.DAT
ACSSB Carrier Rec.:	NONIDEAL
Receive Filter:	BUT1131.DAT
Multipath Filter:	MUL.DAT
Encoder Type:	DMSK
Detector Type:	SEC

Simulation Characteristics

Block size:	1024
Samples per Bit Period:	4
Bit per Block:	246
Overlap size:	40

Random Number Seeds

Data Seed:	2345678
Multipath Seed:	3456789
Channel Seed:	4567890

System Performance

Estimated Eb/No (dB):	10.000
Estimated Channel K Factor(dB):	-10.000
Operating point of non-linearity:	1.000
Ratio of fading BW to bit rate:	0.04167

Miscellaneous

Estimated channel delay: 25.000

Figure D.4a Typical first page of Output file.

Error Statistics
==========

	Run number 1	2	3	4
Average bit error rate (BER):	8.264E-03	0.000E+00	2.033E-03	1.016E-02
Number of bits simulated:	484	492	492	492
Number of +1 errors:	2	0	1	1
Number of -1 errors:	2	0	0	4
Number of error gaps 0 <...< 10	1	0	0	2
10 <...< 100	2	0	0	1
100 <...< 1000	1	0	1	2
1000 <...< 10000	0	0	0	0
...> 10000	0	0	0	0

	Run number 5	6	7	8
Average bit error rate (BER):	6.098E-03	6.098E-03	0.000E+00	1.016E-02
Number of bits simulated:	492	492	492	492
Number of +1 errors:	1	1	0	1
Number of -1 errors:	2	2	0	4
Number of error gaps 0 <...< 10	2	1	0	3
10 <...< 100	0	1	0	0
100 <...< 1000	1	1	0	1
1000 <...< 10000	0	0	0	1
...> 10000	0	0	0	0

Net average bit error rate: 5.352E-03
Standard deviation: 4.212E-03

Figure D.4b Typical second page of Output file.

that the extension is assumed to be PAR. This is all of the information required of the user. Some information will be output to the terminal at this point but all relevant information will be saved in the output file e.g. MSK01.RES. With this format and in some cases its long execution time, the simulation is suited to submitting to a batch queue if such facilities exist on the computer system.

D.1.5 HELP Facilities

Included with the software are a series of HELP files; these files can be identified by the extension .HLP. These files contain a variety of information which can be useful in running the simulation. Table D.2 gives the help file names and a brief description of their contents.

To read anyone of the help commands simply use the VAX TYPE facility, for example, execute

```
$ TYPE MSAT.HLP
```

to look at the MSAT.HLP file.

D.2 Detailed Software Description

A flowchart of the program is given in Figure D.5, as indicated for any particular simulation run all of the components listed there may not be used. The simulation is carried out in a block processing mode, passing one block of samples completely through the system before starting the next. To maintain continuity between blocks of samples, all devices with memory are implemented causally using the overlap and save technique (see Section D.2.6 for

MSAT	- provides the information in the remainder of this table.
DEVICE	- this provides information on the expected format of the device input files to the simulation program
DEVICEDAT	- provides information on existing device input files to the program
PARAMETER	- provides information on the expected format of the parameter input file to the simulation program
PROGRAM	- provides information on the structure of the program, subroutines, etc., useful for making program changes.
RUN	- provides information on how to run the program
LINK	- provides information on how to compile and link the program
UTILITY	- provides information on utility programs external to the main simulation program

Table D.2: HELP Files

Flow Chart

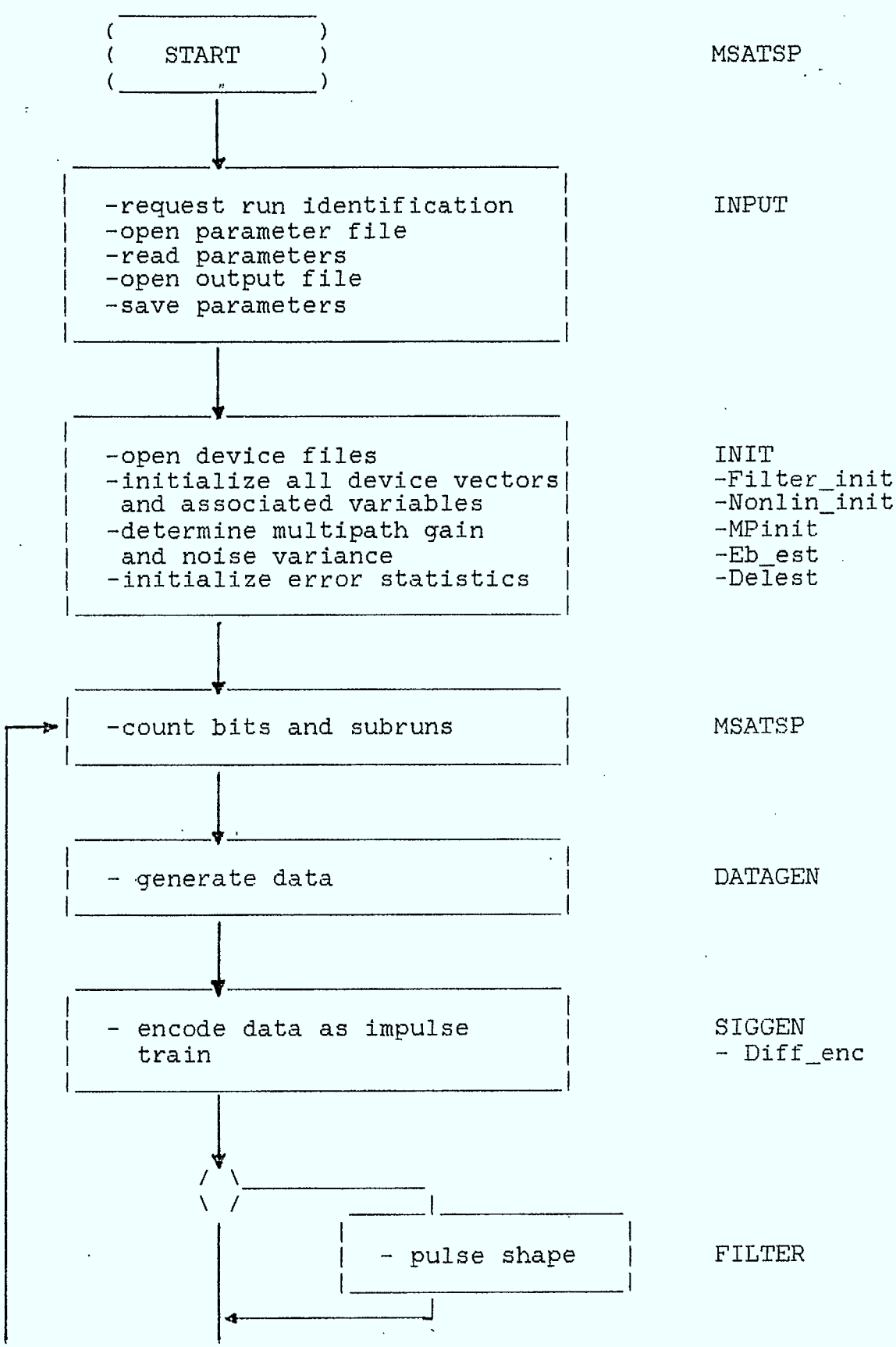

Figure D.5a

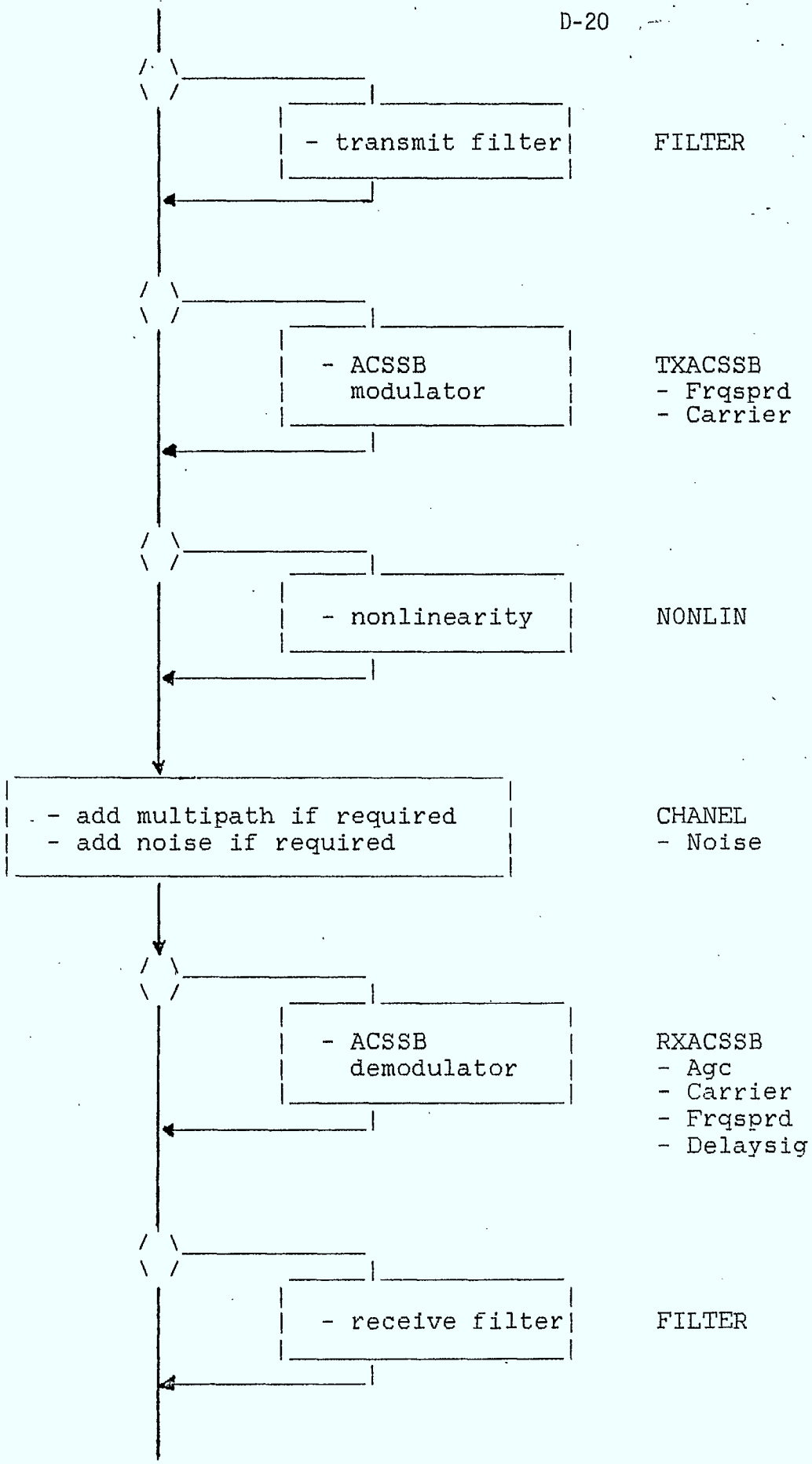
- transmit filter
FILTER
- ACSSB modulator
TXACSSB
- Frqsprd
- Carrier
- nonlinearity
NONLIN
- add multipath if required
- add noise if required
CHANEL
- Noise
- ACSSB demodulator
RXACSSB
- Agc
- Carrier
- Frqsprd
- Delaysig
- receive filter
FILTER

Figure D.5b

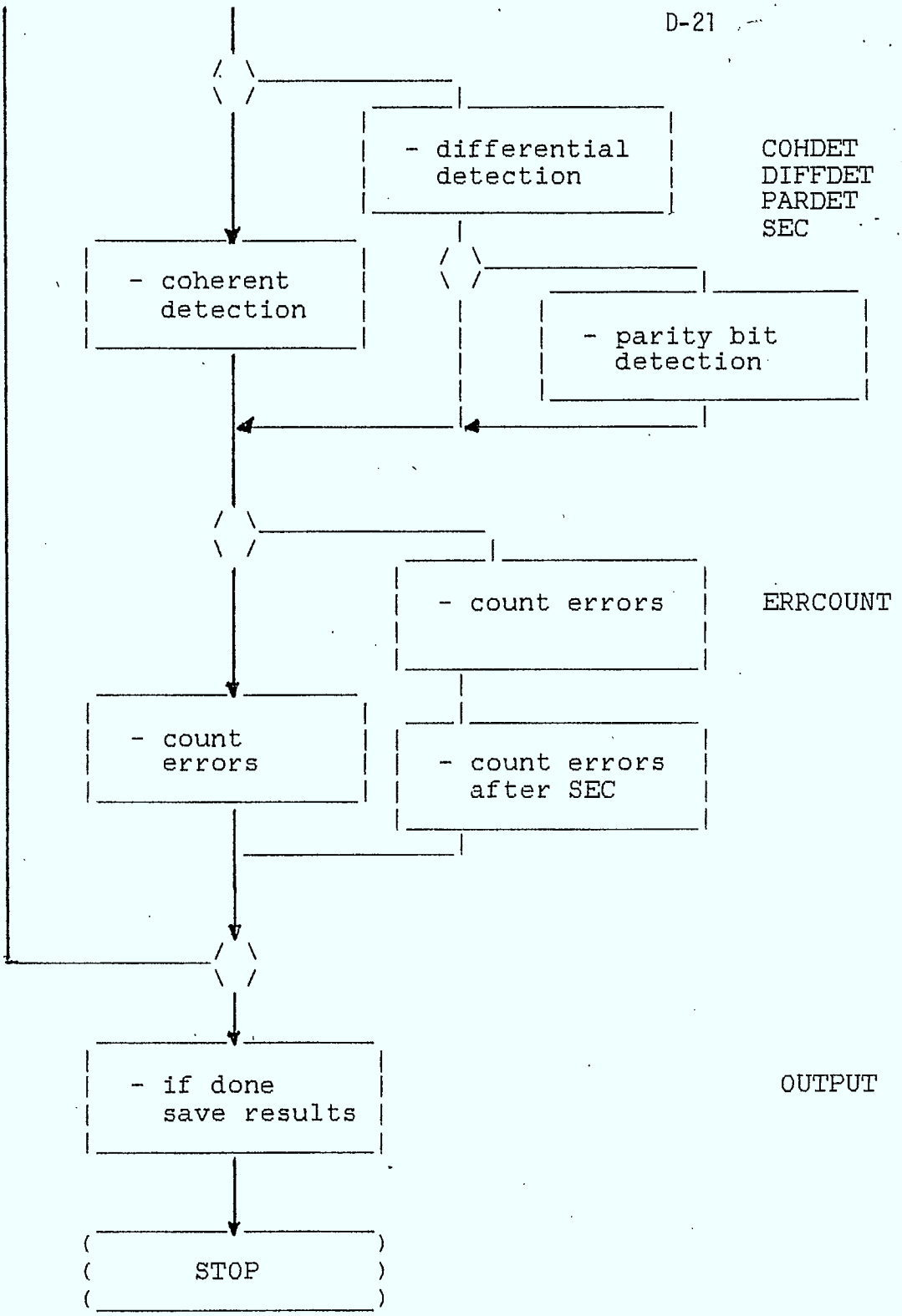
- differential detection
COHDET
DIFFDET
PARDET
SEC
- coherent detection
- parity bit detection
- count errors
ERRCOUNT
- count errors
- count errors after SEC
- if done save results
OUTPUT
STOP

Figure D.5c

more details). All memory devices such as filters are assumed to have finite memory, the upper bound on the memory length provides the maximum size of the overlap. Note that program efficiency decreases with increasing overlap, so the overlap should be kept to a minimum wherever possible.

Since block processing is the approach used, the overall simulation has a loop structure. An outer loop is executed eight times (this number can be reprogrammed), each iteration represents a subrun. The inner loop corresponding to each subrun is executed according to the number of bits per subrun as specified by the user in the parameter file. The splitting of the simulation into subruns allows the calculation of some standard deviations on the results, which would not be possible with one single large run. The first subsection following describes the standard format used for the device files. This is followed by a description of the program subroutines.

D.2.1 Device File Formats

There are two standard device file formats used by the MSAT simulation program. The first applies to filters and the second applies to nonlinear devices.

In the testing of the simulation, the vast majority of the filters used were of finite impulse response (FIR), and thus the simulation is more suited to FIR filters than infinite impulse response filters (IIR) although this does not preclude the use of the latter. The format of a filter device file is simply a list of the complex frequency domain samples of the filter, one per line, with the zero

frequency corresponding to line N/2 + 1 where N is the total number of samples. Note that N must be a power of 2, and must correspond to the block size used in the simulation (in most cases 1024). This file is usually created by taking the time domain samples of a FIR filter padding it with the appropriate number of zeros and then performing the forward FFT operation.

In those few cases where an IIR filter was required (e.g. ACSSB modem) it was found to be more efficient to code an implementation of the filter and fix it in the software. This is the approach that is recommended if further IIR filters are required. The alternative is to sample the frequency domain response of the IIR filter as was done above for the FIR filter. This will work well if the delay of the filter is comparable to the other filters used in the simulation and if it can be closely approximated by an FIR filter of length less than or equal to the number of samples of overlap allowed (in the input parameter file).

The nonlinear devices allowed in the simulation are assumed to be of the general AM-AM/AM-PM variety (see Section 2.0). The device file for this type of nonlinearity has the following format. The first line contains, M, the number of complex samples of the nonlinearity transfer characteristic which follow, (e.g. 61) the second line of the file contains the maximum amplitude (A) for which a gain is specified (e.g. 3.0). The following 61 lines are the complex gain samples of the nonlinearity corresponding to the determined step size μ, where $\mu=(A)/(M-1)$ (= 0.05 in this case).

Further details on the information in this section may be found in the file DEVICE.HLP.

D.2.2 Input - Subroutine INPUT

This subroutine opens and reads the input parameter file. Some of the input parameters are checked for validity and that they satisfy certain range conditions. In some cases the parameters are converted to the units used by the program. This subroutine also opens the output file and writes out most of the input parameters. Obviously this subroutine is outside the main loop of the program and is only executed once per simulation run. This subroutine also adjusts overlap so that there is an integer number of bits per non-overlap segment of a block.

D.2.3 Initialization - Subroutine INIT

The primary task of this subroutine is the creation of all the device profiles to be used by the simulation and initializing all of the overlap vectors to zero. However it also performs several other functions concerned with the calibration of the channel which are described in the following.

D.2.3.1 Filter Initialization - Subroutine FILTER_INIT

This is a general routine which reads a filter's characteristics from a file, stores it in the designated filter vector and initializes the overlap vector to zero.

D.2.3.2 Delay Estimation - Subroutine DELEST

Since all filters are assumed to be causal, there is a finite delay associated with each. The overall delay of the system must be determined accurately before the transmitted bits can be compared to the received bits, and the system performance determined.

The delay of each filter is estimated by determining the slope of its phase about the centre frequency. The best mean square fit of a straight line to the centre three phase values is obtained by minimizing

$$J = \sum_{i=-1}^{+1} (y_i - mx_i - b)^2$$

where (x_i, y_i) $i=-1,0,+1$ are the centre three frequency-phase points: with the result that

$$m = \frac{(y_1 - y_{-1})}{2} \cdot \frac{(\text{no. of samples per block})}{2\pi} .$$

In practice, some checking must be done to avoid the modulo 2π problem.

This slope is a simple estimate of the delay of the filter in samples.* The delays associated with all of the

*This technique will work for all linear phase filters but when applied to nonlinear phase filters, the accuracy may be suspect and a more complex method may be required.

elements are added, and if the result is not an integer number of samples, the slope of the phase of the receiver filter is adjusted (multiplied by $e^{j\alpha w}$ where α = int(m) - m + 1 where m is the calculated delay) to provide a delay of an integer number of samples.*

Note that this adjustment of the phase of the receive filter may change it from an FIR to an IIR filter, however the FIR assumption will still be reasonably accurate.

It is desirable to have a delay of an integer number of samples because it allows optimum bit sampling to be done without the introduction of further interpolation. The above 'adjustment of phase' causes the required interpolation to be performed.

Note that for linear phase FIR filters with N taps, the delay is known to be (N-1)/2 [24], and this can be used as one check of the delay estimation.

D.2.3.3 Nonlinearity Initialization - Subroutine NONLIN_INIT

This subroutine reads the nonlinear device characteristics from a file and saves them in the appropriate vector. It also determines the scale factor to apply to the signal to result in the desired nonlinearity operating point.

This calibration of the nonlinearity is done as follows. A 128 bit pseudo-random sequence was generated and used to fill a signal vector with impulses at the appropriate positions (see SIGGEN). This length of sequence will characterize all patterns of intersymbol interference caused by the three adjacent bits on either side of the data bit. With no allowance for overlap this sequence will

*The delay of the multipath spectral shaping filter is not included in this calculation of delay because it does not delay the transmitted signal.

completely fit in a signal vector an integer number of times. This sequence is then circularly filtered by the pulse shaping and transmit filters. This is the only place in the simulation where circular operations can appropriately be used.

The power of this sequence is measured immediately after pulse shaping and transmit filtering with the calculation

$$P_i = \frac{1}{N} \sum_{k=1}^{N} |s_i(k)|^2$$

If the non-linearity operating point was specified to be β, then the input scaling factor, γ, to the nonlinearity is given by

$$\gamma = \beta / \sqrt{P_i}$$

With this scaling factor applied to the input of the nonlinearity, the power of the output sequence is measured

$$P_o = \frac{1}{N} \sum_{k=1}^{N} |s_o(k)|^2$$

The estimated bit energy used in calculating the noise variance is then given by

$$E_b = P_o \cdot r$$

where r is the number of samples per bit. This estimate of E_b can then be used in the equations of the following Sections to determine σ^2.

D.2.3.4 Noise Parameter Estimation

The input parameters with regard to the channel are the E_b/N_o and K, the Rician channel factor. However to use these values in the simulation, they must be converted to noise amplitudes and multipath gains.

D.2.3.4.1 Gaussian Noise Variance Without Nonlinearity

Given a desired E_b/N_o ratio, we wish to determine the appropriate noise variance to add to the transmitted signal. Let E_b be the received energy per bit, corresponding to the received baseband symbol pulse, g(t). Then

$$E_b = \int |g(t)|^2 dt$$

$$= \tau \sum_k |g(k\tau)|^2$$

$$= \frac{\tau}{N} \sum_{k=0}^{N-1} |G(k)|^2 = \tau S$$

by Parseval's Relation [24], where G(k) is the DFT of g(k).

It is shown in Appendix A that to obtain a desired E_b/N_o, the <u>complex</u> noise variance is given by

$$\sigma^2 = \frac{S}{(E_b/N_o)} \quad .$$

D.2.3.4.2 Gaussian Noise Variance With Nonlinearity

When there is a nonlinearity, the energy per bit must be estimated using the E_b calculated in the nonlinearity initialization, and then proceeding as above.

D.2.3.4.3 Multipath Gain Estimation

If s(t) is the input to the Rician channel then the output is

$$r(t) = s(t) + A(t)\ s(t - \tau)e^{j\theta(t)}.$$

For our purposes, the bit rate will be assumed low enough that the delay is negligible ($\tau \approx 0$) and the Rician channel K factor, the ratio of reflected path to direct path power is

$$K = 10 \log E[A^2(t))].$$

The expected value $E[A^2(t)]$ is approximately given by

$$E[A^2(t)] \approx \frac{k^2}{N} \sum_{n=1}^{N} |x(n|^2$$

where k is a multipath gain factor, and x(n) is the sampled output of the multipath spectral shaping filter (see Section 2.5 and D.2.8). The input to this filter is white Gaussian noise of unit variance, thus this can also be represented as

$$E[A^2(t)] \approx \frac{k^2}{N} \left(\frac{1}{N} \sum_{k=1}^{N} |G(k)|^2\right)$$

where G(k) are the sample values of the DFT of the filter. From this and the desired K, the required multipath gain, k, can be determined.

However, because the output of the reflected channel is added to the direct path it can have the effect of

increasing (or decreasing) the instantaneous received energy per bit. Therefore the average energy per bit must be recalculated after the Rician channel. This can be done analytically as follows

$$E[\,|r(t)|^2] = E[\,|(1 + Ae^{j\theta})s(t)|^2]$$

$$= E[\,|(1 + Ae^{j\theta})|^2][E|s(t)|^2]$$

This is true because the complex fading gain is independent of the signal so that

$$E[\,|r(t)|\,]^2 = (1 + E(A^2))E|s(t)|^2$$

This means that the energy per bit must be adjusted to

$$E_b^1 = (1 + E(A^2))\ E_b$$

$$= (1 + 10{**}(K/10))E_b$$

and the Gaussian noise variance must be calculated accordingly.

D.2.4 Data Generation - Subroutine DATAGEN

This subroutine uses the Fortran random number generator to create a sequence of random bits. The cycle length of this generator is approximately 2^{32}. Since any simulation run will only use a portion of this sequence this implies that we are dealing with a Monte Carlo simulation of the mobile channel.

On each iteration of the loop, only enough bits for one block of data are generated, and the updated seed is saved for the next pass through the loop.

D.2.5 Signal Generation - Subroutine SIGGEN

The function of this subroutine is to differentially encode the data, if required, and then insert the data as a string of impulses at the appropriate points in the signal vector. Mathematically the underlying strategy of all the modulation techniques was to convert the data bits, $\{a_i\}$, $i=1,\ldots,N$, to an impulse train described by

$$m(t) = \sum_{i=1}^{N} b_i \delta(t-T)$$

where T is the bit period, and $\{b_i\}$ is an encoded form of the data $\{a_i\}$. In the case of differential detection then $\{b_i\}$ must be a differentially encoded version of $\{a_i\}$, that is,

$$b_i = a_i + b_{i-1}$$

where + is a modulo 2 adder. If in addition, we are using a signaling scheme which has two orthogonal channels, then every second b_i must be rotated in the complex domain to become purely imaginary. This is accomplished by rotating each successive b_i by 90°, that is,

$$b_i \leftarrow b_i \, e^{j\frac{i\pi}{2}} \qquad i = 1,\ldots,N$$

Note that this type of continuous rotation is required for a differential detection scheme using two orthogonal channels.

All modulation strategies studied for signaling over two orthogonal channels only included the case when the bits

are offset in the two channels. Strategies such as QPSK, where the bits are not offset, were not considered.

Note that at the beginning of each signal vector space is left to allow for signal overlap.

D.2.6 Filtering - Subroutine FILTER

The filtering operations of pulse shaping, transmit and receive filtering are all done in the same manner and use the same subroutine but with different parameters passed. The signal vector is by convention, always in the time domain when in the main program, and since the filtering operations are done in the frequency domain, both a forward and reverse FFT is required by each filtering operation. Continuous filtering is performed by using the overlap and save technique which is illustrated in Figure D.6. This involves copying the overlap from the previous vector into the beginning of the new signal vector, and saving the overlap for the next case. This is followed by an FFT based filtering operation.

Several notes can be made about this technique. The overlap space allowed at the beginning of each block is essentially overhead space as far as the simulation results are concerned but is required to maintain continuity. To reduce overhead, this overlap should be kept to a minimum but note that the size of the overlap is constant for the entire simulation, thus the length of the overlap must allow for the maximum required by any device.

In cases where there are two filtering operations in a row it would be more efficient to combine the two filters into one to perform the filtering operation. This is not done in the program but can be done using an external utility

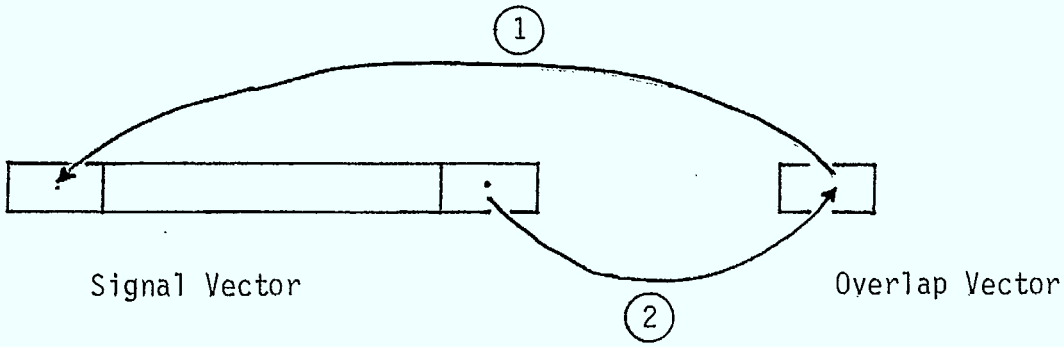

3 FFT(signal)
4 Multiply by Filter Profile
5 IFT(signal)

Figure D.6 Implementation of Overlap and Save Technique of Continuous Filtering.

program, and then entering only the new filter in the simulation configuration. However, one must be careful to check that the size of the overlap required by the combined filter does not exceed the overlap bounds.

D.2.7 Nonlinearity - Subroutine NONLIN

The program is set up to handle a general memoryless nonlinearity with both AM to AM and AM to PM distortion. The nonlinearity is implemented as a look up table, with the input amplitude as the abscissa and a complex gain as the ordinate.

The input amplitude is used as an index into the table, avoiding the need to search, and then the points on either side of the input amplitude are linearly interpolated between to obtain the appropriate nonlinearity gain.

The implementation of the nonlinearity requires a number of steps. They are the following:

- the input to the nonlinearity is scaled to the specified operating point. This scale factor was determined in the initialization routine.

- the signal magnitude is then used as an index into a table of complex gain coefficients which represent the nonlinearity

- linear interpolation between the two closest points in the table determines the complex gain to use

- the nonlinear action is then carried out by multiplying the signal by the determined gain.

Before a nonlinearity can be implemented properly it must be calibrated as described in 2.3.2. In the case the input amplitude exceeds the table size, the last two points of the table are linearly extrapolated to provide an estimate of complex gain.

D.2.8 Mobile Channel - Subroutine CHANEL

The mobile communications channel is assumed to be approximated by a Rician fading channel as illustrated in Figure D.7. In this model, there is a direct path for the signal and a Rayleigh fading path. On the fading path the signal is multiplied by a time-varying gain before being combined with the direct path. This time-varying gain is a complex Gaussian process of zero mean, with a spectral shape and variance determined by H(f). The spectral shape used in this simulation is described in Section 2.5.

The multipath channel is implemented in the following manner. The gain of the multipath channel is determined by filtered white Gaussian noise as shown in Figure D.7. This noise is generated in the time domain but because the spectral shaping filter is narrow, the noise samples need only be generated at specific sample intervals with zeros in between and then allowing the filter to interpolate between these values. The multipath spectral shaping filter is at present implemented as an FIR filter in the frequency domain. However because this filter is so narrow, it has a long overlap and requires doubling the FFT size to process the same number of samples. This implementation is not as efficient as a time-domain IIR implementation, but it is in general easier to find an FIR approximation to a given spectral shape than an IIR approximation, which may be more efficient from a user's viewpoint.

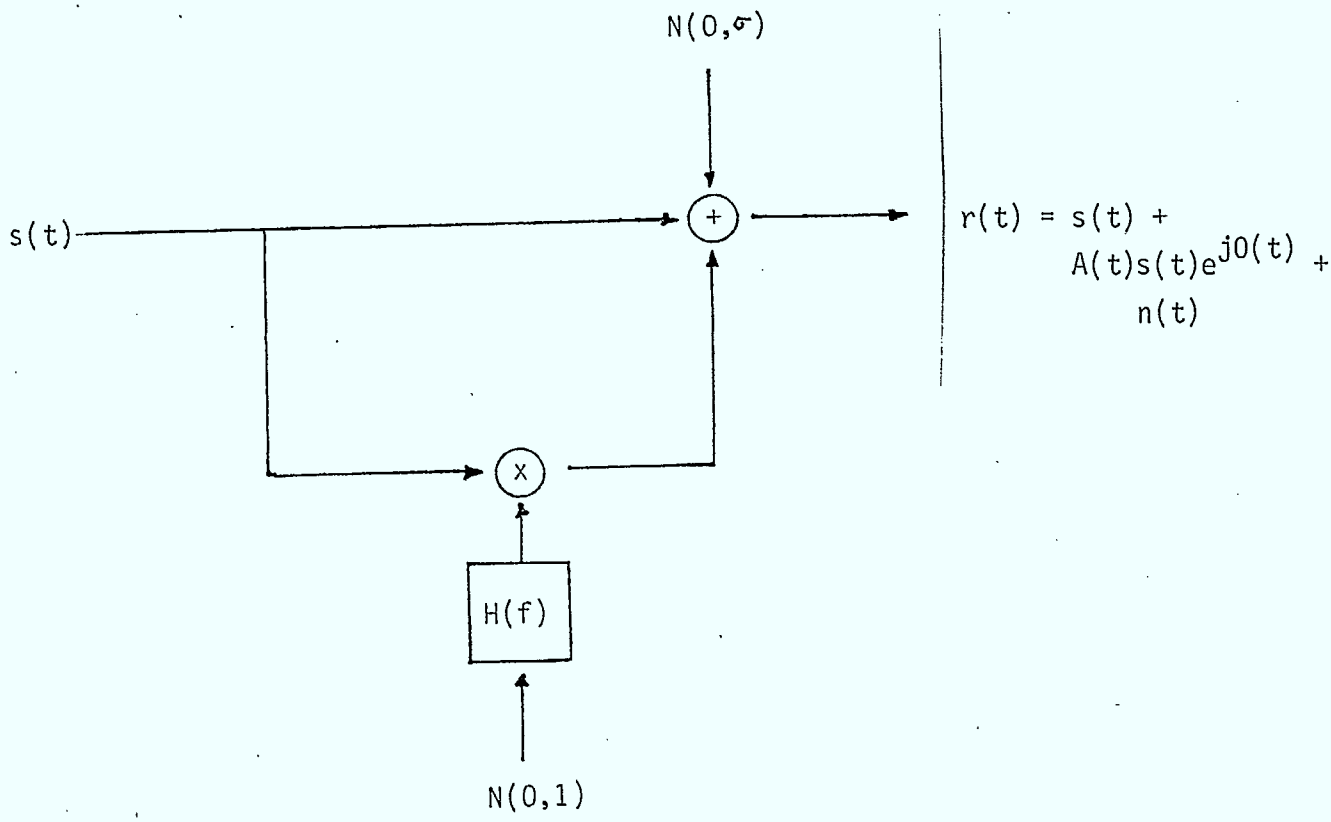

Figure D.7 Rician Fading Channel

To the output of the Rician channel is added sampled white noise. The variance of this noise is determined from the desired E_b/N_o as discussed in Section D.2.3.4.3 and D.2.3.4.1.

D.2.9 Differential Detector - Subroutine DIFFDET

This subroutine implements a differential detector as shown in Figure D.8. There are basically five steps to the differential detector

- copy overlap from previous signal block into the beginning of this block

- save overlap from end of this block

- estimate the optimum sampling point from the delay estimate discussed in Section D.2.3.2

- form the product

$$b_i = \mathrm{Re}\left\{s(iT)\ \overline{s((i-1)T)}e^{-j\pi/2}\right\}$$

where T is a bit interval and b_i are the received bit estimates.

The estimated data bits are then output in a separate array leaving the signal vector unchanged and suitable for further processing e.g. parity checking. Note that there are no filtering operations in the implementation of the data detector.

D.2.10 Coherent Detection - Subroutine COHDET

There is also the option of using a coherent detector as opposed to a differential detector. This option simply

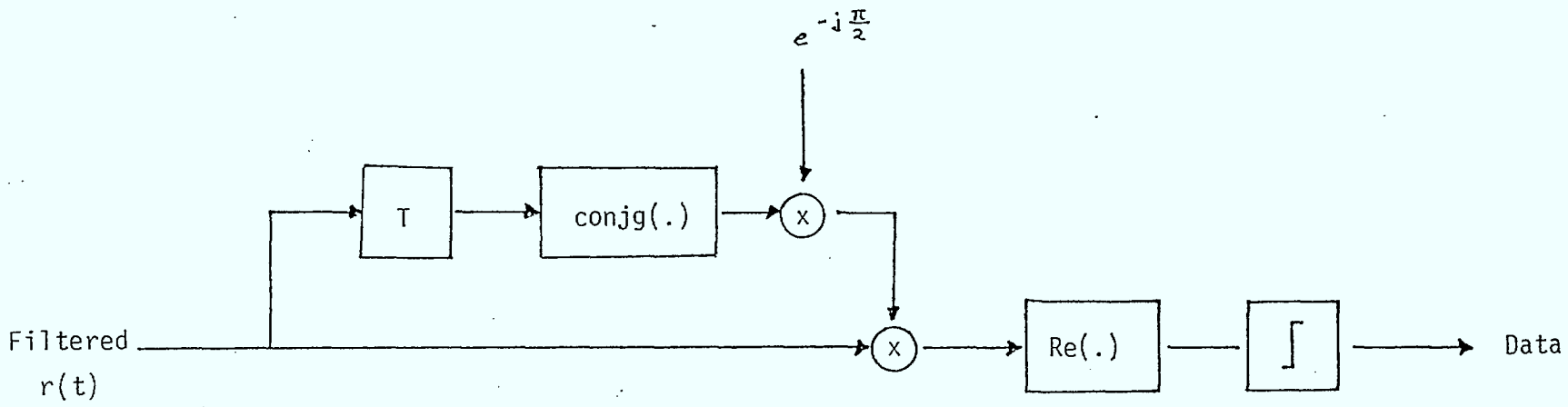

Figure D.8 The differential detector.

samples the received filtered signal at the appropriate instants and estimates the data bits.

D.2.11 Nonredundant Single Error Correction - Subroutine SEC

With differential detection schemes there is the possibility of performing non redundant single error correction to improve performance. This is described in Section 2.8 and has been implemented directly in software in this routine.

D.2.12 Gathering Error Statistics - Subroutine ERRCOUNT

This subroutine gathers information to estimate the performance of the data link. In this routine the transmitted bits are delayed and compared to the received bits. The following information is gathered concerning the number of errors.

- total number of bit errors
- total number of "+1" errors
- total number of "-1" errors

The following information is gathered concerning the distribution of error free gaps between errors.

- number of error free gaps of $\leqslant$ 10 bits
- number of error free gaps 10 $\leqslant$ ... $\leqslant$ 100 bits
- number of error free gaps 100 $\leqslant$ ... $\leqslant$ 1000 bits
- number of error free gaps 1000 $\leqslant$ ... $\leqslant$ 10000 bits
- number of error free gaps $\geqslant$ 10000 bits

It is the former statistics which are the main performance criteria of the system but the latter statistics may lend some insight into the error process.

D.2.13 The ACSSB Modem

The following set of subroutines implement the modulator and demodulator portions of the ACSSB modem which was described in Section 5.0.

D.2.13.1 The ACSSB Modulator - Subroutine TXACSSB

This subroutine implements the ACSSB modem in the following steps

- the input signal is first separated into two subbands by filtering the signal by the transmit subband filter and its conjugate symmetric version using the overlap and save approach

- if non-ideal carrier recovery is to be performed then
  - the two subband signals are IFFTed to the time domain.
  - a 300 Hz phase continuous tone is generated and passed through the CARRIER routine to generate +600 and -600 Hz tones
  - the +600 Hz and -600 Hz tones are used to spread the subband signals in the time domain
  - the spread subband signals are added together with the 300 Hz tone and the d.c. pilot

- if ideal carrier recovery is performed then
  - the two subband signals are simply shifted in the frequency domain with the appropriate phase adjustment to make them continuous (subroutine FRQSPRD)
  - and the 300 Hz tone and d.c. pilot are added in the frequency domain
  - the combined signal is then IFFTed to the time domain.

D.2.13.2 The ACSSB Demodulator - Subroutine RXACSSB

The ACSSB demodulator basically undoes everything the ACSSB modulator does, but it is done in a manner which allows the coherent recombining of the subband signals. The front end of the demodulator includes a complex AGC which compensates for the amplitude and phase variations of the Rician channel. The following steps are performed

- the complex AGC (and carrier recovery) is performed (subroutine AGC).

- the signal is then passed to the subroutine CARRIER where the 300 Hz tone is stripped off and used to generate the coherent +600 Hz and -600 Hz subcarriers.

- the spread data signal is then passed through the receiver subband filter and its conjugate symmetric filter to separate the two subbands

- if subcarrier recovery is nonideal then
  - the signal is then delayed to match the delay of the subcarrier recovery process
  - the two recovered subcarriers are used to coherently recombine the signal.

- if subcarrier recovery is ideal then the two subband signals are simply shifted together in the frequency domain, with the appropriate phase correction to account for the delay of the channel and the receiver front end (subroutine FRQSPRD)

D.2.13.3 Ideal Subcarrier Recovery - Subroutine FRQSPRD

This subroutine is used in both the modulator and demodulator portions of the ACSSB modem. It simply shifts

both input signals an integer number of samples in opposite directions in the frequency domain. A phase adjustment is performed to maintain signal continuity.

D.2.13.4 Non-ideal Subcarrier Recovery - Subroutine CARRIER

This subroutine is used in both the modulator and demodulator portions of the ACSSB modem and performs the function described in Section 5.2.2.3. It performs the following steps.

- the input signal is filtered by a bandpass filter centred at 300 Hz, to remove the 300 Hz tone.

- if the subroutine is in the demodulator the original signal is also notch filtered to remove the 300 Hz tone.

- the 300 Hz tone is then passed through two one-sided filters to produce +300 Hz and -300 Hz tones respectively

- the +300 Hz and -300 Hz tones are then averaged in phase and squared to produce the +600 Hz and -600 Hz subcarriers.

D.2.13.5 AGC and Carrier Recovery - Subroutine AGC

This subroutine performs the carrier recovery portion of the modem, and also compensates for the phase and amplitude variations caused by the Rician fading channels as described in 5.2.2.1. The following steps are performed

- the input signal is split among two paths

- on the first path the signal is lowpass filtered to remove the d.c. pilot. This estimate of the d.c. plot is then subtracted from the second path which has simply been delayed to match the filter delay.

- the estimate of the pilot is then inverted and lowpass filtered

- the other signal path is delayed to match this filter delay

- the two signals are then multiplied to produce the output signal

D.2.13.6 Delaying the Signal - Subroutine DELAYSIG

This subroutine simply delays the signal the amount required by the subroutine AGC and updates the appropriate overlap vectors.

D.2.14 Program Results - Subroutine OUTPUT

As described in Section D.1.3, this subroutine saves all of the error statistics gathered through the course of the simulation and places them in an output file. It also calculates an overall bit error rate and the standard deviation observed in this value.

D.3 Compiling and Linking The Simulation Program

If it is necessary to modify the simulation program, or if it is being transferred to new system with a VAX-11 Fortran-77 compatible compiler, then all of the previously described program modules can be recompiled using the command

```
$FOR module_name
```

There are no compiler options or switches which are necessary. If all of the modules must be compiled then the command file COMPILE.COM can be used to do this.

If a re-compilation has been necessary, then re-linking will also be necessary and this can be done with the following command

```
$LINK MSATSP/OPTIONS
```

This command requires the presence of the file MSATSP.OPT, which lists all of the module names. This also assumes that object code versions of all modules exist and are in the directory as specified in MSATSP.OPT. If the source code is modified to add an additional module then MSATSP.OPT must also be updated.

D.4 Array Processor Version of The Simulation Program

The array processor version of the MSAT simulation has a structure which is nearly identical to that of the VAX compatible version. In fact, the majority of the code is identical because it was only a few time-consuming routines which were converted to array processor code. These routines were

- FILTER
- CHANEL
- some of the subroutines associated with the non-ideal ACSSB.*

To distinguish these routines the prefix 'AP' was added to their file name e.g. APFILTER.FOR. The structure and actions of these subroutines is virtually identical to the

*Note the array processor version does not include an ideal subcarrier recovery ACSSB option.

VAX compatible version and they were validated against one another. The only major difference is the inclusion of the module APMEMMAP, which initializes the array processor and transfers the necessary filters and constants to the array processor memory. This subroutine also sets all address variables used to point to data in the array processor memory. For example, the vector SIGNAL in the VAX has a corresponding address in the array processor which is saved in the variable ASIGNAL.* All operations on array processor data refer to these addresses.

---

*The prefix A is standard.